Carnegie Mellon University

CARNEGIE INSTITUTE OF TECHNOLOGY

THESIS

SUBMITTED IN PARTIAL FULFILLMENT OF THE REQUIREMENTS

FOR THE DEGREE OF Doctor of Philosophy

TITLE Informing ankle-foot prosthesis design and prescription through systematic experimentation with a tethered robotic prosthesis

PRESENTED BY Joshua M. Caputo

ACCEPTED BY THE DEPARTMENT OF

Mechanical Engineering

_____ _____
ADVISOR, MAJOR PROFESSOR DATE

_____ _____
DEPARTMENT HEAD DATE

APPROVED BY THE COLLEGE COUNCIL

_____ _____
DEAN DATE

Informing ankle-foot prosthesis design and prescription through systematic experimentation with a tethered robotic prosthesis

Submitted in partial fulfillment of the requirements for

the degree of

Doctor of Philosophy

in

Mechanical Engineering

Joshua M. Caputo

B.S., Mechanical Engineering, Carnegie Mellon University
B.S., Electrical and Computer Engineering, Carnegie Mellon University

Carnegie Mellon University
Pittsburgh, PA

May, 2015

joshua.m.caputo@gmail.com

Acknowledgments

Thank you Steve for catalyzing my passion for biomechatronics and providing me with a world-class research environment. Thank you Peter for your advice and invaluable contributions to commercialization. Thank you Jon, Mark, and Andy, for your recommendations regarding this work and participation on my committee.

Thank you Hartmut for so generously sharing your space and gait lab hardware. Thank you Dr. Miknevich, the staff of DeLaTorre O&P, Connie Lewis, and Bambi Brewer for your invaluable contributions to the clinical applications of this work. Thank you Manoj, Karl, and Greg for providing an outside perspective.

Thank you to the Mechanical Engineering Department, especially Dr. Aubry, Dr. Robinson, Dr. Steif, Dr. Reid, and Chris Hertz, for helping me to make the most of my experience at CMU. Thank you John, Jim, and Ed, for teaching me everything I know about fabricating metal parts and tons of laughs over the years. Thank you Ginny and Bobbi for so kindly fulfilling countless purchases on my behalf.

Thank you Rachel, Myunghee, J.J., Matt, Soongeun, Michiel, Tianyao, Robbie, Philippe, Pepin, Jon Boerner, Roberto, Anne, Julie, Patrick, and all the other CMU-EBLers–it was a genuine pleasure to work with you all, keep in touch!

Thank you Mom, Dad, Em, and Elise.

Doctoral committee:

Steven H. Collins (committee chair)

Associate Professor, Mechanical Engineering, Carnegie Mellon University

Peter G. Adamczyk

Assistant Professor, Mechanical Engineering, University of Wisconsin–Madison

President, Intelligent Prosthetic Systems LLC

Jonathan Cagan

G. Tallman and F. B. Ladd Professor, Mechanical Eng., Carnegie Mellon University

Mark S. Redfern

W. K. Whiteford Professor, Bioengineering, University of Pittsburgh

Andy L. Ruina

Professor, Mechanical and Aerospace Engineering, Cornell University

Funders:

This thesis was made possible by financial support from the Carnegie Mellon University Department of Mechanical Engineering, the National Science Foundation under Grant No. CMMI-1300804, the National Institutes of Health under Award No. 1R43HD076518-01, and a John and Claire Bertucci Graduate Fellowship.

Preface

My objective is to provide individuals with lower-limb amputation with prosthetic limbs that enable users to restore (or even exceed) their pre-amputation levels of mobility. Despite great progress in the field over recent decades, the design and prescription of prosthetic limbs still falls rather short of our imaginations. It is deceptively challenging to effectively design and prescribe lower-limb prostheses. State-of-the-art methods rely on human intuition informed by simple observations, and are unlikely to result in optimal decisions. The robotic technology ubiquitous in everyday items such as cell phones, automobiles, and children's toys promises to revolutionize prosthetics, and yet it is mostly absent from the industry. When this technology has been incorporated, adoption has been limited by an inability to justify the 10–100 times increase in cost over conventional solutions. I believe this technology can provide a benefit at a justifiable cost, but new methods of design and prescription are required to efficiently realize these benefits. In this thesis I detail a few novel approaches to these challenges, which I hope will contribute to accelerating this robotics revolution and enable lower-limb amputees to achieve new levels of mobility.

Abstract

Recently-developed robotic prostheses have demonstrated that it is possible to design a prosthesis which makes it easier for unilateral transtibial amputees to walk. Unfortunately, it is unclear which design features are most important and which users will benefit most from these advanced technologies that increase prosthesis cost by an order of magnitude. I developed a novel experimental approach to resolving these design and prescription uncertainties. Candidate prosthetic feet are emulated during treadmill walking experiments using a high-performance off-board actuated and controlled lightweight robotic prosthesis. Prosthesis behavior is systematically varied while users' walking economy, performance, and satisfaction are measured. This process thereby determines unambiguous relationships between device behavior and outcomes of interest.

In Chapter 1 of this thesis I motivate the approach. In Chapter 2 I detail the design and evaluation of the novel prosthesis emulator system. Then, in Chapter 3, I detail an experiment in which I test the simple walking model prediction that increasing prosthetic ankle push-off work will lessen leading limb collision, thereby reducing users' metabolic energy consumption. I demonstrate that increased push-off instead seems to primarily reduce energy consumption by aiding in the acceleration of the swing leg. In Chapter 4, I emulate the behavior of off-the-shelf prostheses, giving patients the opportunity to test-drive candidate devices prior to purchase, and enabling prescriptions to be justified by predictive experimental data. Finally, in Chapter 5, I demonstrate a human-in-the-loop prosthesis design optimization scheme that enables the manufacture of user-customized prostheses, which could ultimately supersede the need for prosthesis selection.

This thesis lends insight into how powered ankle-foot prostheses can make walking easier and demonstrates that the degree to which individual users will benefit is highly dependent on their specific needs, expected walking conditions, and the choice of outcome measures. I hope that this work serves to improve mathematical models of human walking and contributes to a shift towards individualized prosthesis design and prescription.

Contents

List of Tables

List of Figures

Chapter 1

Introduction

1.1 Motivation

1.1.1 Significance of lower-limb amputation

Lower-limb amputation adversely affects the quality of life of more than 600,000 people living in the United States (Zidarov et al., 2009; Legro et al., 1999; Hagberg and Brånemark, 2001; Ziegler-Graham et al., 2008). Members of disadvantaged demographics are disproportionately affected by amputation and prevalence of amputation is expected to double by the year 2050, driven by population aging and increased incidence of dysvascular conditions (Ziegler-Graham et al., 2008). Reduced mobility is a major component of amputees' reduced quality of life, with the deceptively simple task of walking reported as a major challenge (Zidarov et al., 2009; Legro et al., 1999; Hagberg and Brånemark, 2001). Unilateral transtibial amputation, the most common and simplest major lower-limb amputation, adversely affects walking performance by causing, for example, a 20% increase in metabolic energy expenditure, a 20% decrease in preferred walking speed, and an increased incidence of falls (Miller et al., 2001; Lehmann et al., 1993; Waters and Mulroy, 1999; Torburn et al., 1990; Hsu et al., 2006).

1.1.2 Need for new approaches to design and prescription

The functionality provided by conventional ankle-foot prostheses is likely a component of these performance limitations. Prosthetic foot designs have evolved, especially in recent decades, through an iterative design process driven by intuition based on simple observations of how a variety of users perform while using different prosthetic feet. While significant progress has been made, this process has been slow and has explored but a tiny portion of the possible design space. State-of-the-art prostheses, as prescribed using conventional means, have categorically failed to demonstrate quantitative performance improvements compared to traditional designs (Barr et al., 1992; Casillas et al., 1995; Lehmann et al., 1993). But it is clear that device design does affect performance, as systematic variations of device behavior have demonstrated significant affects on outcomes (Adamczyk et al., 2015; Klodd et al., 2010; Major et al., 2014). Recently developed next-generation device designs have demonstrated that it is possible to improve walking performance (Herr and Grabowski, 2012; Zelik et al., 2011; Grabowski et al., 2010). However, it remains unclear what design features are key to improving performance, since alternative designs deviate in many ways from conventional designs, so these demonstrations have contributed little to our understanding of how to design more effective prostheses. Also, it is unclear if all users will benefit from these novel devices, given differences in physiology and experience across individuals. Prescription of promising new technologies has been limited by the 10-100 times increase in cost they introduce compared to conventional devices, which has limited the gathering of observational data about what types of users will benefit.

It is a deceptively challenging to identify what prosthesis behavior will improve specific performance outcomes for an individual user based solely on intuition and observation. Simulation-based approaches to design, which are ubiquitous in other

domains, are not yet useful for the design of these systems since they have not demonstrated an ability to accurately predict human behavior in response to candidate device designs for either average or individual subjects (see Chapter 3). Inspired by these limitations, I seek to develop new processes for the optimal design and selection of prosthesis behavior that are driven by systematic experimentation which clearly describes relationships between device behavior and walking performance. Throughout this thesis I show that such processes can improve our understanding of the science of how humans respond to changes to particular design features, reduce uncertainty in prescription, accelerate innovation in prosthesis design, and ultimately yield better mobility outcomes for individuals with lower-limb amputation.

1.2 Approach

1.2.1 Avoiding the practical matter of implementation

Progress in the design of prosthetic limbs can partly be explained by and is limited by technology–improved manufacturing methods, materials, and components, such as sensors, batteries and actuators, enable improvements in time. Rapidly improving technology has set the expectation for a robotics revolution for lower-limb prosthetics (Goldfarb et al., 2013). But even with, say, massless batteries and infinitely powerful motors, it is unclear what prosthesis behavior will provide a given individual with the most benefit. Also, physical implementation of prosthesis design concepts is rather challenging given extreme design constraints, unclear design objectives, and tedious human-in-the-loop design iteration. Two prominent examples of next-generation prosthetic feet, the CESR foot (Collins et al., 2005; Zelik et al., 2011) and the MIT robotic foot (Au et al., 2006; Herr and Grabowski, 2012), each required 6 years prototyping before publishing the first conclusive experimental results with amputee subjects.

1.2.2 The tethered robotic ankle-foot prosthesis

Prototyping novel designs can be dramatically simplified by emulating the behavior of physical prototypes using a haptic interface. Instead of building new hardware for each candidate behavior, a single robotic system could be used to rapidly and systematically test a variety of behaviors behaviors. Existing robotic prostheses are limited in their versatility, being specialized for their designed behavior in order to meet practical design constraints such as mass-minimization. So we developed a tethered, off-board actuated and controlled robotic prosthesis with exceptional versatility. The basic premise of this approach is not new (Flowers and Mann, 1977; Abul-Haj and Hogan, 1987; Sawicki and Ferris, 2008; Andersen and Sinkjaer, 1995; Versluys et al., 2008), but given technological improvements over time and having the luxury of hindsight on the successes and shortcomings of these previous demonstrations, we were able to develop a system with notably higher performance.

1.3 Scope

1.3.1 Performance outcomes

Given humans' tremendous ability to adapt, it is straightforward to provide the user with a prosthesis that contains the mechanical functionality sufficient for walking. However, a prostheses should be conducive to walking, or the user will have a limited ability and desire to do so. A variety of walking performance outcome measures have been studied, but it is unclear how to appropriately weigh these different outcomes and, given individual differences in experience and physiology, this weighing is likely to be individual-specific. Some of these outcomes are quantifiable and can be measured experimentally, such as metabolic energy consumption, maximum walking speed, or stability. Users likely weigh such outcomes based on their perception of,

say, effort or balance, but also may consider immeasurable outcomes such as comfort or appearance. Physicians also consider outcomes such as the long-term implications of prosthesis use on physiology, gait symmetry, or similarity to non-amputee gait, and weigh these outcomes in their own subjective manner.

I considered several different outcomes throughout the research described in this thesis. As a roboticist with an interest in energy efficiency, I began with addressing how prosthesis behavior affects mechanics and metabolic energy consumption (Chapter 3). I then added heart rate, as a clinically-relevant energy metric, and maximum walking speed, to address potential differences between steady-state efficiency and maximal performance (Chapter 4). I then also added a measures of user satisfaction in order to capture users' subjective weightings and immeasurable outcomes (Chapters 4 and 5).

1.3.2 Device behavior

The goal of this thesis is to make progress towards identifying how an ankle-foot prosthesis should behave in order to maximize its benefit to the user. I think of 'behavior' as the functional relationship between the forces and motion of the user and the forces and motion of the environment, as governed by the design of the prosthesis. Prostheses have historically consisted of assemblies of passive materials such as foam, wood, metal, plastic, and composites. Through the shaping and selection of these materials, a myriad of possible device behaviors can be achieved. Recent technological advances have made robotic prostheses practical solutions, dramatically expanding the possibilities for device behavior. Sensors can be used to measure quantities such as forces, angles, velocities, and biological electrical signals. These signals can be combined to drive an actuated prosthetic joint through a myriad of possible control strategies. Though the capabilities of such prosthetic feet are far greater than that of a passive feet, this only exacerbates the uncertainty of device design.

It is unclear which of the many possible device behaviors are most relevant to explore, so I considered several throughout the research described in this thesis. Motivated by the predictions of simple dynamic walking models which promote the implementation of powered ankle push-off, I first I studied the effects of prosthetic ankle push-off work on walking performance (Chapter 3). I then emulated the behavior of different off-the-shelf prostheses, considering the effect of these different devices on outcomes (Chapter 4). Finally, focusing on easily-implementable passive device behaviors, I simultaneously optimized several aspects of spring-like behavior (Chapter 5).

In all of these experiments, I chose to describe and control the behavior of the prosthetic ankle joint by the relationship between the plantar/dorsiflexion angle and velocity of the joint and the torque about that joint. This torque vs. angle relationship, also known as quasi-stiffness or impedance, is commonly used to describe the behavior of the human and/or prosthetic ankle joint (Hansen et al., 2004) and to control prosthetic limbs (Sup et al., 2008). By directly controlling this relationship with a robotic prosthesis, a wide variety of steady-state behaviors can be systematically controlled and and compared based on their effect on human walking biomechanics. This torque vs. angle relationship changes with walking speed (Hansen et al., 2004), so for simplicity I conducted all of my experiments on a fixed-speed treadmill, but the torque vs. angle control approach can be extended to be adapted to changes in walking speed or ground conditions (Lenzi et al., 2014).

1.4 Summary

Given that the conventional prosthesis design and prescription replaces complex highly-actuated, finely controlled, and sensitive biological tissue with passive structures built of carbon-fiber, plastic, foam, wood, and metal, through an iterative pro-

cess driven by intuition informed by simple observations, it is likely that the prostheses used by most lower-limb amputees are sub-optimal. This thesis details the use of a high-performance tethered robotic ankle-foot prosthesis as an experimental tool for the rapid optimization of device behavior to individual users' needs. In Chapter 2, I detail the design of this device and demonstrate that it has higher performance than any other lower-limb assistive device. In Chapter 3, I detail an experiment in which we rigorously tested a design principle that has motivated the development of several novel prosthetic limbs, and provide evidence that state-of-the-art mathematical models of human walking may be too simplistic. In Chapter 4, I demonstrate an emulation approach to prosthesis prescription and suggest that patient-specific outcomes could be improved, costs across the prosthetics industry could be reduced, and adoption of effective novel prostheses could be accelerated through such an approach. In Chapter 5, I demonstrate another approach to improving outcomes, reducing costs, and encouraging innovation that could supersede the selection of off-the-shelf prostheses by rapidly optimizing device behavior based on users' verbal cues, thereby generating a blueprint for the manufacture of a user-specific custom prostheses.

Chapter 2

The ankle-foot prosthesis emulator

In this first chapter I detail the design of a tethered robotic ankle-foot prosthesis and demonstrate its exceptional performance through a series of controlled benchtop and walking tests. The key to this device's performance is its off-board power and control system, which enables the prosthesis to be be arbitrarily powerful without affecting the mass worn by the user. This arrangement was motivated by frustration with the inefficient iterative design process required when developing novel mobile ankle-foot prostheses (Collins and Kuo, 2010). In chapters 3–5 I describe several different approaches to informing prosthesis design and prescription using the ankle-foot prosthesis emulator. The development of this system laid the foundation for the development of several other assistive devices at Carnegie Mellon, including a strengthened version for subjects weighing over 210 lbs, a 2 degree-of-freedom ankle-foot prosthesis with ankle inversion/eversion control (Collins et al., 2015), a prosthetic knee, several ankle foot orthoses (Witte et al., 2015), and a knee exoskeleton.

Caputo, J. M., Collins, S. H. (2014) A universal ankle-foot prosthesis emulator for human locomotion experiments. *Journal of Biomechanical Engineering*, **136**:035002.

A preliminary version of this work appears in:

Caputo, J. M., Collins, S. H. (2013) An experimental robotic testbed for accelerated development of ankle prostheses. In Proceedings *International Conference on Robotics and Automation*, pages 2630-2635.

Preliminary versions of this work were presented at:

Caputo, J. M., Collins, S. H. (2012) An externally powered and controlled ankle–foot prosthesis for use in push-off experiments. Poster presentation at *36th Annual Meeting of the American Society of Biomechanics*.

Caputo, J. M., Collins, S. H. (2011) Externally powered and controlled ankle–foot prosthesis. Poster presentation at *Dynamic Walking*.

Abstract

Robotic prostheses have the potential to significantly improve mobility for people with lower-limb amputation. Humans exhibit complex responses to mechanical interactions with these devices, however, and computational models are not yet able to predict such responses meaningfully. Experiments therefore play a critical role in development, but have been limited by the use of product-like prototypes, each requiring years of development and specialized for a narrow range of functions. Here we describe a robotic ankle-foot prosthesis system that enables rapid exploration of a wide range of dynamical behaviors in experiments with human subjects. This emulator comprises powerful off-board motor and control hardware, a flexible Bowden cable tether, and a lightweight instrumented prosthesis, resulting in a combination of low mass worn by the human (0.96 kg) and high mechatronic performance compared to prior platforms. Benchtop tests demonstrated closed-loop torque bandwidth of 17 Hz, peak torque of 175 N·m, and peak power of 1.0 kW. Tests with an anthropomorphic pendulum 'leg' demonstrated low interference from the tether, less than 1 N·m about the hip. This combination of low worn mass, high bandwidth, high torque, and unrestricted movement make the platform exceptionally versatile. To demonstrate suitability for human experiments, we performed preliminary tests in which a subject with unilateral transtibial amputation walked on a treadmill at 1.25 $m{\cdot}s^{-1}$ while the prosthesis behaved in various ways. These tests revealed low torque tracking error (RMS error of 2.8 N·m) and the capacity to systematically vary work production or absorption across a broad range (from -5 J to 21 J per step). These results support the use of robotic emulators during early-stage assessment of proposed device functionalities and for scientific study of fundamental aspects of human-robot interaction. The design of simple, alternate end-effectors would enable studies at other joints or with additional degrees of freedom.

2.1 Introduction

Individuals with lower-limb disabilities experience reduced mobility and quality of life compared to their able-bodied counterparts. Major lower-limb amputation is a prominent example, affecting more than six hundred thousand people in the United States, disproportionately affecting disadvantaged groups, and expected to double in prevalence by the year 2050 (Ziegler-Graham et al., 2008). Individuals with amputation experience decreased walking performance using conventional, passive prostheses, including increased metabolic energy consumption, slower preferred walking speed, increased likelihood of falling, increased loading and injury of the unimpaired limb, and restricted social and recreational engagement (Ralston, 1958; Skinner and Effeney, 1985; Lehmann et al., 1993; Torburn et al., 1995; Hoffman et al., 1997; Waters and Mulroy, 1999; Hagberg and Brånemark, 2001; Miller et al., 2002; Hsu et al., 2006; Silverman et al., 2008; Zidarov et al., 2009; Morgenroth et al., 2011).

Robotic devices with active assistance show promise for improving locomotor performance for people with lower-limb amputation (Au et al., 2007; Hitt et al., 2007; Sup et al., 2009; Zelik et al., 2011; Morgenroth et al., 2011; Cherelle et al., 2012; Segal et al., 2012). For example, the first robotic ankle-foot prosthesis to reduce the energetic cost of walking for amputees has recently been demonstrated (Herr and Grabowski, 2012). A similar function can be provided by recycling energy that would otherwise be dissipated, suggesting that this benefit might be obtained in designs without motors or batteries (Collins and Kuo, 2010). These results highlight the potential for positive impact through robotic technology development.

Advances in robotic ankle prosthesis technology have been achieved despite very limited exploration of possible functionalities. A primary goal is to improve locomotor performance, which is a deceptively challenging task (Madden, 2007). Human adaptations to mechanical interactions with a prosthesis are very difficult to predict.

Although computational models can predict some qualitative aspects of human walking (Anderson and Pandy, 2001; Srinivasan and Ruina, 2006), and underlying control (Song and Geyer, 2012), they are not yet capable of predicting responses to subtle mechanical changes (Adamczyk et al., 2006; Fregly et al., 2012). Experimental studies are therefore crucial to evaluating the effects of a proposed design on humans, but such tests require a physical device that can be worn and used by a person. This has led to the development of product-like prototypes, each embodying a candidate functionality (we use this term in the manner of (Hirtz et al., 2002)), and each requiring several years of design and refinement prior to evaluation by human users (Pratt et al., 2004; Au et al., 2007; Hitt et al., 2007; Sup et al., 2009; Herr and Grabowski, 2012; Collins and Kuo, 2010). Autonomy presents the greatest design challenge, leading to specialized devices that are not versatile enough to express other candidate functionalities. This limits their usefulness as experimental tools and prevents studies with broadly generalizable findings; even in the cases where results have been positive, we have not understood why or whether better solutions exist. Our field has thereby invested heavily in answering 'how' to implement various functionalities, while the more important question of 'what' functionalities would most benefit the user remains largely unanswered.We propose that decoupling the critical task of testing proposed functionalities from the arduous task of designing specialized devices would speed the development of robotic prostheses with predictable benefits.

Laboratory testbeds, which have often been used as versatile exploratory tools in basic locomotion research, may provide the foundation for such an approach. These systems have typically been used as probes, providing measurable, though not tightly-controlled, disturbances in experiments designed to gain insights into reflexes (Andersen and Sinkjaer, 1995), adaptations to external (Veneman et al., 2007) and internal (Sulzer et al., 2009) forces on the legs, adaptations to altered effects of muscle activity (Sawicki and Ferris, 2008), and balance strategies (Bruijn et al., 2010). This

approach has cleverly leveraged machines with modest mechatronic performance to obtain useful insights. With improved fidelity, perhaps similar tools could be used to emulate behaviors relevant to specialized, wearable robots.

We propose that high-performance testbeds, or 'emulators', could be used to explore potential robotic assistance strategies, allowing measurement of human responses without the time-consuming development of specialized prototypes. Studies could be conducted during early product development, emulating, testing and refining proposed product designs quickly and with low cost. Emulators could also facilitate scientific investigations that address fundamental aspects of human-robot interaction during biomechanics tasks. This approach seems to have been first suggested by (Flowers and Mann, 1977) in the context of prosthetic knees, and later extended to prosthetic elbows by (Abul-Haj and Hogan, 1987).

Experimental emulators for these purposes should provide versatile, high-performance control and actuation capabilities without restricting other natural motions of the body. Torque control allows the testbed to be used as a haptic interface (Ellis et al., 1996), in which forces mimic the presence of a virtual system designed by the experimenter, such as springs or force fields. Torque control provides excellent versatility compared to, e.g., position control for which interactions are dominated by robot position, which can restrict human engagement (Hidler et al., 2009). Such a system should of course be capable of human-like torque and power magnitudes, but the limiting factor that must be maximized for dynamic emulation is closed-loop torque bandwidth (Griffiths et al., 2011). In this context, bandwidth is a measure of the responsiveness of the system, characterizing how quickly joint torque can be changed. High bandwidth might suggest large motors worn by the person, but such an approach would conflict with the requirement that interference with natural motions be minimized; mass worn on the limbs strongly affects coordination patterns and energetic cost (Browning et al., 2007). Instead, emulators can leverage the advan-

tages of a laboratory setting by placing motor and control components off-board and transmitting mechanical power through flexible tethers to lightweight end-effectors worn on the body. This organization of components has the added advantage of allowing a single actuator and tether to control multiple swappable end-effectors, with each being significantly simpler to design and fabricate than a fully integrated system. External forces from tethers could also interfere with natural motions of the limbs (Gordon et al., 2006; Veneman et al., 2007), so tethers should be designed to be lightweight and flexible, and their effects on gait should be measured and minimized.

Here we describe the design and feasibility tests of one such emulator for ankle-foot prostheses. We chose the ankle for its commonality to lower-limb disabilities (Waters and Mulroy, 1999) and mechanical importance in locomotion (Whittle, 1996). We used an off-board motor tethered to a lightweight prosthesis through a Bowden cable. We performed a variety of tests, in isolation and during human walking, to characterize performance and suitability of the platform as an experimental tool.

2.2 Methods

We designed and constructed a tethered ankle-foot prosthesis system incorporating a powerful electric motor, a low-interference transmission, and a lightweight instrumented prosthesis. We implemented plantarflexion torque control at the prosthetic ankle joint, including a demonstration mode suitable for walking tests, and measured system performance in a series of benchtop tests and human walking trials.

2.2.1 Mechatronic Design

The electromechanical system comprises an off-board motor and control system, a flexible tether, and an instrumented prosthesis end effector (Fig. 2.1). We selected a powerful, low inertia electric motor and a high-speed, real-time control module for

off-board actuation. We used a 1.61 kW AC servomotor with a 5:1 planetary gearhead (BSM90N-175AF with GBSM90-MRP120-5, Baldor Electric Corp., Fort Smith, AR). We made this selection using computer simulations of closed-loop torque control characteristics in which inertia, motor constant, and gear ratio were varied and step response and bandwidth were estimated. We regulated motor voltage using an industrial motor drive (MFE460A010B, Baldor) with embedded velocity control. Desired motor velocity commands were generated using a real-time controller (ACE1103, dSPACE Inc., Wixom, MI) based on high-level control laws (see *Sensing and Control*) and were communicated on an analog channel at 500 Hz. We used a Bowden cable transmission comprised of a coiled-steel outer conduit (415310-00, Lexco Cable Mfg., Norridge, IL) and a 3 mm synthetic inner rope (Vectran Fiber Inc., Fort Mill, S.C.). The cable measured 3.5 m in length and was routed to minimize bending, thereby minimizing friction while allowing desired end-effector motions (Fig. 2.1A). We fixed the outer conduit to the motor frame on one end and to the prosthesis frame on the other end, then wrapped the inner rope onto the motor pulley on one end and onto the prosthesis pulley on the other end (Fig. 2.1C). Forces generated by the motor were thereby transmitted to the prosthesis independent of its position in the workspace. Sensor cables were bundled with the Bowden cable to complete the tether.

We designed an instrumented prosthesis end effector to convert transmission forces into ankle plantarflexion torques. The prosthetic ankle joint (Fig. 2.1C) allows the toe segment to rotate with respect to the prosthesis frame. A series leaf spring on the toe segment protrudes backwards relative to the ankle joint axis. Transmission forces pull upwards on the end of this spring, generating a plantarflexion moment about the ankle joint (Fig. 2.1B), similar to the action of the Achilles tendon in the human ankle. We included a series spring to decouple motor inertia from the toe segment, which can improve torque tracking during, e.g., intermittent ground contact (Pratt and Williamson, 1995; Wyeth, 2006). We also used spring deflection to measure ankle

torque based on a calibrated model (see *Sensing and Control*). We used a low-tension spring to pull the toe upwards, leading to ankle dorsiflexion when transmission forces were low. We directly attached a compliant heel segment to the prosthesis frame.

Prosthesis dimensions were selected based on those of an average human foot (Hawes and Sovak, 1994). The distance between the heel and the toe was 0.22 m. The foot was aligned on the user's leg such that the heel was 0.07 m to the rear of the centerline of the tibia or pylon. The ankle was 0.07 m from the ground plane during standing. The toe was 0.07 m wide and the heel was 0.04 m wide, slightly narrower than the typical human dimensions of 0.10 m and 0.07 m, respectively. This allowed for a variety of foot widths to be explored using toe and heel attachments. Although the prosthesis fit inside an unmodified shoe, interference with the series leaf springs prevented its use during the tests reported here. Instead, rubber at the toe and heel contact points approximated the effects of the sole of a walking shoe.

We constructed the prosthesis end effector using a variety of custom and catalog components. Series leaf springs and heel springs were machined from fiberglass (unidirectional E-Glass, GC-67-UB, Gordon Composites Inc., Montrose, CO). Heel and toe pads were 3D printed using fused deposition modeling (FDM) of acrylonitrile butadiene styrene (ABS). Rubber strips (Pro Tania, Vibram, North Brookfield, MA) were affixed with adhesive at ground contact locations. The frame, toe segment, spring attachment, pulley, and Bowden cable termintation components were machined from 7075-T651 aluminum. We connected the pulley and series springs with an ANSI 25 hardened steel sprocket and roller chain (6Q 7-H25 and A 6C 7-25011C, Stock Drive Products/Sterling Instrument, New Hyde Park, NY) including a custom machined 1074/1075 spring steel link at the spring attachment. The device was connected to the user's pylon with a standard titanium prosthesis adapter (FND-227014, Ohio Willow Wood, Sterling, OH). We measured ankle rotation with a 10 bit absolute magnetic encoder with analog transmission, geared 8:1 for increased resolution,

and pulley rotation with a 9 bit optical incremental encoder (MAE3-A10-250-220-7-1 and E8P-512-250-D-H-D-2, respectively, US Digital, Vancouver, WA). See *Supporting Materials* for models of all custom components and a complete bill of materials.

2.2.2 Sensing and Control

We computed measured ankle torque based on measurements of spring displacement and ankle position using a calibrated model. We performed calibration trials in which the prosthesis was fixed upside down while masses of known weight were hung from the toe. We applied a range of masses and ankle angles that spanned the expected operating conditions. Maximum torque during calibration was limited by the rated continuous current of the motor (which is lower than the maximum intermittent current). We modeled measured ankle torque as a function of ankle angle and prosthesis pulley angle, and fit coefficients using least squares regression. We first determined a relationship between ankle and pulley angles under zero load, then determined a stiffness coefficient for the deviation of the pulley angle from the zero-torque relationship under various loads.

Torque control was achieved using proportional feedback on torque errors:

$$\omega_m = K_p \cdot (\tau_d - \tau) \tag{2.1}$$

where ω_m is the velocity commanded to the motor driver, K_p is the proportional gain, and τ_d and τ are desired and measured ankle torque, respectively. K_p was determined from a mathematical model, then hand tuned. We used a similar feedback control law to perform ankle position control under conditions with no external load, such as the swing phase of walking, by substituting a position error for torque error and using a modified gain. See *Supporting Materials* for a complete set of software used to control the device.

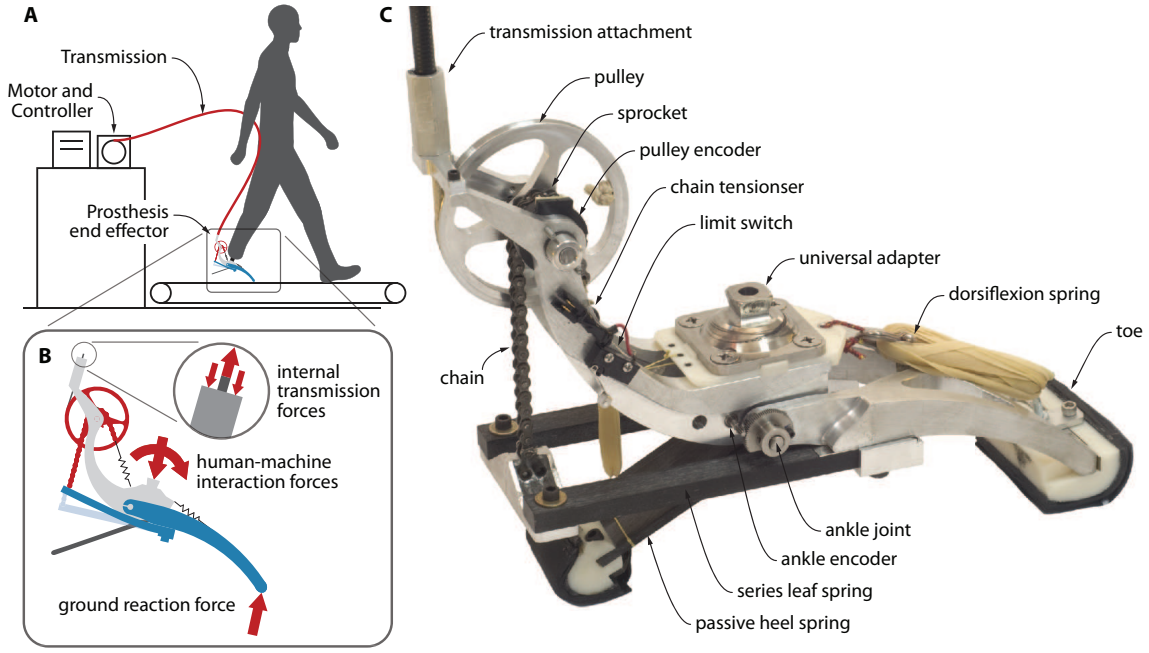

Figure 2.1: Mechatronic design of the universal prosthesis emulator. **A** The system comprises three elements: (1) powerful off-board motor and control hardware, (2) a flexible tether transmitting mechanical power and sensor signals, and (3) a lightweight instrumented end-effector. This division of components was chosen to maximize responsiveness and minimize end-effector mass during treadmill walking. **B** Free-body diagram of the end effector. Internal Bowden cable transmission forces pull the synthetic rope upwards while equally and oppositely pushing the aluminum frame downwards. Rope tension is transmitted through the pulley, sprocket, chain, and leaf spring, giving rise to a ground reaction force at the toe. The effect is equivalent to an ankle plantarflexion torque, resulting in a reaction force and moment at the interface with the human user. **C** Photograph of the instrumented prosthesis. A pulley-sprocket component magnifies transmission forces and allows direct measurement of spring deflection. A tensioning spring keeps the chain engaged. A limit switch protects against excessive plantarflexion. A universal adapter attaches to the socket or prosthesis simulator worn by the user. A dorsiflexion spring comprised of rubber bands retracts the toe, e.g., during leg swing. Fiberglass leaf springs provide series elasticity for ankle torque measurement and control. A separate leaf spring directly connected to the frame (not the toe) comprises the heel.

We designed several safety features, in both software and hardware, to limit the forces exerted by the prosthesis on the human user. We placed software limits on the maximum desired torque and motor velocity, and used software stops to prevent travel beyond the range of motion of the prosthesis ankle joint. We incorporated an electrical plantarflexion limit switch (Fig. 2.1C) and electrical buttons accessible to the subject and experimenter that deactivated the motor when pressed. Mechanical fail-safes included a transmission break-away, composed of an empirically-determined number of loops of thin synthetic rope, and hard stops at the ankle's range of motion.

2.2.3 Benchtop Testing Methods

We conducted benchtop tests characterizing device performance in terms of torque measurement accuracy, peak torque, closed-loop torque step response, closed-loop torque bandwidth, peak power, and tether interference. These tests were designed to reveal fundamental aspects of system performance and to allow comparison with existing platforms.

We first evaluated the accuracy of our calibrated torque measurement. We applied a range of known ankle torques using static loading with free weights (Fig. 2.3A). We separately applied each load with the ankle joint maximally dorsiflexed, in a neutral position, and maximally plantarflexed. We then compared measured and applied torques, computing the root mean square (RMS) error and the maximum absolute error. Validation and calibration were performed separately, comprising independent data sets.

We performed step response tests with the toe fixed in place to characterize closed-loop torque response time and demonstrate peak torque capacity. We rigidly fixed the prosthesis frame and toe to the benchtop, locking the ankle joint (Fig. 2.3B), and programmed desired torque as a square wave with a magnitude of 175 N·m. We then tuned K_p so as to minimize rise time and overshoot. We collected data for 10

complete cycles, averaged the measured torque trajectories, and computed 90% rise and fall times.

We performed similar step response tests with a compliant load to demonstrate peak power. We rigidly fixed the prosthesis frame to the benchtop and attached the toe to the benchtop through a coil spring. We chose a spring with stiffness of 26,000 $N \cdot m^{-1}$, which we found allowed motor velocity saturation. We collected data for 10 complete cycles, averaged the computed power trajectories, and computed peak power as the maximum of the average power trajectory.

We characterized closed-loop torque control bandwidth using frequency-domain transforms of the system's response to a chirp in desired torque. During bandwidth trials, we rigidly fixed the prosthesis frame and toe to the benchtop, locking the ankle joint (Fig. 2.3C), and programmed desired torque as an offset chirp oscillating between 56.5 and 113 N·m at frequencies rising from 0 to 30 Hz. We tuned K_p to maximize bandwidth with acceptable resonance. We mathematically approximated both input (desired torque) and output (measured torque) signals in the frequency domain using a fast Fourier transform (FFT). We calculated magnitude responses as the ratio of the magnitudes of the complex FFTs and frequency response as the difference of the angles of the complex FFTs. Accuracy of the FFTs obtained in each trial was limited by the number of data points captured at each input frequency, which was limited by trial duration prior to reaching motor temperature limits. We collected data for 10 trials, smoothed each resulting Bode plot to remove FFT artifacts, and averaged across trials. We calculated bandwidth as the minimum frequency for which the average magnitude response was above -3 dB. We calculated phase margin as the difference between -180° and the average phase response at the frequency where the magnitude response was 0 dB.

We performed experiments with an anthropomorphic pendulum 'leg' to characterize interference in natural leg motions due to tether stiffness and damping. In

order to generate dynamic leg-like motions under controlled, repeatable conditions, we constructed a single-link pendulum with mass properties of a 50^{th} percentile male leg (Winter, 1990). We attached the instrumented prosthesis to the end of this "leg", and performed trials under two conditions: *tethered* and *untethered*. In *tethered*, peak ankle plantarflexion torque was applied to maximize resistance to leg motions. For each trial, we raised the prosthesis to a consistent initial angle, allowed it to swing freely until a lower threshold amplitude was crossed, and recorded the number of cycles and the time elapsed. We conducted 10 trials and calculated the average frequency and decay time for each condition. We then calculated the stiffness and damping coefficient attributed to tether forces (see *Appendix A* for a detailed model and calculation).

2.2.4 Human Walking Testing Methods

We developed a high-level impedance control law that calculated desired torque based on ankle angle and gait cycle phase. This control law enabled evaluation of device performance during walking, and provided an example of one of many high-level torque control techniques that could be embodied by the system, such as impedance matching (Sup et al., 2009), proportional electromyography (Gordon et al., 2006), positive force feedback (Eilenberg et al., 2010), or time-trajectory control variants (Aoyagi et al., 2007). In the example control law (Fig. 2.2), desired torque was determined using the piecewise linear function:

$$\tau_d = k_i \cdot (\theta - \theta_{0_i}) \tag{2.2}$$

where τ_d is desired ankle torque, θ is ankle joint angle, and k_i and θ_{0_i} are the piecewise constant stiffness and offset terms, respectively, that remained constant over a range of joint angles and during each finite state, ϕ. A finite-state machine advanced ϕ

through three phases: *dorsiflexion*, during the beginning of stance, characterized by negative ankle velocity; *plantarflexion*, during the end of stance, characterized by positive ankle velocity; and *swing*, characterized by no ground contact. During each of the stance phases, two values of k_i and θ_{0_i} were used, based on a transition threshold value for θ, such that the ankle joint behaved as a stiffening spring comprised of two linear stiffness regions. Different values of k_i and θ_{0_i} were used during dorsiflexion and plantarflexion phases, enabling control of the net work produced or absorbed over the course of a step cycle, equivalent to the area within the resulting work loop.

We chose default values of k_i and θ_{0_i} for each linear segment such that the overall curve approximated the relationship observed for the human ankle during normal walking (Fig. 2.2). We also determined alternate sets of curve parameters for the plantarflexion phase that resulted in a range of values of net ankle work. During the swing phase, a separate position control mode reset the ankle angle to prepare for the next stance phase.

We used a configuration prediction term to improve tracking of desired torques generated using the impedance control law. We found that communication delays and motor dynamics typically led to a lag of about 16 ms between commanded and observed motor velocity changes. This caused measured torque to lag the impedance-based desired torque, especially during fast ankle motions, e.g., push off. We modified the ankle angle used to generate desired torque in Eq. 2.2 to account for expected changes in desired torque as follows:

$$\theta_p = \theta + t_{pred} \cdot \dot{\theta} \tag{2.3}$$

where θ_p is the predicted ankle angle substituted for θ in Eq. 2.2, t_{pred} is a prediction time constant, and $\dot{\theta}$ is the current ankle angular velocity. This adjustment was based on a simplified model of the system dynamics, in which motor dynamics are much

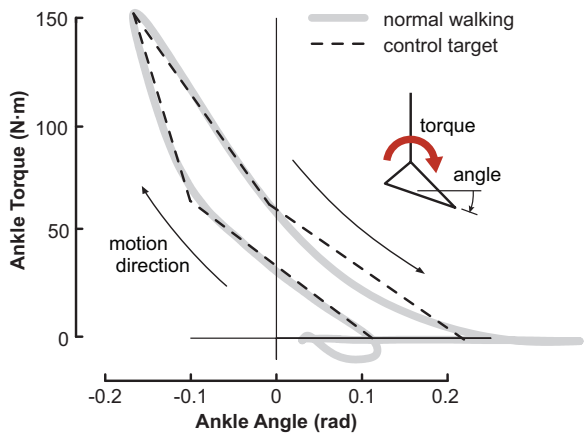

Figure 2.2: Impedance control law used during walking trials. Desired torque is a piecewise linear function of ankle position, with separate dorsiflexion (negative velocity) and plantarflexion (positive velocity) phases. Default curve parameters were selected to roughly match the torque-angle relationship observed for the biological ankle during normal walking. Plantarflexion segments were manipulated across conditions to alter the net positive ankle joint work over the step cycle.

faster than ankle dynamics, and resulted in improved torque tracking. This is mathematically identical to including a derivative term in the desired torque calculation (Eq. 2.2).

We performed a series of walking tests to evaluate torque tracking performance and demonstrate system versatility under realistic operating conditions. One subject with unilateral transtibial amputation (male, 88 kg, 0.92 m greater trochanter height, 44 years) wore the instrumented prosthesis while walking on a treadmill at a speed of 1.25 $\mathrm{m{\cdot}s^{-1}}$. Five conditions were applied, in which the prosthesis followed the impedance control law with condition-specific plantarflexion parameters k and θ_0 corresponding to net work values of roughly -1, 0, 1, 2, and 3 times the normal net work observed during walking. The subject walked for 7 minutes under each condition. Data from the final minute of each trial (about 50 prosthesis steps) were captured and normalized to percent stance (scaled time). For each condition, we calculated RMS error between desired and measured torque and the average and standard deviation of net ankle work per step.

2.3 Results

The instrumented prosthesis had a mass of 0.96 kg (weighed without the tether). The ankle range of motion was 14° (17°) in dorsiflexion and 35° (27°) in plantarflexion when unloaded (maximally loaded). Torque measurement errors were always less than 7.9 N·m, with 3.3 N·m RMS error (or 1.9% of maximum torque, Fig. 2.3A). Peak operating torque was demonstrated to be at least 175 N·m (Fig. 2.3B).

Peak ankle power output was 1036 ± 44 W (mean ± st. dev.), with a corresponding ankle torque of 144 ± 1 N·m and velocity of 7.2 ± 0.3 rad·s^{-1}. At the instant of peak ankle power output, both the series spring and tether were being stretched (absorbing energy) and therefore did not contribute to peak power, e.g., through oscillations. The motor reached velocity saturation during each peak power trial.

We measured closed-loop ankle torque step response rise times (90% of final value) to be 0.062 ± 0.000 s and 0.051 ± 0.001 s for increasing and decreasing steps, respectively (Fig. 2.3B). We calculated closed-loop ankle torque response to have a bandwidth (-3 dB magnitude criteria) of 17.1 ± 0.2 Hz and a phase margin of 23.6 ± 5.3° (Fig. 2.3C). We found that increasing K_p from the tuned value resulted in resonance at about 15 Hz.

In experiments with the anthropomorphic pendulum leg, we characterized tether interference as a rotational stiffness, k_t, and damping, b_t, about the hip joint. We found very low stiffness and damping, with $k_t = 2.6 \pm 0.11$ N·m·rad^{-1} and $b_t = 0.26 \pm 0.023$ N·m·(rad·s^{-1})$^{-1}$. For comparison, the damping coefficient for untethered trials, b_0, attributable to the ball bearing and air resistance, was calculated to be 0.12 ± 0.002 N·m·(rad·s^{-1})$^{-1}$. The calculated tether stiffness and damping would result in an estimated 1 N·m resistance torque at maximum hip flexion and 1 N·m (or 1.9% maximum torque) at maximum hip velocity, under maximum transmission loads (i.e. peak ankle torque, the worst case). See *Appendix A* for detailed calculations.

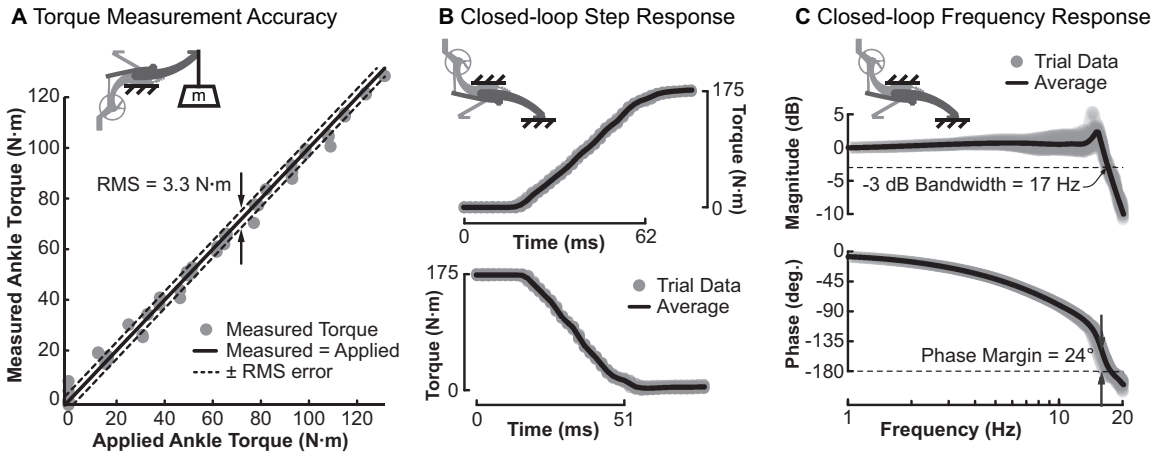

Figure 2.3: Results of benchtop tests of mechatronic performance with the experimental prosthesis emulator. **A** Torque measurement accuracy. We performed tests in which we applied known torques by suspending weights from the toe in a range of known configurations, and found RMS measurement error of 3.3 N·m. **B** Closed-loop torque step response. We fixed the base and toe of the prosthesis and applied 175 N·m step changes in desired torque. Across 10 trials, we measured average 90% rise times of 0.062 s. **C** Bode plot of frequency response under closed-loop torque control. We fixed the base and toe of the prosthesis and applied chirps in desired torque from 56.5 to 133 N·m, then smoothed the resulting curves and averaged over 10 trials. We calculated an average -3 dB bandwidth of 17 Hz.

During walking trials, measured torque closely matched desired torque for a variety of control parameters. In the condition corresponding most closely to normal ankle function, RMS torque error over time was 2.8 N·m, or about 2% of peak torque (Fig. 2.4B), characterizing temporal tracking performance. Torque tracking in joint angle space resulted in net ankle work production of 7.88 ± 1.28 J (Fig. 2.4A). Variability in work production was primarily due to natural variations in subject kinematics from step to step, evidenced by a similar standard deviation in desired work (1.08 J). The average work error was -1.61 J, due predominantly to tracking errors during rapid motions at terminal stance. The standard deviation of error in mechanical work was 0.48 J, or about 6% of the net work, characterizing the consistency of dynamical emulation. In trials with systematic variations in the control law (Fig. 2.5), we measured net ankle joint work values of -4.8 ± 0.7 J, 2.2 ± 0.8 J, 7.9 ± 1.3 J, 14.4 ± 1.9 J, and 20.9 ± 2.6 J, again including variability due to natural variations in human stride kinematics. Average stance duration was 0.58 ± 0.02 s and average stride period was 1.15 ± 0.05 s. These results demonstrate incremental improvements on results from earlier walking trials with an able-bodied subject wearing a simulator boot (Caputo and Collins, 2013).

2.4 Discussion

We developed an experimental platform for use in early-stage assessment of robotic ankle-foot prosthesis design concepts and conducted thorough tests of the system's mechatronic performance. Walking trials demonstrated precise torque tracking, both in time and in joint angle space, and versatile mechanical behavior through systematic changes in high-level control law parameters. Benchtop tests revealed superior performance compared to prior torque-controlled devices, particularly in terms of worn mass and torque bandwidth. These results suggest tethered robotic prosthesis

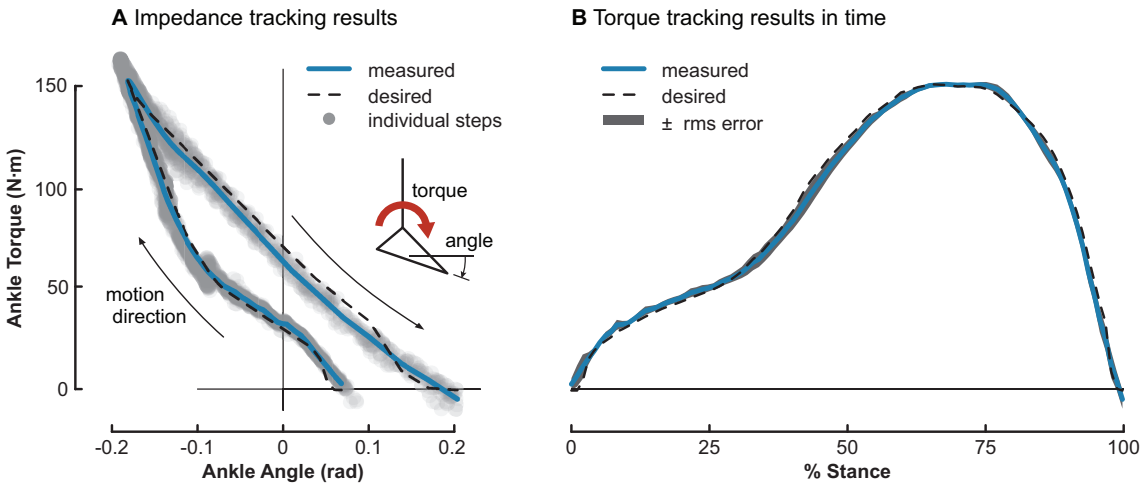

Figure 2.4: Tracking of impedance control law during walking. **A** Measured torque-angle relationship as one subject with unilateral transtibial amputation walked at 1.25 m·s^{-1} for one minute (52 strides). Each step resulted in a similar amount of net joint work, 7.88 ± 1.28 J, visible here as work loop area. **B** Joint torque over the stance period during one minute of walking, normalized to % stance. Average stance duration was 0.58 ± 0.02 s. The average RMS torque error was 2.8 N·m. Note that time-trajectory error appears smaller than error in angle-torque space, while the latter is more meaningful in terms of work production or absorption.

could be used to emulate and evaluate novel functionalities as part of an experimental approach to device development.

Pilot tests of walking with the prosthesis demonstrated the suitability of this experimental tool for emulating a wide variety of functionalities under realistic conditions. We measured very low torque tracking errors in time and in torque-angle space (Fig. 2.4), and found that work production could be systematically and consistently altered across conditions (Fig. 2.5). Prosthesis energy contributions are strongly involved in human performance (Collins and Kuo, 2010; Herr and Grabowski, 2012), and affect key device design requirements, such as motor, battery, or spring size. Consistent work production is challenging in torque-controlled actuator systems, however, because small changes in the timing of torque production can result in significant changes in mechanical power. For instance, the push-off phase of gait occurs very rapidly (Fig. 2.4B, 75-100% stance) and is characterized by a large ankle plantarflex-

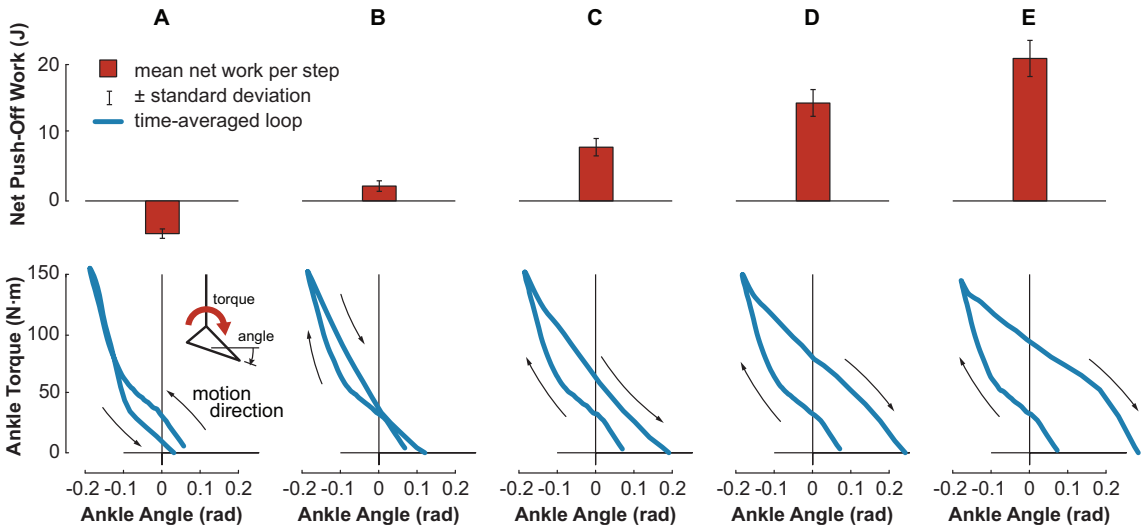

Figure 2.5: Modulating the impedance control law parameters resulted in a variety of work loops during walking, demonstrating system versatility. We measured average net work per step as one subject with unilateral transtibial amputation walked at 1.25 m·s^{-1} for one minute (52 strides) with plantarflexion curve parameters set to five different values (A-E). *Top:* Average net joint work produced (positive) or absorbed (negative) during each step, mean ± st. dev.. *Bottom:* Average impedance relationship for each condition, computed as the time-averaged ankle torque by time-averaged joint angle. We measured energy absorption of -5 J in condition A, similar to the damping effects of conventional dynamic-elastic response prostheses. In condition C, 8 J of work was produced per step, similar to the contribution of ankle plantarflexor muscles during human walking. We measured energy production of 21 J in condition E, which would constitute a very large input from a robotic prosthesis.

ion velocity and a large drop in ankle torque. Leading or lagging the desired torque alters the resulting torque-velocity relationship, causing large changes in power and work. Most developers of lower-limb devices with torque control have not reported these errors. We demonstrated this system's capacity to systematically manipulate the torque-displacement relationship during this phase of gait, leading to a range of overall ankle behaviors consistent with damped springs, passive springs, human ankle musculature, or high-powered robotic devices (Fig. 2.5A-E). These effects were highly repeatable, characterized by small standard deviation in prosthesis work error. Dynamic consistencies were not due to fixed features of the mechanical structure, such as parallel springs or dampers, which would limit versatility. This system can therefore emulate prosthesis designs with a wide range of mechanical features, and can even alter these features online, e.g., to optimize device performance for an individual user. Controlled step-by-step changes could also be used to address a variety of scientific questions, allowing direct measurement of human response to systematic changes in, e.g., dynamic stability (Su and Dingwell, 2007) or altered metabolic cost landscapes (Snaterse et al., 2011; Collins and Jackson, 2013).

The versatility observed during walking trials was achieved by leveraging the laboratory setting to improve mechatronic performance, particularly in terms of worn mass and closed-loop torque bandwidth. High closed-loop torque bandwidth is important for dynamic emulation during periods of rapidly-changing conditions, such as the initial contact of the foot with the ground (Roy et al., 2009), while low mass is needed to avoid affecting natural limb motions or increasing user effort (Burse et al., 1979). The prosthesis end-effector had lower mass than the lightest reported for comparable designs (0.96 kg vs. 1.37 kg in (Gordon et al., 2006)), yet with an order of magnitude greater bandwidth. Benchtop tests demonstrated higher closed-loop torque bandwidth than the highest *open-loop* bandwidth values reported for prior designs (17 Hz vs. 14 Hz in (Au et al., 2007)), but with less than half the mass.

The emulator also exhibited higher peak torque (175 N·m vs. 134 N·m in (Au et al., 2007)) and peak power (1036 W vs. 270 W in (Hitt et al., 2009)) than prior experimental results. These results also compare well with observations of the human ankle and foot. We demonstrated peak torques 50% greater than those observed during human walking (1.6 $N \cdot m \cdot kg^{-1}$ in (Whittle, 1996)), device mass less than a human foot (1.5% body mass in (Winter, 1990)), and torque bandwidth twice that of ankle muscles (6-10 Hz in (Bawa and Stein, 1976; Agarwal and Gottlieb, 1977)). Some other actuators have demonstrated similar torque bandwidth, but with substantially lower peak torque and greater mass (Pratt et al., 2004; Noël et al., 2008; Sulzer et al., 2009; Stienen et al., 2010). While adjustments to the features of other designs could result in improvements in one or another category of performance, overall performance differences seem to be related to qualitative differences in system design.

The primary feature allowing for improved mechatronic performance in this emulator was a Bowden cable tether separating the prosthesis end-effector from driving hardware. This division of components allowed the use of a powerful but heavy gearmotor (1.61 kW, 16.4 kg) without additional mass worn by the user. The tether itself did exert measurable forces on the prosthesis as it moved in the treadmill workspace, but tests with the anthropomorphic pendulum "leg" demonstrated these were minor compared to the forces typically measured in the leg during human locomotion. We estimated that, under worst-case assumptions, the tether would produce effective hip torques of at most 1 N·m, or about 1.9% of the peak torque attributed to hip muscles during normal walking (Winter, 1991). By contrast, an additional 2 kg in end-effector mass due to a smaller actuator (Pratt et al., 2002) would increase peak hip torque by about 18 N·m, or 48% (Browning et al., 2007), and metabolic cost by at least 17% (Browning et al., 2007) or as much as 48% (Adamczyk et al., 2006). The tether does, however, impose a restriction on the size of the workspace, and this limitation must be weighed against such benefits. Overground walking would be enabled by a longer

tether with serpentine routing, but this would result in poorer mechatronic performance due to increased cable compliance and friction. Overground walking might also be achieved by, e.g., mounting the motor on a moving platform, but at a cost of greatly increased system complexity. It is therefore likely impractical to use the device for overground tests, restricting it to use in activities such as treadmill walking, stairmill climbing, and standing. This restriction does not interfere with measurement of common steady-state outcomes such as energy economy or maximum speed, but would interfere with tests of intrinsically overground activities. In a laboratory setting, replacing on-board hardware with a Bowden cable tethered to more capable off-board hardware is therefore advantageous in terms of increased versatility and decreased interference with natural human motions, but restricts the types of activities that can be tested.

For this type of application, Bowden cable tethers appear to have advantages over hydraulic or pneumatic transmissions in terms of mass, bandwidth, and interference with natural motions. Other designs utilizing Bowden cables have demonstrated strong mechatronic performance in their domains, such as ankle perturbation (Andersen and Sinkjaer, 1995), low-interference knee actuation (Sulzer et al., 2009), or upper-extremity force feedback (Schiele et al., 2006). Tethered hydraulic systems have demonstrated high torque bandwidth, but have been limited by the need for heavy cylinders at the end effector (Zoss et al., 2005) and relatively stiff, heavy hoses (Stephens and Atkeson, 2010). Transmission tubes in conventional pneumatic systems are often more flexible, as they are operated at lower pressure, but heavy cylinders are still needed (Noël et al., 2008) and gas compressibility limits bandwidth. Artificial pneumatic muscles can result in low end-effector mass (Gordon et al., 2006), but have more severe bandwidth limitations due to increased resting volume (Versluys et al., 2008, 2009a) and are still heavier than a Bowden cable termination. Like conventional hydraulic or pneumatic systems, Bowden cables can introduce stick-slip

dynamics, due to cable-conduit or piston-cylinder friction, but these can be remedied by measuring torque on the joint side of the transmission (Schiele, 2008). Anecdotally, we found the Vectran cable used here to be quite durable (more than 10^6 cycles), flexible (minimum bending radius ≈ 3 cable radii), and tidy (no oil leaks, for example). We also found Vectran to be more robust than any of the steel wire rope constructions we tried. In tethered applications where mass and torque bandwidth are critical, a synthetic Bowden cable architecture is likely to be advantageous.

Fiberglass leaf springs also contributed to low end-effector mass in this emulator. Physical series elasticity can reduce torque errors at instants of large position disturbance (Pratt and Williamson, 1995) such as the instant when ground contact is initiated at the beginning of the stance phase of gait (Fig. 2.4A). However, these have often been designed as steel coil springs in compression (Pratt et al., 2002, 2004) or torsion (Sulzer et al., 2009), which can result in designs with greater mass than necessary. Fiberglass is eight times lighter than spring steel for a given strain energy capacity ($\rho \cdot E \cdot \sigma_y^{-2}$, see *Appendix B* for derivation). This benefit is offset by spring geometry, since conventional fiberglass manufacturing limits spring shapes to simple beams, which are three times heavier than coil springs for a given energy capacity. Coil springs require additional structures to convert axial spring forces into joint torques, a function implicitly satisfied by the leaf spring itself, and the added mass of these structures can be approximated as that of the leaf spring for purposes of comparison. The use of fiberglass leaf springs can therefore reduce spring mass by about 70% compared to steel coil springs, and saved an estimated 0.19 kg, or 20% end effector mass, in this application.

Numerous aspects of this experimental emulator prototype could be improved to enhance overall performance. System responsiveness (bandwidth) was limited by peak motor velocity, which could be at least doubled for the same motor by the use of a power supply with higher voltage. Torque control could also be improved by the use of

more sophisticated low-level programming than the proportional control scheme used here (Eq. 2.1). The Bowden cable used here exhibited significant stick-slip dynamics, and reducing conduit coefficient of friction could lead to improvements in torque tracking. We explored a tether with explicit joints to reduce friction and interference with leg motions, but found that our prototype increased stiffness, damping, and mass compared to the Bowden cable. Prosthesis end-effector mass could be reduced by elimination of the force-amplifying pulley, which appears not to be necessary following tests of maximum Bowden cable tension. Torque could then be measured using a load cell (Collins and Jackson, 2013) or by instrumenting the toe with strain gauges. We have observed a threefold reduction in torque measurement error using strain gauge sensing in a separate prototype prosthesis end-effector. Improved accuracy was due to the simpler relationship between torque and electrical signal, which was not affected by mechanical elements, such as the chain and sprocket used here, that are difficult to model and may wear over time. Of course, strain gauge sensing is susceptible to electromagnetic interference. Unless an amplifier and A/D converter are mounted to the end-effector, analog wires routed through the tether can lead to increased measurement noise. The mechanical architectures of some end-effectors might also make it inconvenient to incorporate either strain gauges or encoders to measure spring deflection. These factors must be weighed against each other when choosing a torque measurement method. Leaf springs with length-varying cross section could be used to further reduce spring mass. Under higher loads, the Bowden cable itself might exhibit sufficient series compliance, removing the necessity for a spring and allowing incrementally-lighter toe structures. We did not carefully quantify the trade-off between torque bandwidth, which favors stiffer springs, and torque disturbance rejection, which favors more compliant springs, and such an analysis could improve performance while adding to the literature on series elastic actuator design. Refinements to the curvature of the passive heel element and toe pad could allow more

human-like center of pressure progression and greater comfort. Improved geometry could also prevent interference between the series leaf springs and the heel section of conventional shoes, perhaps allowing the device to operate within an unmodified shoe. We are presently developing a higher-load prosthesis end-effector that would accommodate larger subjects, a prosthesis with separate inversion-eversion torque control to impact lateral motions as well as the dominant sagittal motions addressed here, and an orthosis end-effector as a testbed for rehabilitation techniques. There is much work yet to be done in developing a complete set of high-performance prosthesis and exoskeleton emulators.

We have developed an experimental platform that decouples the challenges of mobile device design from the exploration of human-prosthesis interactions. Our results suggest that platforms of this type will enable rigorous human-subject experiments with the flexibility to evaluate a wide range of parameters and behaviors without laborious tuning of overly-specialized devices. This type of technology could become part of a new experiment-centered approach to the development of biomechatronic devices, in which design requirements and trade-offs are established prior to product design tasks such as minimization of mass, envelope and electricity use. Such an approach could be used to address emerging scientific topics in active prosthetics and orthotics, such as dynamic stability, co-adaptation, and identification of human coordination goals.

Acknowledgments

This material is based upon work supported by the National Science Foundation under Grant No. CMMI-1300804. The authors thank Soongeun Cha for contributions to mechanical design, Michiel Plooij for contributions to motor and tether design, John Fulmer and James Dillinger for advice on design for manufacture, Gordon Composites

for donating leaf springs, Myunghee Kim and Rachel Jackson for contributions to emulator control, and Peter Adamczyk for contributions to the emulator concept.

2.5 Appendix A: Tether Characterization

We performed tests with an anthropomorphic pendulum "leg" to characterize the effects of wearing the instrumented prosthesis while tethered to the off-board motor and controller. We performed 10 trials each for two conditions: *tethered*, in which both prosthesis and tether were attached normally and maximum ankle torque (and cable tension) were applied, and *untethered*, in which the prosthesis was attached normally but tether was removed. In each trial, the pendulum was initialized to a starting angle, then allowed to swing freely until an amplitude threshold was crossed (evaluated at the apex of pendulum swing). The trial duration, T, and number of cycles, n, were recorded. We modeled the effects of the tether on the pendulum as a rotational stiffness about the hinge, k_t, and a rotational damping component, b_t. The equations of motion for the resulting system, with the small angle approximation, were:

$$I\ddot{\theta} + (b_0 + b_t) \cdot \dot{\theta} + (m \cdot g \cdot c + k_t) \cdot \theta = 0 \tag{2.4}$$

where I is the mass moment of inertia of the pendulum about the hinge, θ, $\dot{\theta}$, $\ddot{\theta}$ are the angle, velocity, and acceleration of the pendulum respectively, b_0 is the damping coefficient in the untethered condition, m is the pendulum mass, g is the gravitational constant, and c is the distance from the hinge to the center of mass of the pendulum.

Assuming the pendulum is initially at rest ($\dot{\theta}(0) = 0$) and at a prescribed angle ($\theta(0) = \theta_0$), θ can be described as a function of time t:

$$\theta(t) = \theta_0 \cdot e^{-a \cdot t} \cdot \cos(\omega \cdot t) + \frac{a}{\omega} \cdot \theta_0 \cdot e^{-a \cdot t} \cdot \sin(\omega \cdot t) \tag{2.5}$$

Where a is the decay constant and $\omega = 2{\cdot}\pi{\cdot}n{\cdot}T^{-1}$ is the oscillation frequency. Solving for the poles of the system described by Eq. 2.4 yields:

$$a = \frac{b_0 + b_t}{2 \cdot I} \tag{2.6}$$

and

$$\omega = \sqrt{\frac{m{\cdot}g{\cdot}c + k_t}{I} - \frac{(b_0 + b_t)^2}{4 \cdot I^2}} \tag{2.7}$$

Evaluating Eq. 2.5 at the moment when the oscillation amplitude reaches the lower threshold ($\theta(T) = \theta_f$, where θ_f is the angle at the end of the trial, and $\cos(\omega \cdot T) = 1$), and manipulating appropriately, we have the following equation relating damping coefficients to experimental measurements of decay time:

$$b_0 + b_t = -\frac{2 \cdot I}{T} \cdot \ln\left(\frac{\theta_f}{\theta_0}\right) \tag{2.8}$$

Substituting Eq. 2.8 into Eq. 2.7, setting $k_t = 0$, and rearranging, we have the following relationship between pendulum mass moment of inertia and experimental measurements of decay time and oscillation frequency for the untethered condition:

$$I = m{\cdot}g{\cdot}c \cdot \left(\omega_u^2 + \frac{\ln\left(\frac{\theta_f}{\theta_0}\right)^2}{T^2}\right)^{-1} \tag{2.9}$$

where ω_u and T_u are the frequency and decay period, respectively, for the untethered condition. Finally, solving Eq. 2.7, we have the following relationship between tether stiffness and experimental measurements:

$$k_t = I \cdot \omega^2 + \frac{(b_0 + b_t)^2}{4 \cdot I} - m{\cdot}g{\cdot}c \tag{2.10}$$

We determined m to be 12.0 kg by weighing the pendulum and c to be 0.34 m by

balancing the pendulum horizontally on a string. From Eq. 2.9, we calculated I to be 2.40 N·m^2. We used Eq. 2.8, with $b_t = 0$, to calculate b_0 from untethered trials. We then used Eq. 2.8 and Eq. 2.10 to determine b_t and k_t from tethered data.

2.6 Appendix B:

Spring Mass, Material, and Geometry

The theoretical minimum mass of a spring that meets design requirements for peak load and stiffness (or energy storage) can often be derived in terms of material properties and a geometric constant. We performed calculations for the optimal mass of leaf and coil springs using simple models from classical mechanics. Let us first consider the case of a prismatic member in tension, for which we have the following basic mechanics formulae:

$$\sigma = \frac{F}{A} = E \cdot \epsilon, \quad \Delta x = l \cdot \epsilon, \quad m = \rho \cdot A \cdot l \tag{2.11}$$

where σ is the (uniform) stress in the material, F is the force on the spring, A is the cross-sectional area of the spring, E is the elastic modulus of the material, ϵ is the strain of the material, Δx is the displacement of the spring, l is the length of the spring, m is the spring mass, and ρ is the density of the material.

In designing a spring, we can set geometric parameters l and A such that when the maximum force, F_m, is applied, a desired maximum displacement, Δx_m, and maximum allowable stress, σ_a (typically the failure stress divided by the factor of safety), are simultaneously achieved:

$$A = \frac{F_m}{\sigma_a}, \quad l = \frac{\Delta x_m}{\epsilon_m} = \frac{\Delta x_m \cdot E}{\sigma_a}, \quad and \quad m = \frac{\rho \cdot E}{\sigma_a^2} \cdot F_m \cdot \Delta x_m \tag{2.12}$$

This value of m represents the minimum spring mass required to obtain the desired

combination of peak load and deflection. Note that this equation for spring mass is independent from geometric parameters. Many spring shapes result in minimum mass relationships of the same form, expressed more generally as:

$$m = 2 \cdot C_g \cdot \frac{\rho \cdot E}{\sigma_a^2} \cdot U \tag{2.13}$$

where C_g is a constant arising from spring geometry and $U = {}^1\!/_2 F_m \cdot \Delta x_m$ is the maximum energy stored by the spring. For a prismatic member in tension, $C_g = 1$. This is the lowest possible value for C_g, corresponding to the case in which all spring material is maximally strained at peak load. For all other spring shapes, some material will be sub-maximally strained, and store less energy than possible, but will still contribute equally to spring mass. Other shapes are still useful, however, since the solution to Eq. 2.11 often leads to small values for A and large values for l, which are inconvenient given practical design constraints.

For leaf springs, we begin with the following equations for bending in a rectangular cantilevered beam:

$$\sigma_m = \frac{M \cdot y}{I}, \quad \Delta x = \frac{F \cdot l^3}{3 \cdot E \cdot I}, \quad I = \frac{1}{12} \cdot b \cdot h^3, \quad m = \rho \cdot b \cdot h \cdot l \tag{2.14}$$

where σ_m is the maximum stress, $M = F \cdot l$ is the moment at the spring support, $y = {}^1\!/_2 \cdot h$ is the maximum distance from the centroid, I is cross-sectional area moment of inertia, b is spring width, and h is spring height. By eliminating the geometric parameters b, h, and l, we have an equation of the same form as Eq. 2.13, with

$C_g = 9$:

$$\begin{aligned}
\sigma_a &= \frac{6 \cdot M}{b \cdot h^2} \Rightarrow b = \frac{6 \cdot F_m \cdot l}{\sigma_a \cdot h^2} \\
\Delta x_m &= \frac{4 \cdot F_m \cdot l^3}{E \cdot b \cdot h^3} \Rightarrow h = \frac{2 \cdot l^2 \cdot \sigma_a}{3 \cdot E \cdot \Delta x_m} \\
m &= 9 \cdot \frac{\rho \cdot E}{\sigma_a^2} \cdot F_m \cdot \Delta x_m
\end{aligned} \tag{2.15}$$

For coil springs, we can model the wire as a rod in torsion:

$$\tau_m = \frac{T \cdot r}{J}, \quad \Delta\theta = \frac{T \cdot l}{G \cdot J}, \quad J = \frac{1}{32} \cdot \pi \cdot r^4, \quad m = \rho \cdot \pi \cdot r^2 \cdot l \tag{2.16}$$

where τ_m is the maximum shear stress, T is peak torsion, r is the wire radius, J is cross-sectional polar moment of inertia, $\Delta\theta$ is peak wire rotation, G is the shear modulus, and l is the uncoiled wire length. For steel, we can approximate $\tau_m \approx 2 \cdot \sigma_m$ and $E \approx {}^8\!/_3 \cdot G$ (Budynas and Nisbett, 2011). By eliminating the geometric parameters r and l, and noting $U = {}^1\!/_2 \cdot T \cdot \Delta\theta$, we have an equation of the same form as Eq. 2.13, with $C_g = 3$:

$$\begin{aligned}
2\sigma_a &= \frac{32 T_m}{\pi r^3} \Rightarrow r^3 = \frac{2^4 T_m}{\pi \sigma_a} \\
\Delta\theta_m &= \frac{8 \cdot 32 T_m l}{3\pi E r^4} \Rightarrow l = \frac{3\pi E r^4 \Delta\theta_m}{2^8 T_m} \\
m &= \frac{3\pi^2 \rho E r^6 \Delta\theta_m}{2^8 T_m} = 3 \frac{\rho E}{\sigma_a^2} T_m \Delta\theta_m
\end{aligned} \tag{2.17}$$

Coil springs can therefore be 3 times lighter than constant cross-section leaf springs, considering geometric effects alone. However, conventional manufacturing techniques limit the material types that can be formed into useful helical spring shapes.

For any shape that can be expressed in the form of Eq. 2.13, the ideal spring material will minimize $\rho \cdot E \cdot \sigma_y^{-2}$. The unidirectional fiberglass material used in the series leaf springs reported here has $\rho = 1.9 \times 10^3$ kg·m^{-3}, $E = 3.8 \times 10^{10}$ kg·m^{-1}·s^{-2},

and $\sigma_u = 1.1\times10^9$ kg·m^{-1}·s^{-2} (Composites, 2012), or $\rho{\cdot}E{\cdot}\sigma_y^{-2} = 6.4\times10^{-5}$. Music wire, the best of conventional spring steels, has $\rho = 7.8\times10^3$ kg·m^{-3}, $E = 1.9\times10^{11}$ kg·m^{-1}·s^{-2}, and $\sigma_u = 1.7\times10^9$ kg·m^{-1}·s^{-2} (for $r = 0.25$ in. (Budynas and Nisbett, 2011) pp. 525), or $\rho{\cdot}E{\cdot}\sigma_y^{-2} = 5.2\times10^{-4}$. Springs optimized for mass and having the same geometry will therefore be about 8 times lighter if manufactured from this type of fiberglass than if manufactured from the best spring steel.

2.7 Supporting Materials

A bill of materials, CAD files, control software code, and more supporting materials can be found on the Publications section of the Carnegie Mellon University Experimental Biomechatronics Lab webpage: biomechatronics.cit.cmu.edu.

2.8 Additional discussion of future work

2.8.1 Torque tracking

The prosthetic ankle torque controller is practically limited in its ability to track rapidly changing desired torques. Over the course of the experiments I have conducted, this has become apparent when emulating very high stiffness behaviors (e.g. Chapter 4, SACH mode) and behaviors with large quantities of net work (e.g. Chapter 4, HIPOW mode). I demonstrate in Chapter 4 that an iterative learning controller can effectively eliminate steady-state torque tracking errors (inspired by (Zhang et al., 2015)), proving that the selected combination of electric motor and gearhead is sufficient for the task. While the iterative learning control approach is highly effective at reducing torque tracking errors, it requires many consecutive steady-state walking steps to stabilize, and therefore does not respond ideally to variability in cadence that is ubiquitous during normal daily life activities. Though this is not an issue for the

steady-state treadmill walking experiments described in this thesis, one can imagine future experiments including, e.g., push disturbances applied to the subject or an uneven treadmill surface, where the utility of such a control approach would be limited. Given the simplicity of the feedback controller (proportional control only), it is likely that more sophisticated feedback control techniques, even very simple improvements such as implementing a derivative term, could significantly improve torque tracking performance. It might also be beneficial to tune the stiffness of the Bowden cable transmission to suit the desired torque vs. angle relationship by optimizing motor dynamics to minimize drive current. Performing a rigorous optimization would be a valuable contribution to the field of biomechatronics as it is unclear, in general, how to optimally select series spring stiffness when developing a series elastic actuator. A simple empirical test of several different transmission stiffnesses could significantly improve torque tracking performance. Transmission friction has a deleterious effect on torque control, effectively lowering the ceiling on the amount of current available to control ankle torque. These frictional effects are complex and nonlinear, therefore hard to measure and model, and so ultimately it is unlikely that model-based friction compensation will effectively remove their effects. Reducing the degree of bend in the transmission would reduce the frictional forces acting on the cable (according to $T_{pros} = T_{motor} * e^{-\theta_{bend}}$). Some transmission bend is unavoidable given normal leg swing kinematics and users' drift on the treadmill, but it is conceivable that the motor could be repositioned to avoid the permanent 90° bend in the transmission where it transitions from horizontal to the direction along the leg. If the Bowden cable were to originate at a structure which floated above the users hip, transmission bend would be limited to that which is caused by hip and knee rotations. This introduces other practical challenges, but promises to reduce transmission losses by nearly 80%. Further experimentation with Bowden conduit lining materials and lubrication may also improve upon the off-the-shelf components used here.

2.8.2 State transitions

The implemented high-level control strategy includes three distinct states (stance dorsiflexion, stance plantarflexion, and swing) which requires discrete state transitions over the course of a walking stride. This implementation, though straightforward and versatile, comes with several limitations. To time these transitions optimally requires individual subject tuning at the beginning of each experimental session. Since this is impractical, and since sensor noise makes transition detection a challenge in general, transition thresholds are set conservatively such that the controller reliably moves through the states but transitions then tend to occur later than ideal. This is particularly problematic for two of the state transitions.

First, once the swing controller achieves a target ankle angle, it switches to control motor velocity at zero. This is done because once the user makes ground contact they initially experience a comfortably compliant behavior prior to the switch to torque control. If the controller were to instead maintain a fixed ankle angle, initial ground contact would be uncomfortably stiff and give rise to large plantarflexion torques. If the controller were to simply switch to torque control during swing, sensor noise causes vibrations and positional drift. So instead the controller switches to torque control once it becomes evident that the foot is on the ground, based on reaching a positive torque threshold. Depending on the nature of the desired torque vs. angle relationship, given a fixed series compliance, the torques experienced by the user in the time before the threshold is reached could be considerably different from the desired torques. The passive compliance of the emulator system was selected to emulate the compliance of the biological ankle, and for most of the behaviors that users have reported being comfortable this is not an issue. But for very stiff behaviors (e.g. Chapter 4, SACH mode) this passive response results in a large tracking error which the controller must quickly correct upon switching to torque control mode, and

makes tracking these stiff behaviors more challenging than theoretically required. It might be possible to lower this threshold considerably by using improved sensors that exhibited better signal/noise ratio and linearity–perhaps, high resolution digital encoders and/or strain based sensing with onboard A/D conversion.

Second, while the ankle is dorsiflexing during stance, the controller monitors ankle velocity and transitions to a plantarflexion control state once the ankle velocity changes sign. This transition also has a positive threshold on it, because of sensor non-idealities. This forces the transition to plantarflexion to be late, so for the time before the transition while the toe is plantarflexing but still in the dorsiflexion state, the provided torque vs. angle behavior is not as it should be according to the reference data. This is particularly a problem for behaviors where the plantarflexion behavior is considerably different from the dorsiflexion behavior, which is not ideal for, e.g., accurate device emulation (Chapter 4). Again, improved sensing would improve this situation, but it is possible that this state transition could be eliminated altogether. This was achieved in the prosthesis timing experiment by controlling push-off torque as a function of time (Malcolm et al., 2015), which is guaranteed to increase monotonically over the course of the step. Such a control strategy is unfortunately not very robust to changes in cadence, but perhaps some other monotonically increasing state, such as center of mass position, could be fed back to similar effect.

2.8.3 Alternative high level control architectures

The high-level control strategy of controlling ankle torque as a function of ankle angle proved effective for the purposes of the experiments described in Chapters 2–4, but alternative control strategies could ultimately provide users with a greater benefit. For example, proportional EMG (Huang et al., 2014) or positive force feedback (Eilenberg et al., 2010) control might accommodate changes in, e.g., users' cadence more simply and effectively. Alternative structures are straightforward to implement given the

versatility of our approach, and I am keenly interested in implementing an array of candidate controllers and optimizing their parameters as in Chapter 5 in order to compare the pros and cons of various control architectures (as in Chapter 4).

Chapter 3

Ankle push-off work magnitude

In this first experiment with the ankle-foot prosthesis emulator we investigated the effects of prosthetic ankle push-off work on simulated amputee walking biomechanics. We performed a 1D parameter sweep that included a wide range of different torque vs. angle relationships during push-off, performing from 0.5 to 2 times normal levels of push-off work, while maintaining consistent behavior during ankle dorsiflexion. We found that increasing prosthetic ankle push-off work sharply decreased the users' metabolic energy consumption, with diminishing returns as push-off approached levels twice that of the biological ankle joint. Through inverse dynamics analysis we observed that the metabolic energy savings appeared to derive from a reduction in prosthesis-side hip work during ankle push-off. These results contrast with the predictions of simple dynamic walking models which predict that energy savings would primarily arise from reduced energy dissipation during leading-limb collision (Kuo, 2001; Kuo and Donelan, 2010).

We have since followed-up this experiment with studies investigating the same relationships for amputee subjects (Quesada et al., 2015) and the relationship between the timing of push-off and walking performance (Malcolm et al., 2015). Similar studies at at Carnegie Mellon have since considered the effects of step-to-step modulation of push-off work magnitude (Kim and Collins, 2015), the effects of ankle-foot orthosis stiffness and work on walking performance (Jackson and Collins, 2015), and the effects of ankle-foot prosthesis inversion/eversion stiffness on walking performance.

Caputo, J. M., Collins, S. H. (2014) Prosthetic ankle push-off work reduces metabolic rate but not collision work in non-amputee walking. *Nature Scientific Reports*, **4**:7213.

Preliminary versions of this work were presented at:

Caputo, J. M., Collins, S. H. (2014) The effect of ankle-foot prosthesis push-off work on walking kinetics and overall effort. Poster presentation at *7th World Congress of Biomechanics*.

Caputo, J. M., Collins, S. H. (2013) Quantifying the Relationship Between Prosthesis Work and Metabolic Rate. Podium presentation at *Dynamic Walking*.

Abstract

Individuals with unilateral below-knee amputation expend more energy than non-amputees during walking and exhibit reduced push-off work and increased hip work in the affected limb. Simple dynamic models of walking suggest a possible solution, predicting that increasing prosthetic ankle push-off should decrease leading limb collision, thereby reducing overall energy requirements. We conducted a rigorous experimental test of this idea wherein ankle-foot prosthesis push-off work was incrementally varied in isolation from one-half to two-times normal levels while subjects with simulated amputation walked on a treadmill at 1.25 $m \cdot s^{-1}$. Increased prosthesis push-off significantly reduced metabolic energy expenditure, with a 14% reduction at maximum prosthesis work. In contrast to model predictions, however, collision losses were unchanged, while hip work during swing initiation was decreased. This suggests that powered ankle push-off reduces walking effort primarily through other mechanisms, such as assisting leg swing, which would be better understood using more complete neuromuscular models.

3.1 Introduction

Unilateral below-knee amputation is an increasingly common lower limb disability (Ziegler-Graham et al., 2008) that reduces mobility and adversely affects quality of life (Zidarov et al., 2009). Individuals with amputation expend more energy to walk (Waters and Mulroy, 1999; Houdijk et al., 2009) and experience increased loading and injury of the intact limb (Gailey et al., 2008). Next-generation robotic prostheses are expected to improve these aspects of performance for amputees (Goldfarb et al., 2013).

The increased effort required to walk with conventional prosthetic limbs may be related to observed biomechanical changes at the hip and ankle joints. During the double-support phase of healthy human walking, the trailing limb generates positive

power against the body's center of mass while the leading limb absorbs energy, referred to as push-off and collision, respectively (Donelan et al., 2002; Kuo et al., 2005). Joint power (Winter, 1991) and muscle contraction effort (Requião et al., 2005) are considerably higher in the ankle than elsewhere in the legs, with most work occurring during push-off. Below-knee amputees exhibit reduced push-off in the affected limb, considering either the ankle (Winter and Sienko, 1988; Silverman et al., 2008; Zelik et al., 2011) or the whole limb (Houdijk et al., 2009; Zelik et al., 2011), presumably as a result of the passive nature of conventional prosthetic feet (Geil, 2001). Individuals with amputation have also exhibited increased hip power on the affected (Winter and Sienko, 1988; Silverman et al., 2008; Zelik et al., 2011) and intact (Silverman et al., 2008) limbs during early (Winter and Sienko, 1988; Silverman et al., 2008) and late (Zelik et al., 2011) stance, along with increased affected-limb hip muscle activation (Fey et al., 2010) during early stance. This change in hip coordination is commonly thought to be a compensation for reduced push-off from the prosthetic ankle (Winter and Sienko, 1988; Silverman et al., 2008; Fey et al., 2010). Similarly, individuals with ankle fixation exhibit reduced push-off (Doets et al., 2009; Wutzke et al., 2012) and increased hip power in early stance (Wutzke et al., 2012; Vanderpool et al., 2008), usually accompanied by increased energy consumption (Doets et al., 2009; Wutzke et al., 2012) (although not always (Vanderpool et al., 2008)). Subjects with ankle push-off assistance from an exoskeleton, by contrast, have demonstrated decreased energy consumption (Malcolm et al., 2013). These observations suggest a trade-off between ankle and hip work (Lewis and Ferris, 2008), leading to the hypothesis that a prosthesis which provides increased positive ankle power will decrease positive hip power, thereby reducing energy consumption.

It is not immediately clear, however, why trading ankle work for hip work would adversely effect walking efficiency. Simple dynamic models of walking, widely used in locomotion research, suggest that hip powering strategies should be less efficient

than push-off powering strategies because of their disparate effects on collision losses (Donelan et al., 2002; Kuo et al., 2005; Ruina et al., 2005; Kuo, 2001; Kuo and Donelan, 2010). In these very simple mathematical models, trailing limb push-off mitigates leading limb collision, reducing overall mechanical energy requirements, while work done at the hip does not. This concept has been used to explain observed coordination patterns in humans (Ruina et al., 2005; Kuo, 2001; Gates et al., 2007; Adamczyk et al., 2006; Gordon et al., 2009; Srinivasan and Ruina, 2006) and animals (Ruina et al., 2005; Ren and Hutchinson, 2008; Bertram and Gutmann, 2009; Usherwood et al., 2007), and to design walking robots (Collins et al., 2005; Hobbelen and Wisse, 2008; Byl and Tedrake, 2008; Sreenath et al., 2010; Bhounsule, 2012), robotic exoskeletons (Sawicki and Ferris, 2009; Malcolm et al., 2013), and robotic prostheses (Versluys et al., 2009b; Collins and Kuo, 2010; Zelik et al., 2011; Au and Herr, 2008; Eilenberg et al., 2010; Herr and Grabowski, 2012).

The relationship between push-off and collision in these simple models has also been used to explain increased energy cost in amputees. Reduced push-off in the affected limb, presumably the result of reduced positive work at the prosthetic ankle (Wutzke et al., 2012; Doets et al., 2009), has been implicated as the cause of the observed increases in the simultaneous intact-limb collision (Houdijk et al., 2009; Zelik et al., 2011). This has led to the hypothesis that a prosthesis which increases positive ankle power during push-off will decrease the energy dissipated during collision of the contralateral limb, thereby reducing overall mechanical work requirements and metabolic energy consumption (Kuo and Donelan, 2010; Soo and Donelan, 2012).

These simple-model predictions have not yet been validated in a well-controlled experiment, and a mixture of supporting and opposing observations can be made from related studies. Some ankle fixation experiments have demonstrated increased leading limb collision losses (Doets et al., 2009), while others have not (Vanderpool et al., 2008). Passive-elastic prostheses with higher rates of energy return can increase push-

off somewhat (Barr et al., 1992; Zmitrewicz et al., 2006), but have not reduced collision losses (Zmitrewicz et al., 2006) or metabolic rate (Hafner et al., 2002; Barth et al., 1992; Torburn et al., 1995) (with few exceptions (Casillas et al., 1995; Grabowski et al., 2010)). Several robotic ankle-foot prostheses that provide ankle push-off work at levels similar to that of a healthy biological ankle have been developed (Sup et al., 2008; Hitt et al., 2009; Versluys et al., 2009b; Cherelle et al., 2013; Au and Herr, 2008; Eilenberg et al., 2010; Herr and Grabowski, 2012; Collins and Kuo, 2010; Zelik et al., 2011), but only one of these has demonstrated improved metabolic cost when compared to conventional devices (Herr and Grabowski, 2012). Such comparisons have been complicated by the many differences between devices other than ankle push-off work, such as mass, geometry, stiffness and control, any of which could be responsible for observed differences in energy use. It remains unclear whether simple model predictions about the relationship between ankle push-off, collision losses, overall mechanical work and metabolic energy cost are relevant to the design of robotic prostheses.

The aim of this study was to isolate and characterize the relationship between ankle push-off work, metabolic energy cost, and underlying mechanics in human locomotion. We performed an experiment in which ankle push-off work was varied over a wide range using a high-performance ankle-foot prosthesis emulator (Caputo and Collins, 2014a). Simulated amputee subjects wearing the prosthesis using an immobilizer boot walked at a fixed speed on a treadmill. We hypothesized that increased prosthesis push-off would reduce contralateral-limb collision, thereby reducing both overall mechanical energy use and the portion borne by the human user, leading to a reduction in metabolic energy consumption. We hypothesized that the proximate cause of reduced metabolic rate would be reduced positive hip work during stance. We expect the quantitative relationships determined in this study to provide new, well-controlled tests of several prevailing theories of the energetics of human walking

while informing the design of improved prosthetic devices.

3.2 Methods

We used an experimental ankle-foot prosthesis emulator to systematically vary ankle push-off in isolation from other prosthesis features. We controlled push-off work by setting a desired relationship between joint torque and joint angle during the push-off phase. We applied conditions with prosthesis push-off work ranging from 50% to 200% of the push-off work observed during normal walking. Ten subjects with simulated amputation completed the protocol while wearing the prosthesis via an immobilizer boot. We compared prosthesis mechanics, metabolic energy consumption, center of mass mechanics and joint mechanics across conditions.

3.2.1 Universal ankle-foot prosthesis emulator

Precise regulation of push-off work across conditions was enabled by an experimental ankle-foot prosthesis emulator (Caputo and Collins, 2014a). The emulator provided an exceptionally broad range of push-off work, from –5 to 30 J of net work per step. Adjustments were made electronically, with all mechanical features of the prosthesis (such as size, mass, heel stiffness, and alignment) unchanged across conditions. Mechanical power and computer control of the prosthesis were generated off-board and provided via a tether as subjects walked on a treadmill (Fig. 3.1). The tether was supported near the subject to minimize interference with natural motions. Participants wore the ankle-foot prosthesis on their right leg via a simulator boot which immobilized the ankle. The prosthesis was attached beneath the biological limb along the centerline of the tibia. To keep leg lengths equal, a lift shoe with a rocker bottom was worn on the other leg (Fig. 3.1). The mass of the prosthesis, simulator boot, and lift shoe were 1.2 kg, 1.9 kg, and 1.0 kg, respectively. The length of the prosthetic

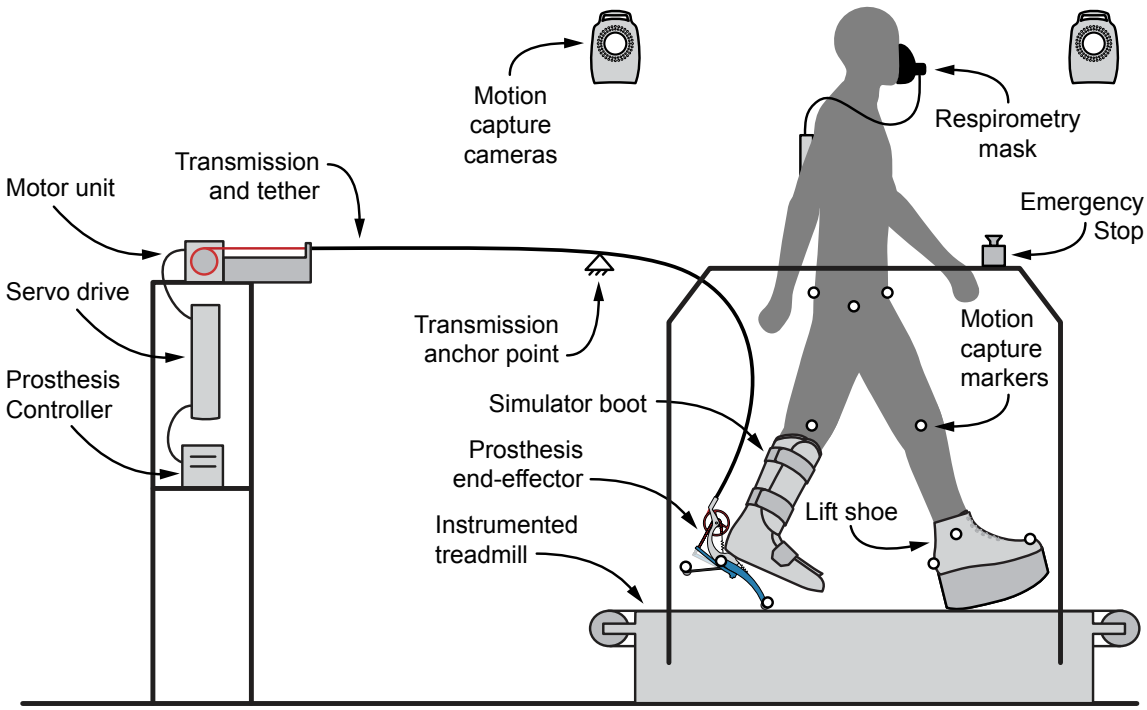

Figure 3.1: Schematic of the experimental setup. The ankle-foot prosthesis emulator comprised a powerful off-board motor and controller, a flexible tether transmitting mechanical power and sensor signals, and a lightweight instrumented ankle-foot prosthesis. Measures of prosthesis function were made using onboard sensors. Human subject mechanics and energetics were calculated from data collected using a reflective-marker motion capture system, a split-belt treadmill with force sensing, and a portable respirometry system.

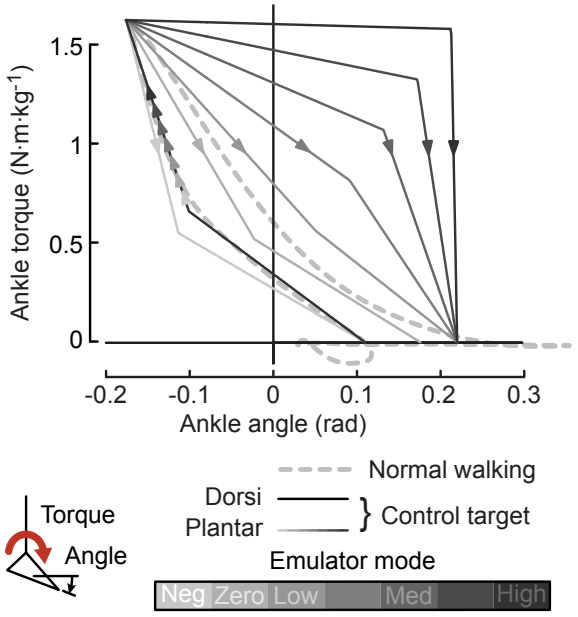

Figure 3.2: Impedance control law used during walking trials. Desired torque is a piecewise linear function of ankle position, with separate dorsiflexion (negative velocity) and plantarflexion (positive velocity) phases. Gray lines indicate programmed trajectories for each condition, with darker lines corresponding to conditions with higher prosthesis push-off work. Plantarflexion segments were manipulated across conditions to alter the net positive ankle joint work over the step cycle. Dashed line indicates biological ankle joint power measured in (Collins and Kuo, 2010).

foot was 0.22 m, the heel of the prosthesis was 0.070 m to the rear of the centerline, and the total added leg length was 0.13 m.

Prosthetic ankle joint work was regulated using impedance control in two phases. In each phase, joint torque was controlled as a function of ankle angle (Fig. 3.2). The Dorsiflexion phase began at heel contact and lasted until the velocity of the ankle joint reversed direction, usually around 80% of the stance period, when the prosthesis switched into the Plantarflexion phase. Dorsiflexion phase behavior was constant across conditions, while the torque profile in the Plantarflexion phase was adjusted. This changed work production during ankle push-off without altering other aspects of prosthesis function. Nominal parameters were selected to emulate the behavior of the biological ankle during normal walking at the same speed (Collins and Kuo, 2010). Ankle push-off work was varied across the widest range possible

without altering the controller or damaging the system.

3.2.2 Experimental protocol

We tested seven conditions across a wide range of net push-off work. Net work, defined as the difference between positive work during push-off and negative work during the rest of the stance period, was linearly increased from -27% to 490% of the value for normal walking (from (Collins and Kuo, 2010)) in conditions referred to as Negative Low, Zero, Low, Medium Low, Medium, Medium High, and High, respectively (Fig. 3.2). Subjects also completed a Quiet Standing trial and a Normal Walking trial in street shoes. Treadmill speed was set to 1.25 $\mathrm{m} \cdot \mathrm{s}^{-1}$. Subjects walked for 7 minutes to reach steady state. To allow adequate time for acclimation, subjects completed the entire protocol three times with one day of rest between each collection. On each day, all prosthesis conditions were presented in random order. Reported measures are from the final collection.

Ten healthy able-bodied male adults participated in the study (N = 10; age = 28 ± 4.4 yrs; body mass = 78 ± 7.7 kg; leg length = 0.87 ± 0.056 m, greater trochanter to lateral malleolus). Sample size was selected according to standard practice for locomotion research. All subjects completed all conditions except Medium Low ($N = 9$) and High ($N = 6$). Data for Medium Low were not obtained for one subject due to hardware failure. The final six subjects were presented with the High condition, which was enabled by hardware improvements midway through the study. This study was approved by the Carnegie Mellon Institutional Review Board, was carried out in accordance with the approved guidelines, and all subjects provided written informed consent. Subjects were blinded to all prosthesis conditions, but experimenter blinding was not possible while operating the control system.

3.2.3 Data analysis

Prosthesis power and work were calculated from on-board sensor measurements. Joint position and torque were measured using encoders and displacement of a series spring (calibrated as described in (Caputo and Collins, 2014a)). Ankle velocity was obtained by differentiating ankle position and applying a 3$^{\text{rd}}$ order low-pass filter with a cutoff frequency of 50 Hz. Prosthetic ankle power was computed as the product of ankle velocity and ankle torque, and ankle work was computed as the integral of ankle power in time. Positive and negative work were considered separately, and their sum was defined as net prosthesis work. Prosthesis work is presented as stride-averaged work rate, or work divided by stride time, to allow direct comparisons with metabolic rate and to account for differences in stride time across subjects.

Metabolic energy consumption was estimated using indirect calorimetry. Gas concentrations and flow rates were measured using a commercial respirometry system. Breath-by-breath data were averaged across the last three minutes of each trial, when subjects had reached steady state, and metabolic energy consumption was then calculated using a standard formula (Brockway, 1987). For each subject, we determined the exponential function of the form $P_m = c_1 + c_2 \cdot e^{-c_3 \cdot P_p}$ that fit the relationship between metabolic rate, P_m, and net prosthesis power, P_p, with least squared error. We defined change in metabolic rate as metabolic rate minus the value of the best fit function corresponding to zero net prosthesis work rate, or $P_m - (c_1 + c_2)$. Change in metabolic rate therefore captured the effects of adding active power to a conventional passive prosthesis. We defined net metabolic rate as metabolic rate minus the metabolic rate during the Quiet Standing trial.

We estimated mechanical power at each joint in the lower limbs using three-dimensional inverse dynamics analysis. The positions of bony landmarks on the legs, and analogous features on the robotic prosthesis, were tracked using a commercial

reflective marker motion capture system. Time derivatives of position trajectories were calculated and filtered with a 3rd order low-pass filter with a cutoff frequency of 7.5 Hz. Body segment mass properties were estimated from anthropometric regression equations (Drillis et al., 1964; de Leva, 1996), and mass properties of the simulator boot, lift shoe, and prosthesis were determined by weighing and suspension in different configurations. Joint torques were calculated as the torques required to cause the observed segment accelerations (Winter, 1990). We calculated positive or negative joint work over periods of interest as the time integral of joint power over those periods. Joint work is presented as stride-averaged work rate, or work divided by stride time, to allow direct comparisons with metabolic rate and to account for differences in stride time across subjects.

We estimated work done on the center of mass by the legs using the individual limbs method. Ground reaction forces were measured using a commercial instrumented split-belt treadmill and passed through a 3rd order low-pass filter with a cutoff frequency of 7.5 Hz. Center of mass velocity was calculated as the time integral of measured force divided by body mass, and center of mass power was calculated as the dot product of center of mass velocity and ground reaction force for each limb. The biological component of center of mass power on the prosthesis side was calculated as whole-limb center of mass power minus prosthetic ankle joint power as calculated by inverse dynamics analysis (so as to include contributions of both the actively-controlled ankle joint and the passive heel). We calculated positive or negative center of mass work as the integral of center of mass power over sequential periods of stance known as collision, rebound, preload and push-off (Kuo et al., 2005). Center of mass work is presented as stride-averaged work rate, or work divided by stride time, to allow direct comparisons with metabolic rate and to account for differences in stride time across subjects. Peak ground reaction force and center of mass velocity during the double-support period were also calculated.

We performed statistical comparisons of metabolic rate, center of mass mechanics and joint mechanics across conditions. Center of mass and joint trajectories were divided into strides, normalized in time as percent stride, and averaged across strides. Scalar values, such as work and peak force, were calculated on individual subjects' average trajectories and then averaged across subjects, so as to avoid artifacts from smoothing. Variability is represented as inter-subject standard deviation. All measures were normalized to subject body mass and averaged across subjects. Analysis of variance was used to determine the significance of each outcome. For each significant outcome, a paired t-test was then applied to compare conditions. We compared each condition to the Zero work condition, thereby capturing effects of adding or removing power from a conventional passive prosthesis. We then applied a Sidak-Holm step-down (Glantz, 2011) and used a significance level of $P \leq 0.05$.

3.3 Results

With increasing prosthetic ankle push-off work, whole-limb push-off work on the prosthesis side increased and metabolic energy consumption decreased. Energy losses at collision were unchanged, while both contralateral-limb rebound work and the biological component of prosthesis-side push-off appeared to decrease. During prosthesis-side swing initiation, positive work at the hip joint decreased substantially and negative work at the knee increased slightly. The average stride period was 1.2 ± 0.093 s (mean $\pm$ s.d.), and did not change across conditions ($P = 1$).

3.3.1 Prosthetic ankle mechanics

Prosthesis mechanics during push-off varied widely across conditions, while behavior during the Dorsiflexion phase of stance remained consistent. As increasing values of push-off were commanded, peak prosthesis power (Fig. 3.3a) and measured prosthesis

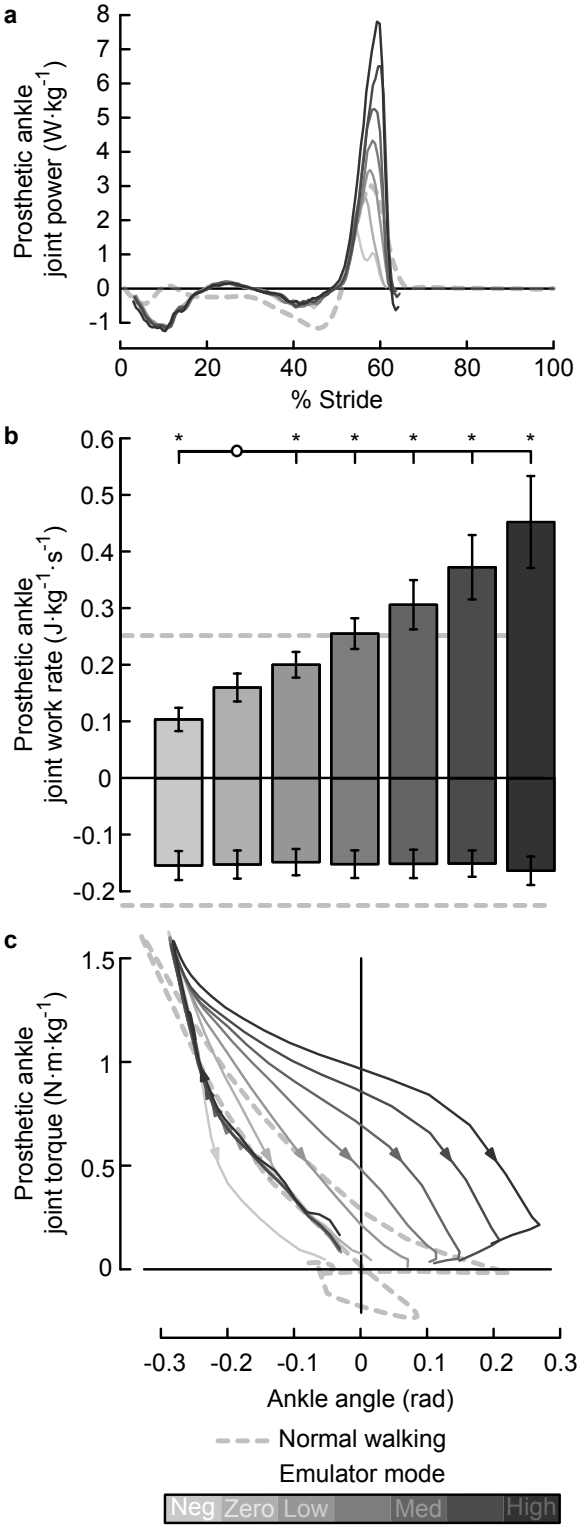

Figure 3.3: Prosthetic ankle mechanics calculated from on-board sensor data. **a** Joint power. Lines indicate average trajectories for each condition, with darker lines corresponding to conditions with higher prosthesis push-off work. Dashed line indicates biological ankle joint power measured using inverse dynamics during Normal Walking. **b** Stride-averaged work rate. Positive and negative work were calculated separately. Error bars indicate inter-subject standard deviation, and *s indicate statistical significance. **c** Joint torque versus joint angle. Direction of motion indicated by arrows. Dorsiflexion curves are overlapping. The area inside each loop is the net prosthesis push-off work for that condition.

push-off work (Fig. 3.3b) increased significantly ($P = 3 \cdot 10^{-25}$). Push-off work was significantly different from the value in the Zero work condition for all other conditions ($P = 6 \cdot 10^{-6}$, $6 \cdot 10^{-6}$, $9 \cdot 10^{-7}$, $4 \cdot 10^{-7}$, $4 \cdot 10^{-7}$, and $2 \cdot 10^{-4}$, for comparisons to Negative Low, Low, Medium Low, Medium, Medium High, and High conditions, respectively). This trend was consistent despite differences between commanded and measured torque at the transition from Dorsiflexion to Plantarflexion (compare Fig. 3.3 to Fig. 3.2). Negative work did not change across conditions ($P = 0.9$). In the Negative Low work condition, positive prosthesis work was 0.41 ± 0.082 times the positive ankle work measured in Normal Walking, negative prosthesis work was 0.69 ± 0.11 times that of Normal Walking, and net prosthesis work was -1.9 ± 0.26 times that of Normal Walking. In the High work condition, positive prosthesis work was 1.8 ± 0.32 times that of Normal Walking, negative work remained unchanged at 0.73 ± 0.11 times that of Normal Walking, and net prosthesis work was 11 ± 2.8 times that of Normal Walking. Positive work was most similar to Normal Walking in the Medium work condition (1.0 ± 0.11 times Normal Walking). Stride-averaged work rate was closest to zero in the Zero work condition (0.0078 ± 0.011 J $\cdot$ kg$^{-1} \cdot$ s^{-1}). Positive, negative and net prosthesis work can also be visualized as the area under and between curves in torque-angle space (Fig. 3.3c).

3.3.2 Metabolic energy consumption

Metabolic rate decreased significantly with increasing prosthetic ankle net work ($P = 1 \cdot 10^{-14}$, Fig. 3.4). Metabolic rate was significantly different from the value in the Zero work condition for all other conditions ($P = 4 \cdot 10^{-3}$, $4 \cdot 10^{-3}$, $2 \cdot 10^{-3}$, $2 \cdot 10^{-3}$, $1 \cdot 10^{-4}$, $7 \cdot 10^{-3}$, respectively). Least squares regression showed the best fitting exponential relationship between the change in metabolic rate, P_m, and stride-averaged prosthesis work rate, P_p, to be $P_m \approx -0.55 + 0.51 \cdot e^{-6 \cdot P_p}$ ($R^2 = 0.7$, $P = 1 \cdot 10^{-17}$). This fit had less residual error than $1^{st}, 2^{nd}$ and 3^{rd} order polynomial fits. In the

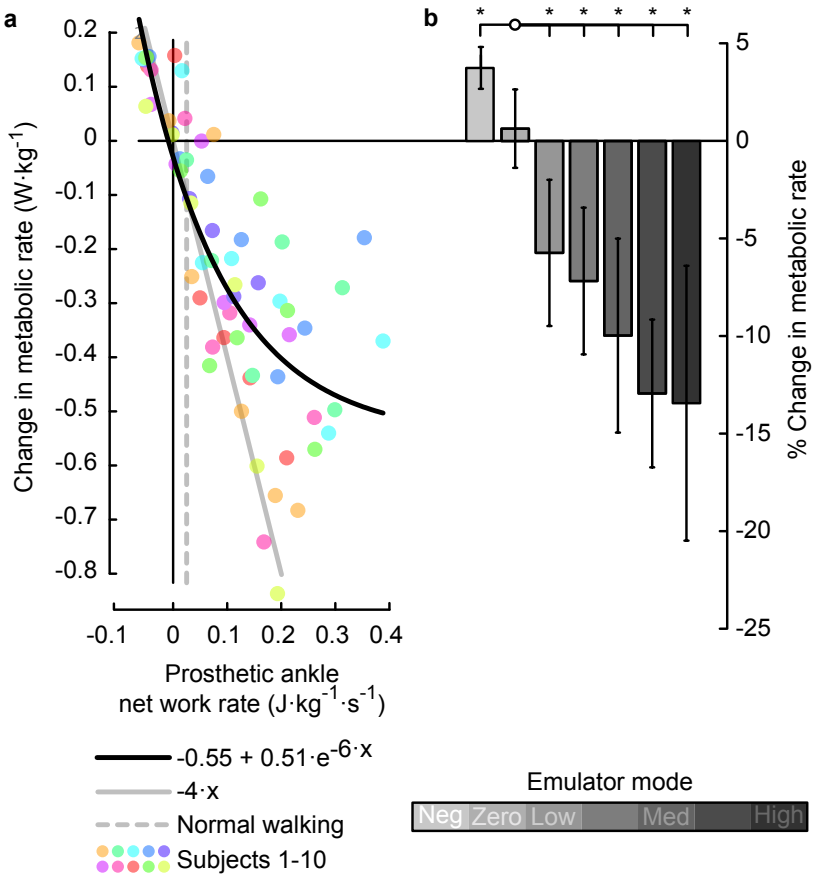

Figure 3.4: Metabolic rate decreased with increasing ankle push-off work. **a** Change in metabolic rate versus net prosthetic ankle stride-averaged work rate. Colored dots indicate data from individual subjects. Heavy black line is an exponential fit to the data. Solid gray line provides a reference for the rate of metabolic reduction if prosthesis work replaced muscle fiber work directly at 25% muscle efficiency. Dashed gray line indicates net biological ankle work rate in the Normal Walking condition. **b** Change in metabolic rate averaged across subjects for each condition. Shading indicates condition, error bars indicate inter-subject standard deviation, and *s indicate statistical significance. % change calculated with respect to the net metabolic rate at zero net prosthesis work.

region between -0.05 and $0.05\ \mathrm{J \cdot kg^{-1} \cdot s^{-1}}$ in net prosthesis work rate, metabolic rate was reduced by approximately $4\ \mathrm{W \cdot kg^{-1}}$ for each $1\ \mathrm{J \cdot kg^{-1} \cdot s^{-1}}$ of additional prosthesis work per second ($R^2 = 0.5$, $P = 2 \cdot 10^{-5}$). This rate of return is consistent with prosthesis work directly replacing muscle fiber work (see Supplementary Fig. 1 for more details). For higher levels of net prosthesis work, metabolic rate continued to decrease but with diminishing returns. Inter-subject variability increased for high values of net prosthesis work rate; for 5 out of the 10 subjects, the greatest prosthesis work rate corresponded to the lowest metabolic rate (individual data provided in Supplementary Fig. 2). In the Negative Low prosthesis work condition the average change in metabolic rate was $0.14 \pm 0.039\ \mathrm{W \cdot kg^{-1}}$, and in the High prosthesis work condition the average change in metabolic rate was $-0.48 \pm 0.25\ \mathrm{W \cdot kg^{-1}}$. Net metabolic rate in the Zero work condition was $3.6 \pm 0.46\ \mathrm{W \cdot kg^{-1}}$ and net metabolic rate during Normal Walking was $2.7 \pm 0.37\ \mathrm{W \cdot kg^{-1}}$.

3.3.3 Center of mass mechanics

Increased prosthesis push-off led to increased prosthesis-side center of mass push-off, but did not decrease contralateral-limb collision work (Fig. 3.5). Increases in whole-limb push-off work on the limb using the prosthesis were significant ($P = 2 \cdot 10^{-12}$, Fig. 3.5b), and push-off work was significantly different from the value in the Zero work condition for all other conditions ($P = 2 \cdot 10^{-3}$, $1 \cdot 10^{-3}$, $2 \cdot 10^{-3}$, $4 \cdot 10^{-5}$, $7 \cdot 10^{-5}$, and $1 \cdot 10^{-3}$, respectively). The biological component of whole-limb push-off work showed a significant downward trend with increasing prosthesis push-off, in both positive and negative components ($P = 0.04$ and $P = 4 \cdot 10^{-5}$, respectively, Fig. 3.5d). In the contralateral limb, negative work during collision was unchanged across conditions ($P = 1$, Fig. 3.5e). Positive work during contralateral-limb rebound appeared to decrease with increased prosthesis push-off ($P = 0.08$, Fig. 3.5f). Negative work during contralateral-limb preload increased with increas-

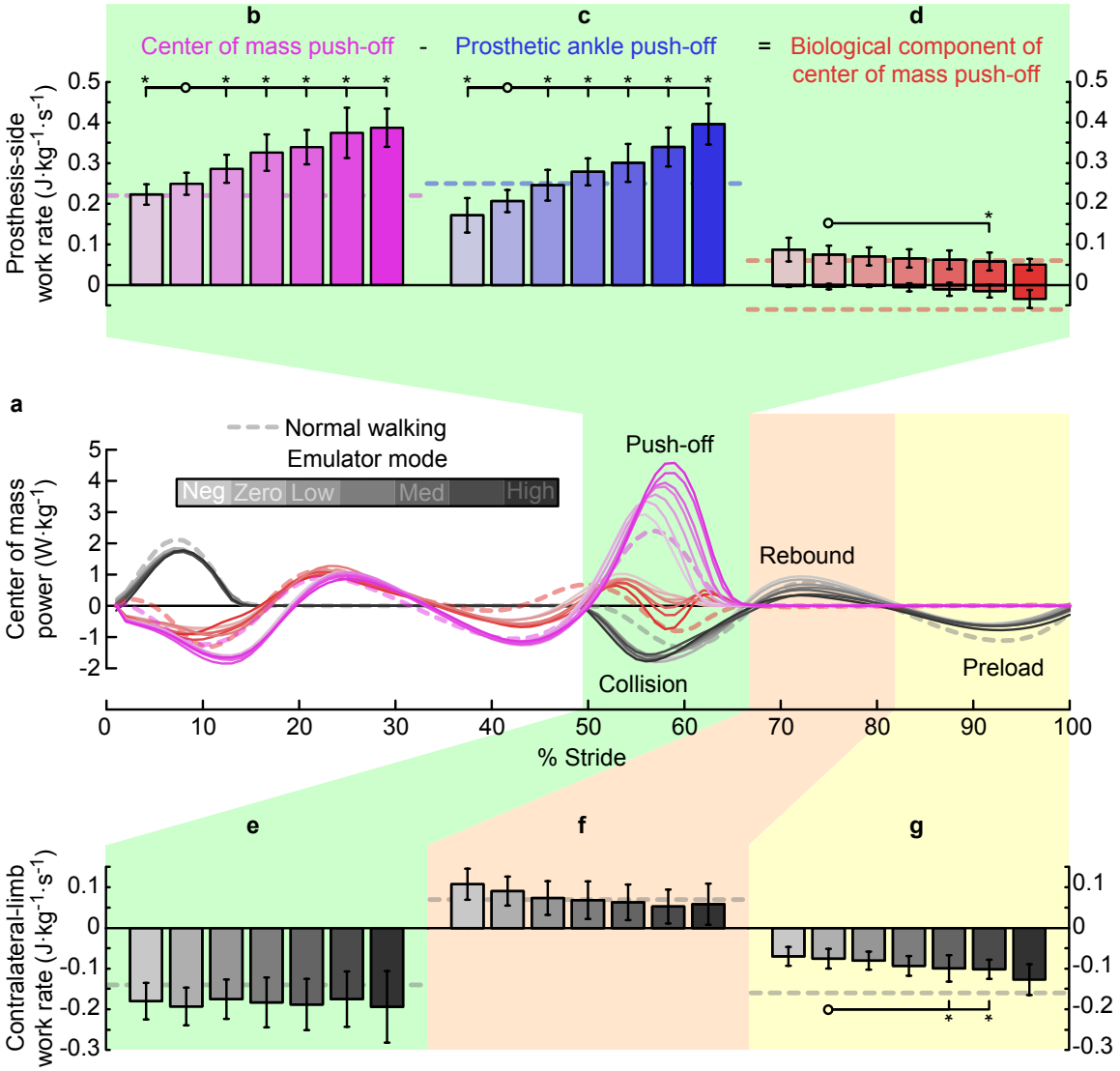

Figure 3.5: Center of mass power for each limb and center of mass work for key phases of the gait cycle. **a** Center of mass power versus percent stride. Lines indicate average trajectories for each condition, with darker lines corresponding to increased prosthesis push-off work. Magenta lines are mechanical power of the prosthesis-side limb on the center of mass. Red lines are the biological component of prosthesis-side mechanical power. Gray lines are contralateral-limb power on the center of mass. *Top:* **b** Prosthesis-side center of mass work rate during push-off, **c** prosthetic ankle joint power during push-off, and **d** the biological component of center of mass work rate during push-off, calculated as b - c. *Bottom:* Center of mass work rate of the contralateral limb during **e** collision, **f** rebound, and **g** preload phases. Error bars indicate inter-subject standard deviation, *s indicate statistical significance.

ing prosthesis push-off ($P = 2 \cdot 10^{-3}$, Fig. 3.5g). Total stride-averaged positive center of mass work rate, the accumulation of all positive work done throughout the stride, increased from 0.58 ± 0.058 J $\cdot$ kg^{-1} $\cdot$ s^{-1} in the Negative Low condition to 0.66 ± 0.11 J $\cdot$ kg^{-1} $\cdot$ s^{-1} in the High prosthesis work condition, an increase of 14% ($P = 0.03$). The biological component of total positive work rate decreased from 0.46 ± 0.043 J $\cdot$ kg^{-1} $\cdot$ s^{-1} in the Negative Low condition to 0.35 ± 0.072 J $\cdot$ kg^{-1} $\cdot$ s^{-1} in the High prosthesis work condition, a decrease of 24% ($P = 0.03$), possibly indicating a reduction in associated muscular effort (Supplementary Fig. 1).

Although contralateral-limb collision work was not affected by prosthesis push-off, contralateral-limb ground reaction forces during double-support were affected (Fig. 3.6a). Peak vertical force decreased significantly with increasing prosthesis push-off ($P = 2 \cdot 10^{-5}$, Fig. 3.6b), and peak vertical force significantly differed from the value in the Zero work condition for all other conditions ($P = 0.04$, $2 \cdot 10^{-3}$, 0.01, $2 \cdot 10^{-4}$, $4 \cdot 10^{-5}$, and 0.01, respectively). Center of mass velocity was oppositely affected (Fig. 3.6c), as peak vertical velocity increased with increasing prosthesis push-off work ($P = 1 \cdot 10^{-3}$, Fig. 3.6d).

3.3.4 Joint mechanics

Prosthesis-side hip work during swing initiation decreased significantly with increasing prosthetic ankle push-off work ($P = 4 \cdot 10^{-6}$, Fig. 3.7a&b). This component of hip work differed significantly from the Zero work condition in all other conditions except the Low work condition ($P = 0.02$, 0.2, $4 \cdot 10^{-3}$, $1 \cdot 10^{-3}$, $5 \cdot 10^{-3}$, and 0.02, respectively). In the Negative Low prosthesis work condition, positive hip work rate during swing initiation was 0.15 ± 0.029 J $\cdot$ kg^{-1} $\cdot$ s^{-1}. In the High prosthesis work condition, this component of hip work rate was 0.077 ± 0.043 J $\cdot$ kg^{-1} $\cdot$ s^{-1}. Prosthesis-side knee work showed a trend toward increased negative work during swing initiation, although the trend was not statistically significant ($P = 0.4$, Fig. 3.7c&d). Total biological

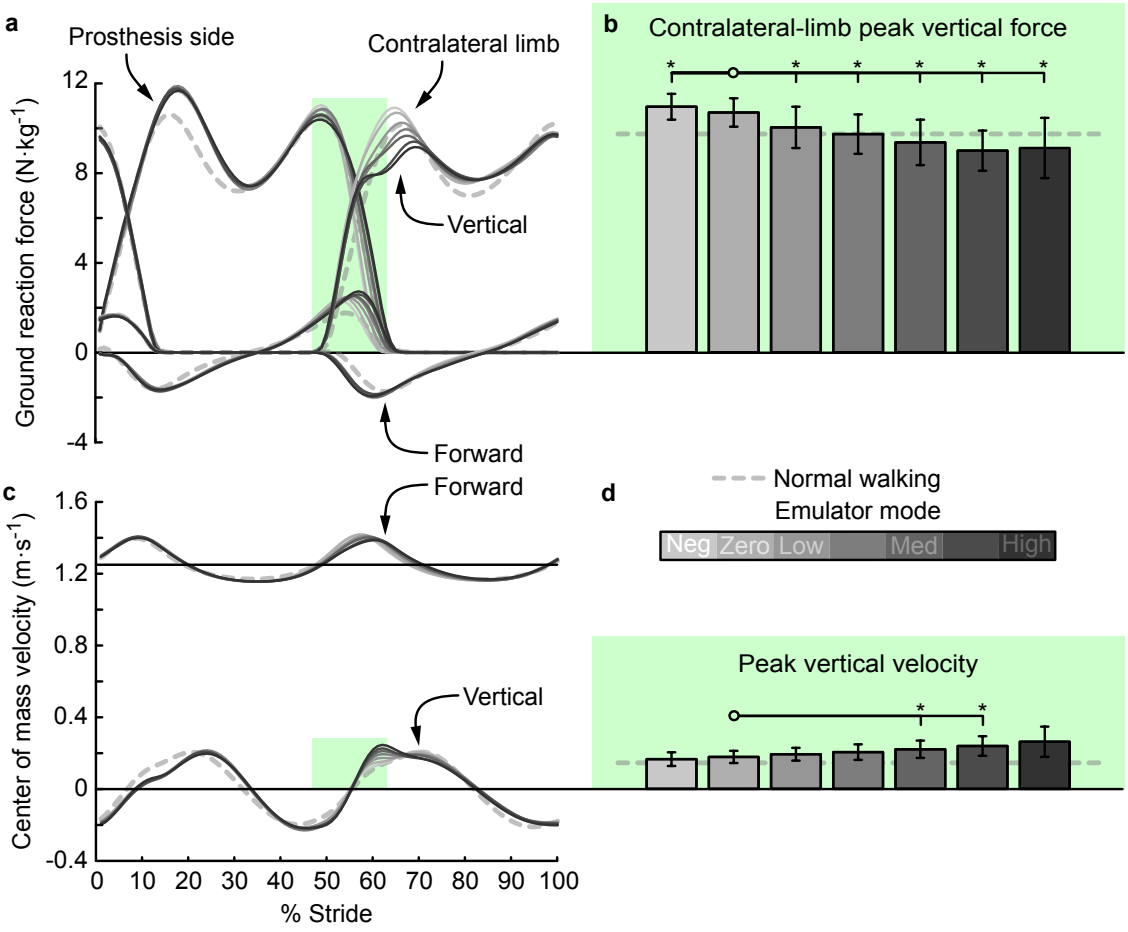

Figure 3.6: Ground reaction forces and center of mass velocity were affected by increasing ankle push-off work. **a** Ground reaction forces versus percent stride. Lines indicate average trajectories for each condition, with darker lines corresponding to conditions with higher prosthesis push-off work. **b** Peak ground reaction force on the contralateral limb during the double support period, indicated by green shading, decreased with increased prosthetic ankle push-off work. **c** Center of mass velocity versus percent stride. **d** Peak center of mass velocity during the double support period, indicated by green shading, increased with increased prosthetic ankle push-off work. Error bars indicate inter-subject standard deviation and *s indicate statistical significance.

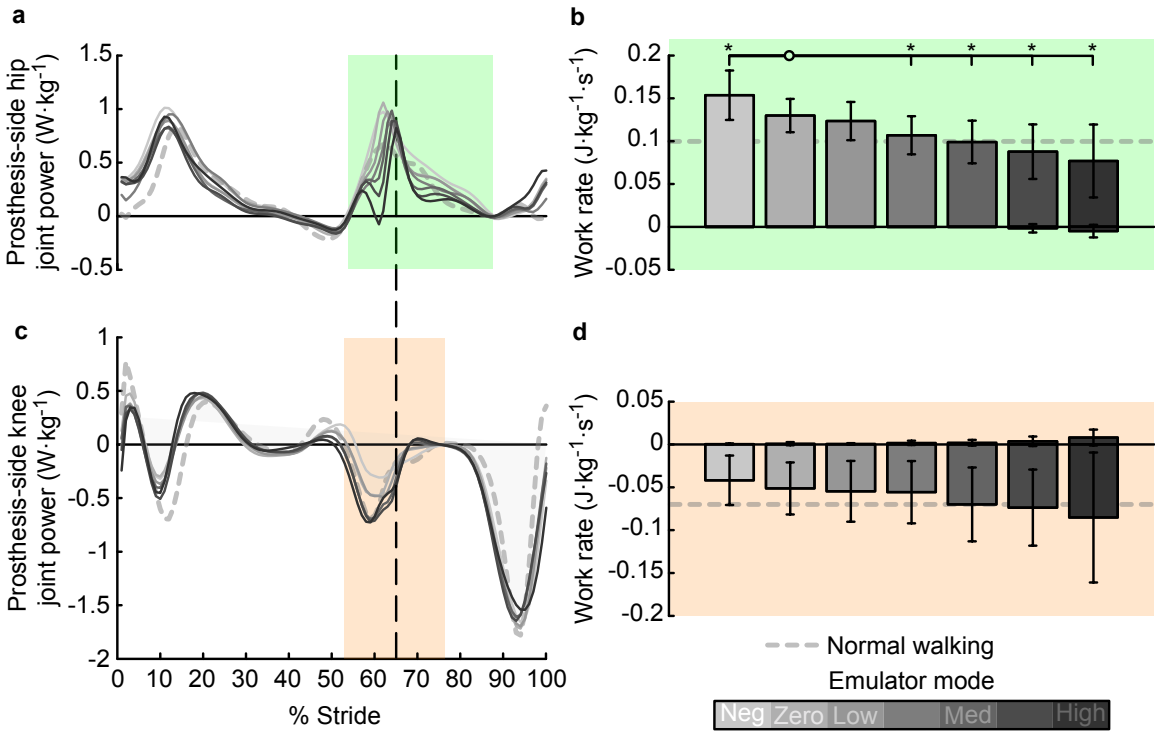

Figure 3.7: Hip and knee joint power on the prosthesis side. **a** Hip joint power versus percent stride. Lines indicate average trajectories for each condition, with darker lines corresponding to conditions with higher prosthesis push-off work. **b** Hip joint work rate during push-off and early swing, or the H3 region (Winter, 1991) indicated by green shading, decreased with increased prosthetic ankle push-off work. **c** Knee joint power versus percent stride. **d** Negative work at the knee joint during swing initiation, or the K3 region (Winter, 1991) indicated by red shading, showed a trend toward increasing in magnitude with increasing prosthetic ankle push-off work. Error bars indicate inter-subject standard deviation, and *s indicate statistical significance.

joint work decreased significantly with increasing prosthesis push-off ($P = 7 \cdot 10^{-14}$, Supplementary Fig. 1). Complete sagittal-plane joint kinematics, kinetics, and power for both limbs are included in Supplementary Fig. 4A & 4B.

3.4 Discussion

A wide variety of mechanical designs and control approaches could be incorporated into robotic prostheses, making it difficult to select device functionalities that provide meaningful benefits to users. Simple dynamic models of walking provide predictions that could, if validated, greatly simplify this design problem. Such models have predicted a causal relationship between reduced trailing limb ankle push-off work, increased contralateral-limb collision losses, increased overall mechanical work requirements, and increased energetic cost of walking for amputees using passive-elastic prostheses. We conducted a tightly-controlled experimental test of this concept, wherein simulated amputees were presented with a broad range of ankle push-off work while gait mechanics and energy use were measured. Increased trailing limb push-off reduced the metabolic cost of walking substantially. In direct contradiction with simple model predictions, however, increased push-off did not reduce leading limb collision losses or overall center of mass work. Instead, we observed reduced prosthesis-side hip power during double support and early swing, activity associated with initiation of leg swing (Fox and Delp, 2010; Lipfert et al., 2014). This would suggest a lower ceiling for the maximal energetic benefit of increased prosthetic ankle push-off, since muscle activity during the stance phase is thought to comprise a larger portion of the overall effort of walking than swing phase activity. These results demonstrate the need for more detailed predictive models of human walking and emphasize the value of human experiments early in the process of developing wearable robots.

In a predictive model, human-like limb segmentation and muscle-tendon actuation

would likely be necessary to capture the observed changes in hip mechanics and their implications for whole-body energy cost. Such elements would also allow for catapult-like mechanics that may be important in explaining the presence of normal ankle work disproportionate to its apparent impact on metabolic rate (Sawicki et al., 2009). Early attempts to use this type of model to make predictions about human responses to new device designs are promising (Song et al., 2013; van Dijk and van der Kooij, 2013), but have yet to be validated.

The substantial reductions in metabolic energy use with increased prosthesis work were well explained by concomitant reductions in human joint work. For Negative Low to Medium Low levels of push-off, metabolic rate decreased by about 4 $W \cdot kg^{-1}$ for each additional 1 $J \cdot kg^{-1} \cdot s^{-1}$ of net prosthesis work per second (Fig. 3.4). This reduction is quantitatively consistent with prosthesis work directly replacing muscle fascicle work, since muscles operate at an efficiency of about 25% in converting metabolic energy into positive mechanical work (Margaria, 1976). For higher levels of prosthesis push-off, however, metabolic energy consumption continued to decrease but at a diminished rate. The sum of all positive and negative joint work, scaled according to expected muscle efficiencies, closely corresponded to this trend, with better correlation than either direct replacement of muscle work by the device or changes in the biological component of total center of mass work (Supplementary Fig. 1). The most substantial changes in joint work occurred at the prosthesis-side hip during double-support and early swing, which accounted for approximately 60% of the change in total positive joint work (Fig. 3.7). Increasing absorption at the prosthesis-side knee joint during the same period might also help to explain diminishing returns with increasing prosthesis push-off. These results suggest that total joint work may be a useful component of the objective function when optimizing assistive device designs in simulation, although it is unlikely that this is the precise or complete mechanism by which increased prosthesis work reduced metabolic rate.

For all subjects, energy cost was minimized when the prosthesis provided far more push-off work than the biological ankle. On average, energy cost continued to decrease even at the highest level of prosthesis work, which corresponded to 1.8 times the normal value for positive work and 11 times the normal value for net ankle work. It appears that most subjects would have benefited from even more work input (Supplementary Fig. 2). This finding seems natural in retrospect; unlike energy expended by muscles, prosthesis work incurred no additional effort to the user, shifting the balance of costs. An analogous finding was that the condition in which temporal outcomes were least asymmetric (Medium, (Malone et al., 2012), Supplementary Fig. 5) was not the condition with the lowest metabolic rate. Another benefit of greater-than-normal prosthesis push-off was reduced limb loading associated with osteoarthritis (Supplementary Fig. 3), confirming observations from a prior comparison of multi-featured devices (Morgenroth et al., 2011). Imitating some aspect of unimpaired gait may be a reasonable starting point in the design of robotic prostheses, but these results demonstrate that the human-robot system can have significantly different optimal coordination patterns.

Timing of ankle push-off also seems to affect the energetics of walking, and the value applied here seems close to optimal for this system. Simple dynamic models of walking suggest that pushing off with the trailing limb just before leading limb heel strike minimizes collision losses and reduces energy cost by a factor of two to four (Yeom and Park, 2011; Ruina et al., 2005; Kuo, 2001). In this experiment, the onset of push-off and of collision were coincident, the observed increases in push-off work took place in the later part of collision, and peak push-off power occurred later with increasing push-off work (Fig. 3.5). This raises the possibility that the timing of push-off was too late to have the predicted effects. Fortunately, we have also conducted a study on push-off timing that suggests the onset used here is approximately optimal. In this separate study, the timing of push-off was varied across a wide range while net

push-off work was kept constant [Malcolm, P., Quesada, R. E., Caputo, J. M., Collins, S. H.]. We again found that collision work was unaffected, while metabolic rate was minimized by the latest onset of push-off work. These results are consistent with anecdotal reports of preferred timing from another robotic ankle prosthesis (Au et al., 2006). It therefore seems that push-off timing is not responsible for the mismatch between trends in collision work predicted by simple models and those observed in this experiment.

Large inter-subject variability with higher push-off work suggests a need for individualized device designs. On average, metabolic rate diminished exponentially with increasing push-off, but some subjects exhibited continued improvements while others experienced increased costs and apparent local minima (Supplementary Fig. 2). These differences could be related to physiology, learning or prior experience. Individualized tuning of prosthesis behavior during prescription, check-ups or even online might therefore provide a significant benefit to users.

This experimental protocol must be performed on individuals with amputation in order to make accurate predictions about optimal push-off work in commercial robotic prostheses. People with simulated and actual amputation can exhibit qualitatively different responses to interactions with the same prostheses (Zelik et al., 2011). The immobilizer boot that subjects wore added about 2% body mass to the prosthesis-side limb, which could have increased the metabolic cost of leg swing by up to 20% (Browning et al., 2007). Hip joint mechanics, however, suggested only a 5% increase in metabolic rate in the Negative Low condition compared to Normal Walking, with hip activity lower than in Normal Walking in the High condition (Fig. 3.7), inconsistent with the relative importance of swing being greater due to added mass. Coordination patterns could also be affected by differences in the mechanical interface with the body, differences in leg length and shoe shape, or neuromuscular differences in the residual limb. We are currently conducting this protocol among unilateral below-

knee amputees, and we expect the results to provide quantitative design guidelines for powered ankle-foot prostheses.

Acknowledgments

This material is based upon work supported by the National Science Foundation under Grant No. CMMI-1300804 and by the National Institutes of Health under Award No. 1R43HD076518-01. The authors thank Julie Renkant, Roberto Jaime and Anne Alcasid for assistance with data collection, Hartmut Geyer for use of data collection equipment, John Fulmer for hardware maintenance, Rachel Jackson and Myunghee Kim for help interpreting results, and two anonymous reviewers for helpful feedback on the manuscript.

3.5 Supplementary Information

A video of a representative subject walking in each condition of the experiment can be found on the Publications section of the Carnegie Mellon University Experimental Biomechatronics Lab webpage: biomechatronics.cit.cmu.edu.

3.5.1 Candidate mechanical correlates of metabolic rate

Simple dynamic models of walking are often optimized for energy consumption, with results proposed as predictive of human behavior under similar circumstances. These models often use some measure of mechanical work as a proxy for metabolic energy consumed by muscles, but there are many candidate work values to minimize. We compared the observed changes in metabolic energy consumption across conditions to three candidate correlative models: prosthesis work, center of mass work, and joint work (Fig. 3.8). The Prosthesis model represents the case that prosthesis work

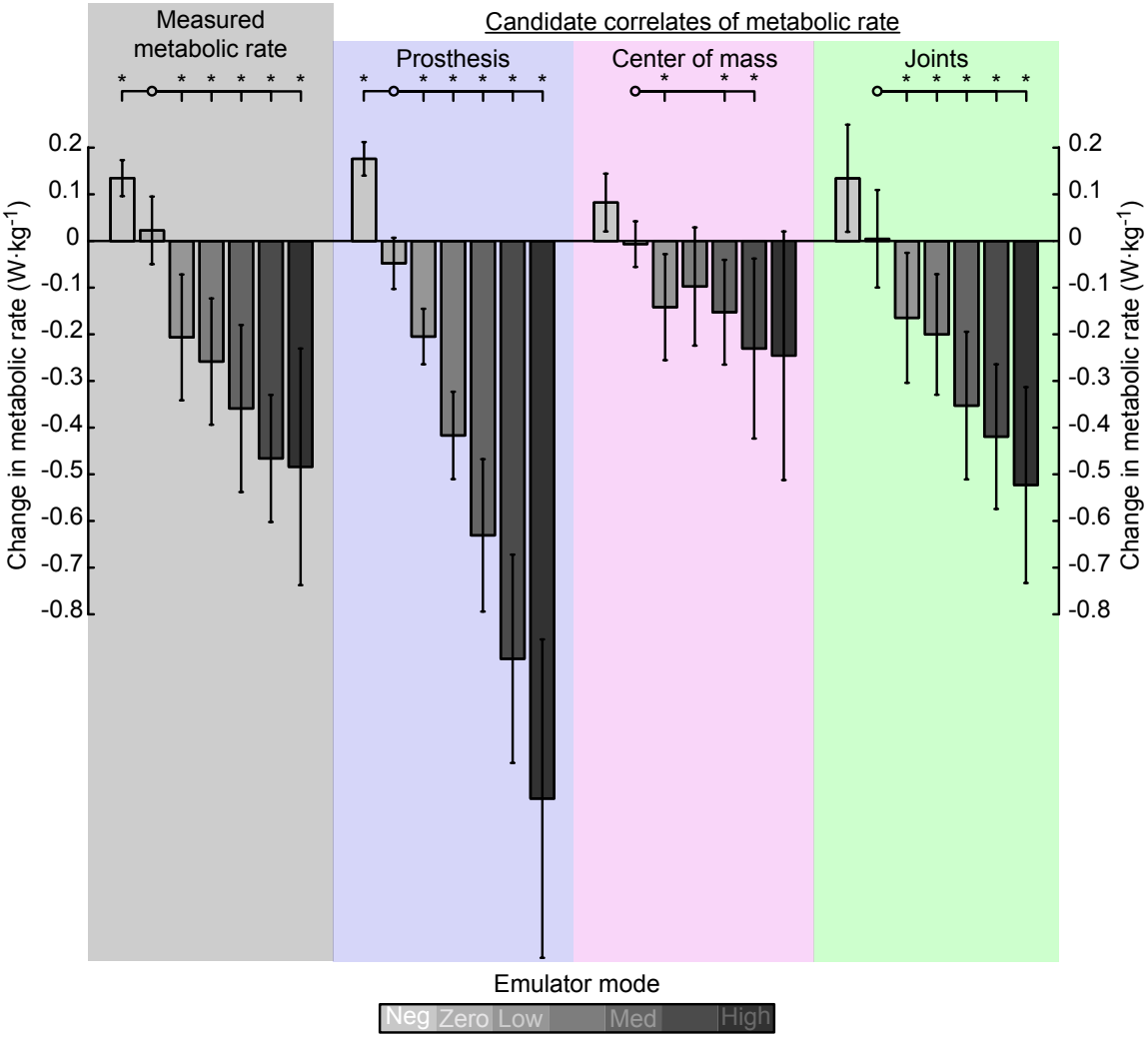

Figure 3.8: Measured change in metabolic energy consumption compared to three candidate mechanical work correlates. Measured metabolic rate decreased with increasing ankle push-off. The change in metabolic rate was less than would be expected if Prosthesis work exactly replaced muscle work. The change in metabolic rate was greater than would be expected if Center of Mass work were equivalent to muscle work. The change in metabolic rate was as would be expected if Joint work were equivalent to muscle work. Error bars indicate inter-subject standard deviation and *s indicate statistical significance.

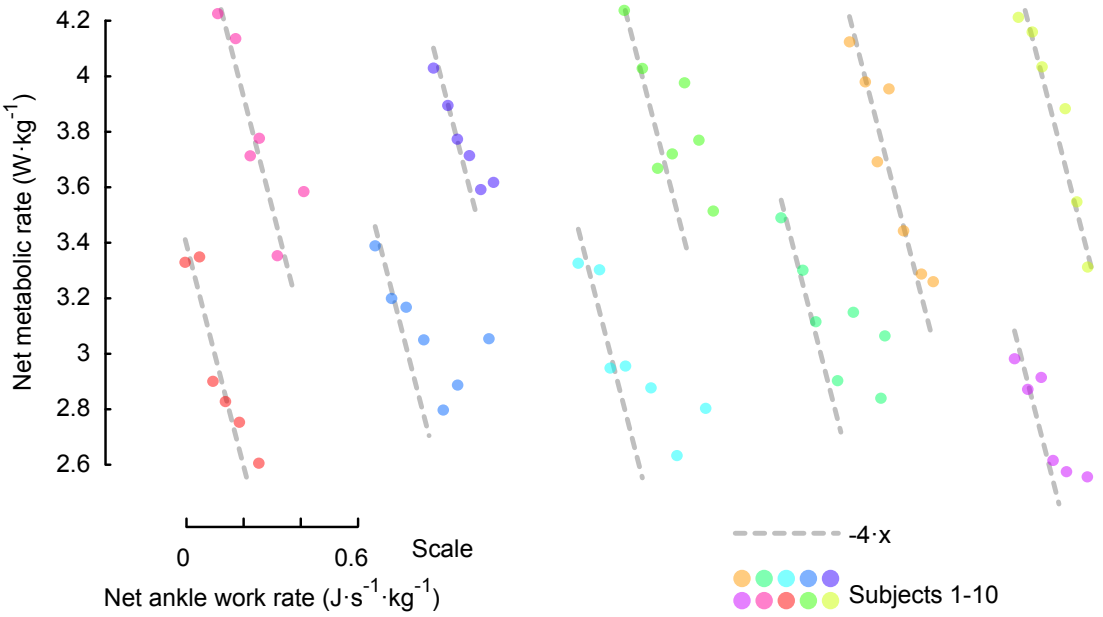

Figure 3.9: Metabolic rate versus net prosthesis push-off work rate for individual subjects. Net metabolic rate (not change metabolic rate) is presented to illustrate inter-subject variability. Dashed lines indicate the predicted decrease in energy consumption if prosthesis work were to exactly replace positive muscle work. All data correspond to the same vertical axis, while horizontal location is self-consistent for each subject and corresponds to the scale provided.

directly replaces muscle fascicle work, and predicts changes in metabolic rate that are about twice as large as those measured for high values of push-off work. The Center of Mass model represents the case that the biological component of mechanical work done by the legs on the center of mass of the body is indicative of muscle fascicle work, and predicts changes in metabolic rate that are about half as large as those measured. The Joint work model represents the case that the sum of mechanical work done across all the joints is indicative of muscle fascicle work, and predicts similar changes in metabolic rate to those observed. In each case, we assumed an efficiency of 25% for producing positive work and -120% for absorbing negative work.

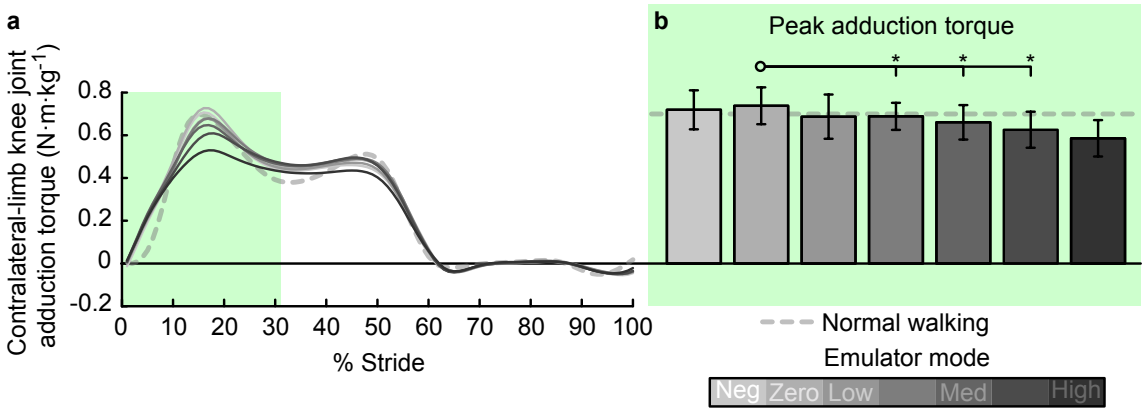

Figure 3.10: Intact-limb adduction knee torque torque decreased with increasing prosthetic ankle push-off work. **A** Joint torque versus percent stride. Lines indicate average trajectories for each condition, with darker lines corresponding to conditions with higher prosthesis push-off work. **B** Peak torque during the collision phase. The apparent mismatch between peak values in these panels is a result of stride averaging to create the trajectories at left; peak values at right were calculated on each individual step and then averaged. Error bars indicate inter-subject standard deviation and *s indicate statistical significance.

3.5.2 Supporting energetics and mechanics figures

Trends in metabolic rate for individual subjects are reported in Fig. 3.9. Changes in contralateral-limb ground reaction forces during double support led to reduced knee adduction torque in the intact-side knee (Fig. 3.10), which is thought to be beneficial in reducing risk of developing osteoarthritis. Joint angle, torque and power for the ankle, knee, and hip joints on the intact (Fig. 3.11) and prosthesis (Fig. 3.12) side legs are also provided for reference. Kinetic and potential energies of the whole prosthesis-side limb, contralateral limb, and the rest of body (assumes torso, head, arms, etc. are a lumped mass at pelvis) as trajectories (Fig. 3.13) and change in energy across the period of prosthetic ankle push-off (Fig. 3.14).

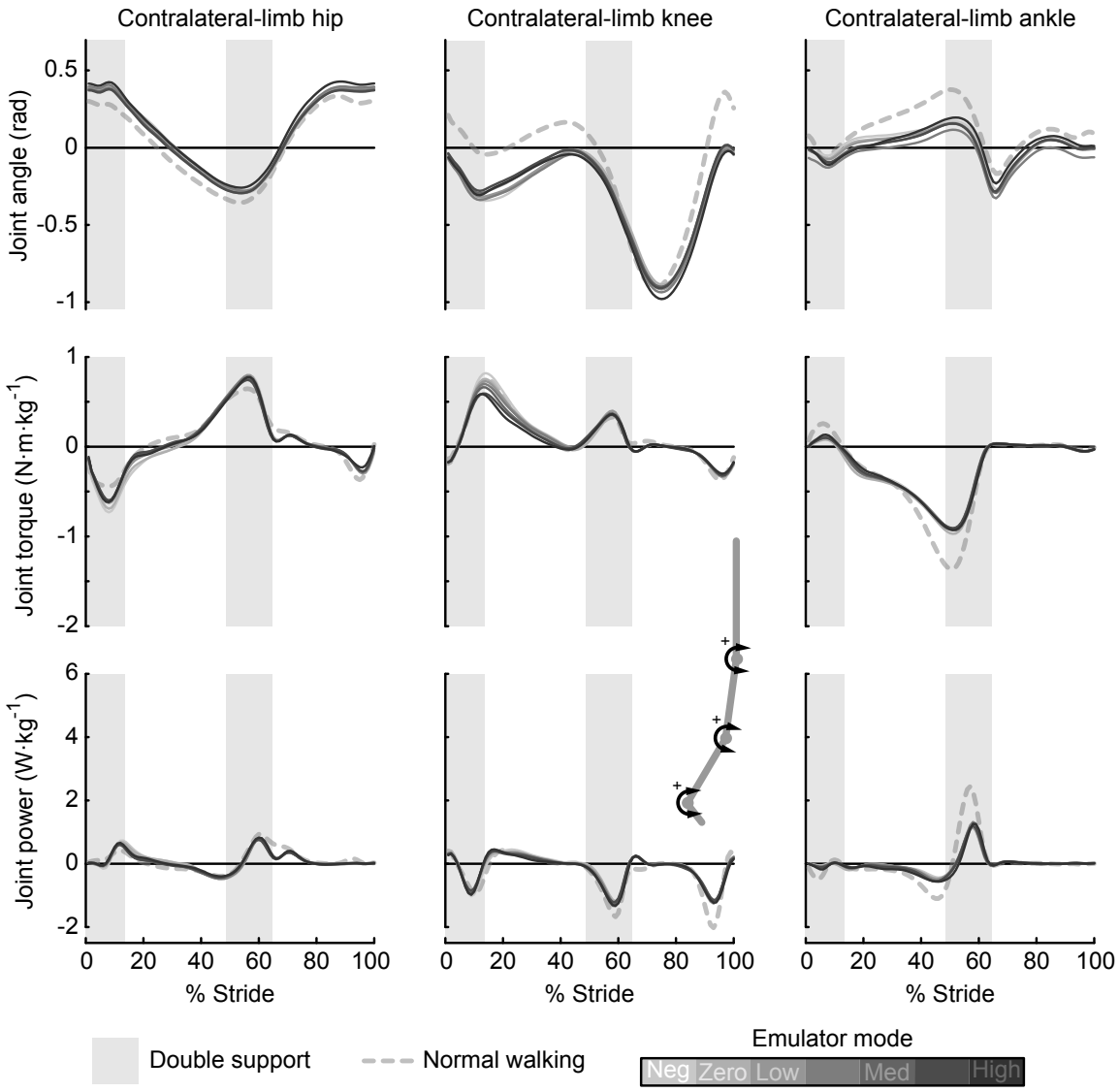

Figure 3.11: Joint angle, torque, and power for the ankle, knee, and hip joints on the intact-side leg. Lines indicate average trajectories for each condition, with darker lines corresponding to conditions with higher prosthesis push-off work. Shaded region roughly indicates the double support period.

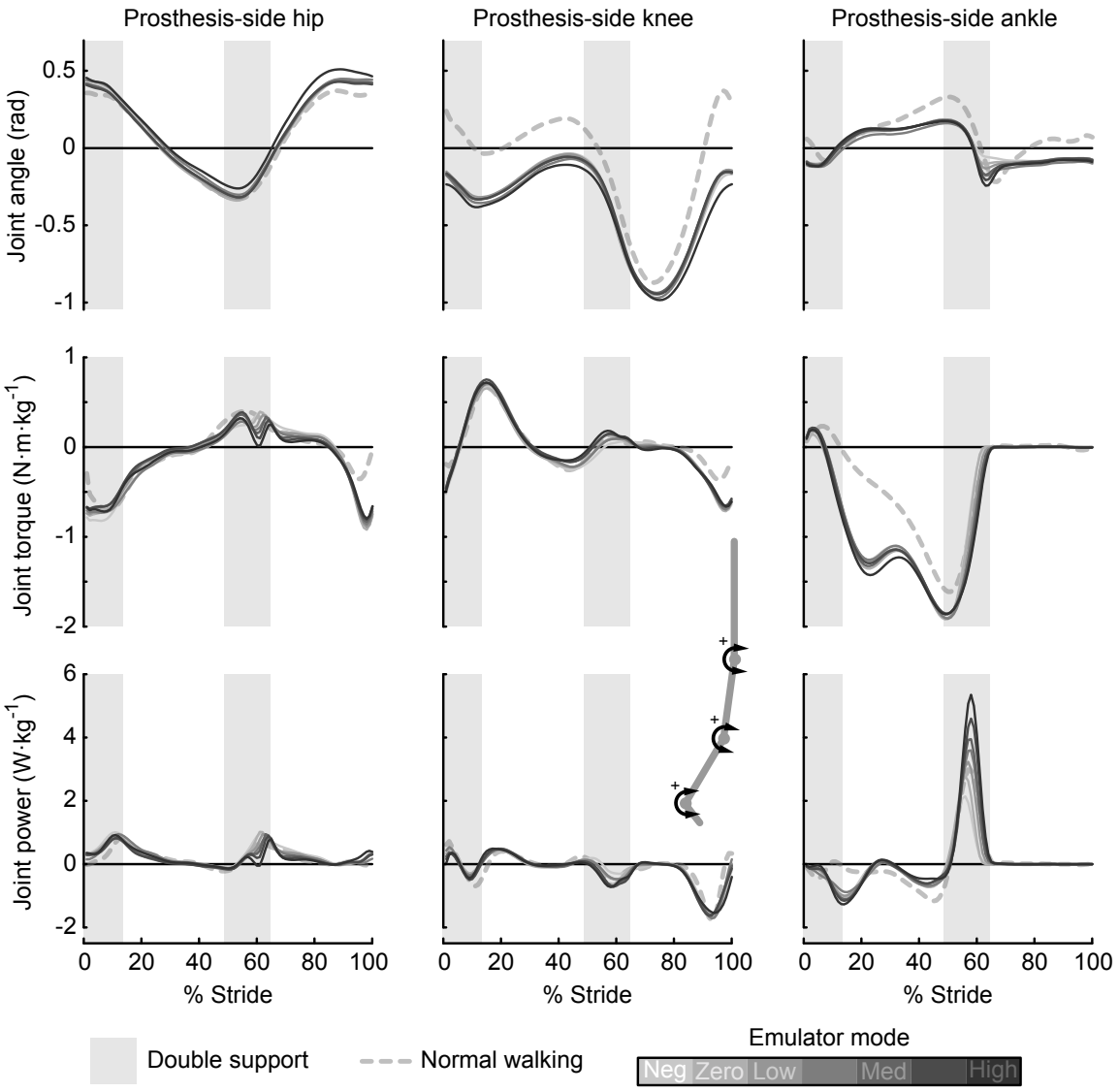

Figure 3.12: Joint angle, torque, and power for the ankle, knee, and hip joints on the prosthesis-side leg. Lines indicate average trajectories for each condition, with darker lines corresponding to conditions with higher prosthesis push-off work. Shaded region roughly indicates the double support period.

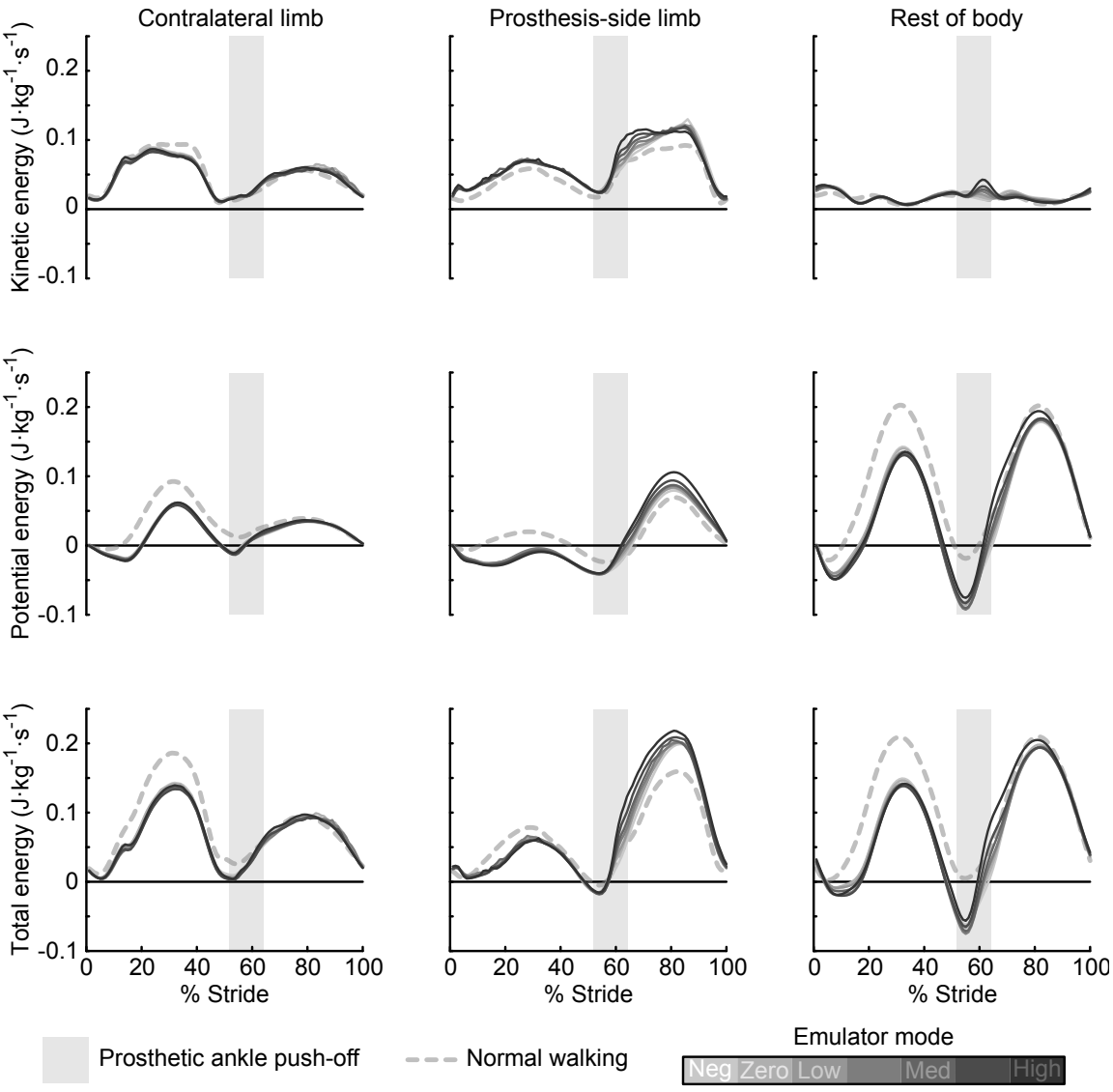

Figure 3.13: Kinetic, potential, and total (the sum of kinetic and potential) energies of the whole prosthesis-side limb, contralateral limb, and the rest of the body, defined as everything other than the legs. 0% Stride corresponds to prosthesis-side heel strike. Lines indicate average trajectories for each condition, with darker lines corresponding to conditions with higher prosthesis push-off work. Shaded region roughly indicates the period of prosthetic ankle push-off.

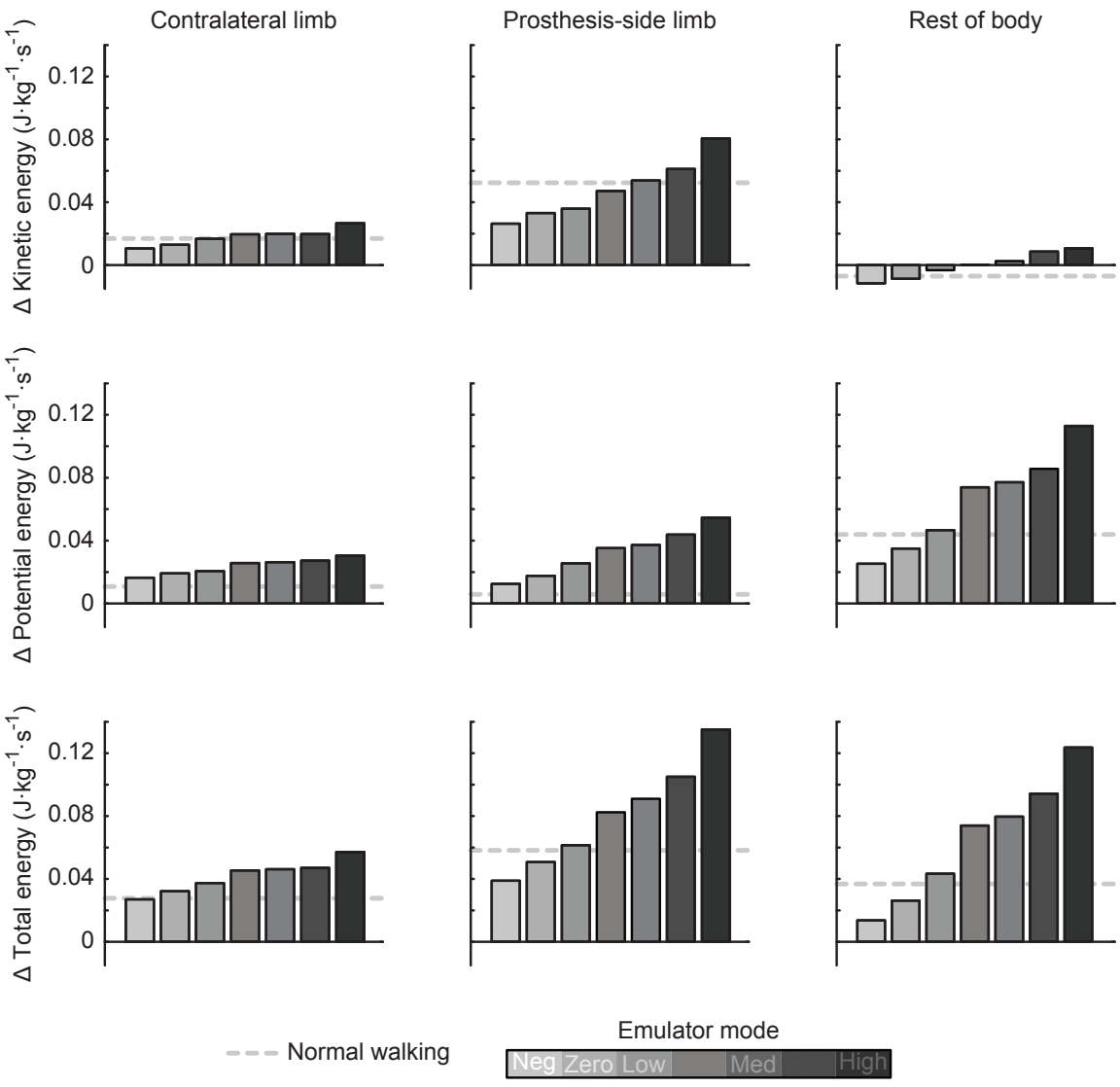

Figure 3.14: Change, across the period of prosthetic ankle push-off, in the kinetic, potential, and total (the sum of kinetic and potential) energies of the whole prosthesis-side limb, contralateral limb, and the rest of the body, defined as everything other than the legs. Shading indicates different conditions.

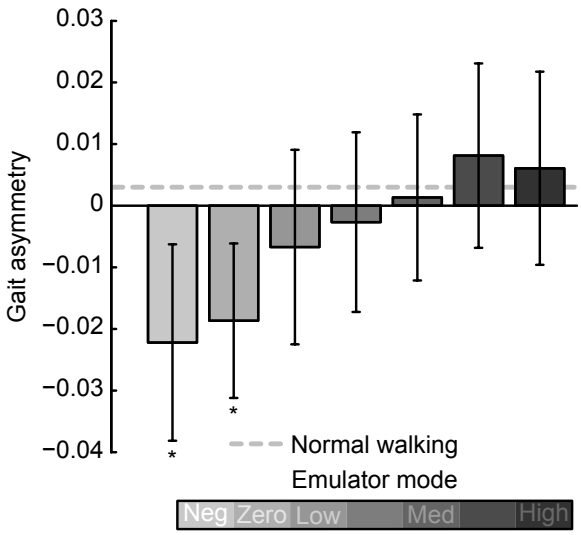

Figure 3.15: Gait asymmetry was affected by prosthetic ankle push-off work. Shading indicates different conditions. Error bars indicate inter-subject variability, *s indicate asymmetry is statistically significant compared to 0.

3.5.3 Temporal symmetry

Healthy humans tend to walk with symmetric gait, and gait symmetry is sometimes suggested as a goal for gait rehabilitation. Disabilities like amputation can create physiological asymmetries, however, so it is not clear that adapting a symmetric gait is always optimal. We measured temporal gait asymmetry across conditions, defined as $Assym = (T_{ps} - T_{is})/(T_{ps} + T_{is})$, where T_{ps} is the time between prosthetic heel strike and intact heel strike and T_{is} is the time between intact heel strike and prosthetic heel strike. Temporal symmetry was significantly affected by prosthesis push-off work ($P = 7 \cdot 10^{-5}$, Fig. 3.15). Asymmetry was minimized in the Medium prosthesis work condition, whereas metabolic energy expenditure was minimized for the High work condiiton. These results demonstrate that symmetric gait can be sub-optimal, at least in terms of energy economy, for individuals using a prosthesis on one leg.

3.6 Additional discussion

3.6.1 Follow-up studies

In a follow-up study with amputee subjects, we found results to have considerably more inter-subject variability (Quesada et al., 2015). Large-enough sample size and statistical analysis allow us to make generalizeable conclusions in spite of variability, as was the case in the N=10 simulated amputee experiment, but in the amputee experiment we observed qualitative differences in users' responses. Confounding factors, such as physiology or experience, could explain such differences. Perhaps future studies with larger subject populations could discover relationships between these factors and users' ability to extract benefit from increases in push-off work. It may also be valuable to measure additional outcomes beyond mechanics and energetics, such as electromyography, stability, or user satisfaction, since we expect degree of benefit to vary across outcome metrics (Chapter 4). Mechanistic explanation is scientifically interesting, potentially useful to the construction of predictive models of human walking, and necessary to extrapolate experimental findings beyond the subject pool in order to inform clinical practice. But, given the vast array of potential factors, this problem could be intractable. Parameters could instead be optimized for every individual in a clinical setting prior to prosthesis prescription–superseding the need for generalization. We explore such techniques in Chapters 4 and 5.

3.6.2 Other interesting 1-dimensional parameter studies

Many interesting 1D parameter studies remain to be performed, including, for example, systematic variation of plantar/dorsiflexion stiffness, inversion/eversion stiffness, prosthesis alignment, device weight, and foot length. Perhaps amputee users' responses to variations in these parameters will be simpler, as these are aspects of

behavior that are currently provided by conventional prosthetic limbs and so users may not require as much accommodation time as with novel behaviors such as powered push-off. Results of these studies could inform the design and prescription of these aspects of prosthetic limbs, which are currently set based mostly on subjects anthropometry.

3.6.3 Further discussion of center of mass mechanics

As reported in Section 3.3.3, increased prosthetic ankle work during push-off led to increased prosthesis-side center of mass push-off work ($P = 2 \cdot 10^{-12}$, Fig. 3.5b). Contralateral-limb collision work was not consequently decreased ($P = 1$, Fig. 3.5e). Contralateral-limb collision impulse did decrease (Fig. 3.6a), which is consistent with the observed reduction in peak contralateral-limb knee adduction torque (Fig. 3.10). However, the metabolic costs associated with walking have been explained by changes in center of mass push-off and collision work (not impulse) (Donelan et al., 2002). It is not required by mechanics laws for these two phases of center of mass work to be balanced. We do expect that the positive and negative components of center of mass work should be balanced across the entire stride, since subjects' velocity was constant over the course of each trial (guaranteed in treadmill walking). Total center of mass work did not change across conditions ($P = 1$), so the increase in center of mass push-off work must have been balanced by a decrease in center of mass work during phases other than contralateral-limb collision. Indeed, this was the case. Increases in negative center of mass work which were statistically significant are presented in Fig. 3.5f&g. Non-significant trends account for the apparent small inconsistency in changes in work presented in Fig. 3.5. Changes in center of mass work do not fully explain the observed changes in metabolic rate (Fig. 3.8).

Chapter 4

Emulation to inform prescription

Results from the amputee push-off work experiments (Quesada et al., 2015) suggest that optimal device behavior depends greatly on individual amputee users' needs and perhaps cannot be generalized across populations (perhaps this was also the case in (Zelik et al., 2011)). So we began to think about how in clinical practice, minimally customizable off-the-shelf devices are selected based on simple assessment of users' ability and needs. This process is unlikely to optimally accommodate individual differences. We envisioned a new prescription process in which a tethered robotic prosthesis emulates the behavior of candidate prostheses and is used to experimentally assess individuals' performance with each device, using a few objective outcome measures. Deployed in a clinical setting, this tool would provide practitioners and payers with hard data to justify that a particular device enables an individual to achieve the highest level of mobility, reducing costs and improving patient-specific outcomes.

Caputo, J. M., Adamczyk, P. G., Collins, S. H. (2015) Informing ankle-foot prosthesis prescription through haptic emulation of candidate devices. In Proceedings *IEEE International Conference on Robotics and Automation*, May 2015.

A preliminary version of this work was presented in:

Collins, S. H., Caputo, J. M., Adamczyk, P. G. (2014) Emulating prosthetic feet during the prescription process to improve outcomes and justifications. In Proceedings *IEEE Workshop on Advanced Robotics and its Social Impacts*, 2 pages.

This work will be presented at:

Caputo, J. M., Adamczyk, P. G., Collins, S. H. (2015) Emulating candidate ankle-foot prostheses to inform prescription. *39th Annual Meeting of the American Society of Biomechanics*.

This work is the subject of the following provisional patent:

Caputo, J. M., Collins, S. H., Adamczyk, P. G. (2014) Methods, Apparatuses, and Systems for Amputee Gait Capacity Assessment. U.S. Provisional Patent No. 62/070,134.

Abstract

Robotic prostheses can improve walking performance for amputees, but prescription of these devices has been hindered by their high cost and uncertainty about the degree to which individuals will benefit. The typical prescription process cannot well predict how an individual will respond to a device they have never used because it bases decisions on subjective assessment of an individual's current activity level. We propose a new approach in which individuals 'test drive' candidate devices using a prosthesis emulator while their walking performance is quantitatively assessed and results are distilled to inform prescription. In this system, prosthesis behavior is controlled by software rather than mechanical implementation, so users can quickly experience a broad range of devices. To test the viability of the approach, we developed a prototype emulator and assessment protocol, leveraging hardware and methods we previously developed for basic science experiments. We demonstrated emulations across the spectrum of commercially available prostheses, including traditional (e.g. SACH), dynamic-elastic (e.g. FlexFoot), and powered robotic (e.g. BiOM® T2) prostheses. Emulations exhibited low error with respect to reference data and provided subjectively convincing representations of each device. We demonstrated an assessment protocol that differentiated device classes for each individual based on quantitative performance metrics, providing feedback that could be used to make objective, personalized device prescriptions.

4.1 Introduction

4.1.1 Typical Prescription Process

The prescription of ankle-foot prostheses is hindered by uncertainty about which device is most suitable for a given individual (Hofstad et al., 2004). Payers expect justi-

fication for prosthesis selection, but without objective data clinicians can only provide their subjective impression, the expressed needs of the individual, and, at best, basic assessment of an individual's pre-prescription mobility (Gailey et al., 2002). Recent robotic devices have intensified this problem, as they have demonstrated benefits to the user (Herr and Grabowski, 2012; Esposito et al., 2015), but at a high price (about \$80,000 for a BiOM® T2 vs. about \$1,000 for a conventional prosthesis). The degree to which individual users will benefit also remains unclear. Given this uncertainty, clinical practice is slow to accommodate disruptive technologies, and is not able to effectively predict a user's activity-level and ability with a device they have never used.

4.1.2 Informing Prescription by Haptic Emulation

We propose a new approach, wherein patients 'test drive' candidate devices, providing hard data on how they perform with each prosthesis. This could be done by buying and trying many different prostheses for each individual, but the process would be laborious and would require expensive inventories of different models of prosthesis (each with variations for different body weights, activity levels, and foot sizes). Instead, clinicians could fit patients with a prosthesis emulator and provide the experience of wearing these different prostheses by simply switching modes in a software interface. Most commercially-available devices can be classified into one of three groups: traditional stiff and dissaptive solid ankle cushioned heel (SACH) prostheses, conventional spring-like dynamic elastic response (DER) prostheses, and actively-controlled robotic prostheses. Emulating these diverse behaviors with a single prosthesis requires versatility beyond the capabilities of currently-available mobile robotic prostheses, which are fine-tuned to exhibit specific behaviors in a convenient autonomous package. To maximize versatility in basic science experiments that do not require autonomy, e.g. (Caputo and Collins, 2014b), we previously developed a

robotic prosthesis system in which a powerful off-board motor and controller actuate a lightweight prosthesis end-effector through a flexible Bowden cable transmission (Caputo and Collins, 2014a). In the present study we test whether such a system can convincingly emulate the behavior of existing off-the-shelf prostheses.

4.1.3 Metrics for Evaluating Benefit

To evaluate the benefits each emulation mode provides to an individual, it would be useful to have outcome metrics that capture aspects of performance that are relevant to daily life. The most-cited measure for the efficacy of an assistive device is metabolic rate (the rate at which biochemical energy is used by the body to perform a task). However, in clinical practice, the expensive equipment required to measure metabolic rate is typically not available. Also, energy consumption must be balanced against other factors such as comfort, stability, versatility, and maximal performance. Therefore, it would be useful to have a set of outcomes that can be measured simply and quickly in a clinical setting, and can estimate energy consumption as well as other important outcomes. Heart rate scales roughly with metabolic rate (Spurr et al., 1988) and could be used as a surrogate that is simpler to measure and responds more quickly to the task. Maximum sustainable walking speed (MSWS) also scales with metabolic rate (Genin et al., 2008), and might include information about perceived stability and comfort. Finally, patient-reported satisfaction scores and comments can include information about perceived effort and stability, comfort, and gait aesthetics.

4.1.4 Summary and Hypotheses

The aim of this study was to test the feasibility of a new approach to the prescription of ankle-foot prostheses that includes quantitative measurements of how an individual will perform with a set of candidate devices. We hypothesize that (1) a tethered robotic prosthesis can accurately emulate different classes of commercially-available

prostheses and that (2) simple, clinically-relevant performance metrics can provide quantitative data on an individual's performance that differentiate device classes and individuals.

4.2 Methods

4.2.1 Overview of the Ankle-Foot Prosthesis Emulator

We developed a prototype haptic emulator capable of exhibiting the behavior of a wide range of commercially available ankle-foot prostheses. The prosthesis emulator consists of a powerful off-board motor and real-time controller, a flexible tether transmitting sensor signals and mechanical power, and an ankle-foot prosthesis end-effector (Fig. 4.1, (Caputo and Collins, 2014a)). The user wears the prosthesis as they would a conventional prosthesis, except that they are constrained by the tether to walk on a treadmill.

Device behavior was controlled by matching the ankle torque vs. angle relationships of commercially available prostheses. We also programmed a behavior that is unlike any commercially available device, to demonstrate the system's ability to emulate candidate designs for testing prior to physical implementation. Emulated behavior was switched by buttons in a simple software interface, without mechanically modifying the emulator hardware. Walking performance was measured for each mode using a variety of techniques that could be used to inform device prescription.

4.2.2 Experimental Methods

We recruited six subjects with unilateral transtibial amputation to test the efficacy of the prosthesis emulator. Subject parameters are listed in Table 4.1. Subjects wore the prosthesis emulator as they would a standard ankle-foot prosthesis: a pylon,

Table 4.1: Human subject parameters

#	K-Level	Cause	TSA [yrs]	Age [yrs]	BW [lbs]	Prescribed device
1	K3	Traumatic	9	42	176	Fillauer Wave
2	K3	Traumatic	6	57	183	Ottobock Triton V. S.
3	K3	Traumatic	1	45	180	Össur Vari-Flex
4	K3	Traumatic	12	48	210	BiOM® T2
5	K3	Congenital	46	49	165	F. I. Renegade A·T
6	K3	DVT	18	53	189	Össur Vari-Flex T. S.

with universal prosthesis adapters at each end, was sized according to each subject's leg length and used to attach the prosthesis emulator to each subject's prescribed socket. Subjects were fitted with the prosthesis emulator by a Certified Prosthetist, who set the alignment of the device, which was then retained throughout the study. Subjects had previous experience with the prosthesis emulator hardware (but not the controller used here) totaling at least four hours of walking. Subjects completed the protocol twice, with data reported for the second repetition. The experimental protocol consisted of two days of walking: one day walking on a level treadmill and the other on an inclined (5°) treadmill. Treadmill speed was set to 1.25 $m{\cdot}s^{-1}$ or each subject's preferred walking speed (measured overground in a 50 m hallway) if it was less than 1.25 $m{\cdot}s^{-1}$. Subjects walked with their prescribed prosthesis (PRES) and with the prosthesis emulator in four modes: SACH (emulating a Solid Ankle Cushioned Heel foot), DER (emulating a Dynamic Elastic Response foot), BIOM (emulating the BiOM® T2), and HIPOW (a custom mode with high power output). Conditions were presented in random order, and subjects were required to rest for five minutes between conditions.

We evaluated users' walking performance in each emulator mode using four different metrics: two objective measures of steady-state walking efficiency and two subjective measures indicating user satisfaction and maximal performance. Metabolic

energy consumption was estimated using indirect calorimetry (Brockway, 1987), performed using gas concentrations and flow rates measured by a commercial respirometry system (Oxycon^{TM} Mobile), averaged over the last three minutes of each trial. Heart rate was measured by the same respirometery system using pulse oximetry, and averaged over the last three minutes of each trial. Net metabolic energy consumption and net heart rate were computed as the average measurement in each condition, minus the average measurement during a quiet standing trial. Percent change in net metabolic energy consumption and percent change in net heart rate were computed relative to the level ground SACH condition, to quantify the marginal benefits of other conditions. Satisfaction was assessed by asking the subjects to rate each of the emulated modes on a Likert Scale (Likert, 1932) which ranged from from -10 to 10, where -10 indicated "walking is impossible", 0 indicated "similar to walking with my prescribed prosthesis", and $+10$ indicated "walking is effortless". Maximum sustainable walking speed was established at the end of each walking trial by progressively increasing the speed of the treadmill in 0.05 m$\cdot$s^{-1} increments every ten seconds until the subject indicated they felt they could no longer sustain walking at the set speed for five more minutes. Measures of ankle torque and angle were calculated using on-board encoders (torque was inferred by measuring the deflection of a series elastic spring).

4.2.3 Ankle Joint Torque vs. Angle Control

Prosthetic ankle torque (τ_a) was controlled as a function of ankle angle (θ), with different relationships for the dorsiflexion ($\dot{\theta} < 0$) and plantarflexion ($\dot{\theta} > 0$) phases of stance (Caputo and Collins, 2014a). Desired ankle torque ($\tau_{a,des}$) was a piecewise linear fit to representative literature data obtained from inverse dynamics measurements made during walking (Fig. 4.2, data from (Torburn et al., 1990) for SACH, (Ferris et al., 2012) for DER and BIOM). To switch the emulator from one mode to

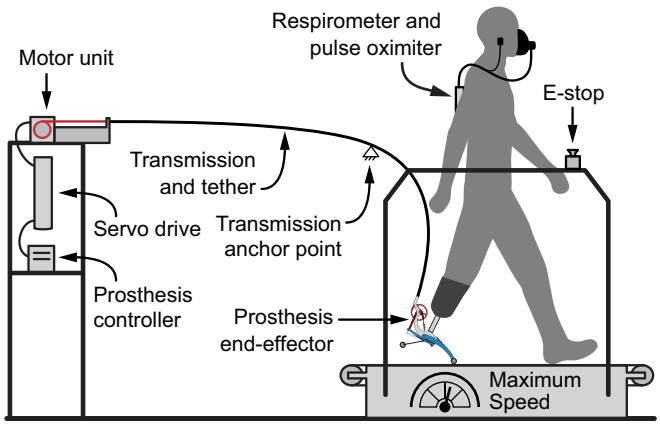

Figure 4.1: The ankle-foot prosthesis emulator consists of a lightweight prosthesis worn by the user and actuated through a flexible tether by a powerful motor and control system. By placing actuation and control off-board, the system can emulate an exceptional variety of behaviors at a worn mass comparable to passive mobile prostheses. Adjustments to the device behavior experienced by the user are made in the prosthesis control software rather than by modifying the end-effector. Metabolic rate, heart rate, maximum walking speed, and user preference are measured to assess which behaviors best suit the user.

another, the experimenter selected a different ankle torque vs. angle reference.

The motor was controlled as a velocity source (low-level control embedded in the motor driver performed velocity control), which was driven according to simple proportional control on torque error.

$$\dot{\theta}_{motor} = k_p * \tau_{a,err} \quad \tau_{a,err} = \tau_{a,des}(\theta) - \tau_{a,mes} \tag{4.1}$$

We tuned k_p to best suit the stiffness of each mode's ankle torque vs. angle relationship: when stiffness was high (e.g., SACH or the plantarflexion phase of HIPOW) larger k_p resulted in better tracking; but when stiffness was low (e.g., DER or the dorsiflexion phase of HIPOW) smaller k_p resulted in more stable torque tracking.

Rapidly decreasing torque during the plantarflexion phase of the BiOM® T2 emulation proved challenging for this simple proportional control scheme, so desired ankle torque was adjusted with an iteratively learned torque ($\tau_{a,lrn}$) to compensate

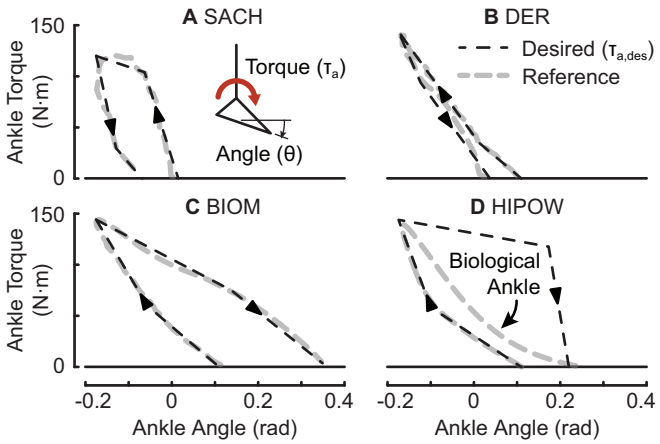

Figure 4.2: Emulation was performed by matching the ankle torque vs. angle relationships of commercially-available prostheses. Ankle torque was controlled as a function of ankle angle, with different relationships for the dorsiflexion and plantarflexion phases of stance. The desired torque (dark dashed) was a piecewise linear fit to literature reference data (light dashed).

for steady-state errors (inspired by (Zhang et al., 2015)).

$$\dot{\theta}_{motor} = k_p * (\tau_{a,des}(\theta) + \tau_{a,lrn}(\theta) - \tau_{a,mes}) \tag{4.2}$$

The learned torque during step n was a function of torque errors ($\tau_{a,err}$) on previous steps.

$$\tau_{a,lrn}(\theta, n+1) = \tau_{a,lrn}(\theta, n) + k_l * \tau_{a,err} \tag{4.3}$$

We tuned k_l to minimize steady-state tracking errors quickly but without overshoot, approximately thirty walking strides.

Because ankle torque is minimal during swing, the proportional controller was switched to control ankle angle when $\tau_{a,mes} < 15$ N·m at the end of stance, driving the joint to the initial dorsiflexion angle (θ_{des}) of the reference data.

$$\dot{\theta}_{motor,swing} = k_s * (\theta_{des} - \theta) \tag{4.4}$$

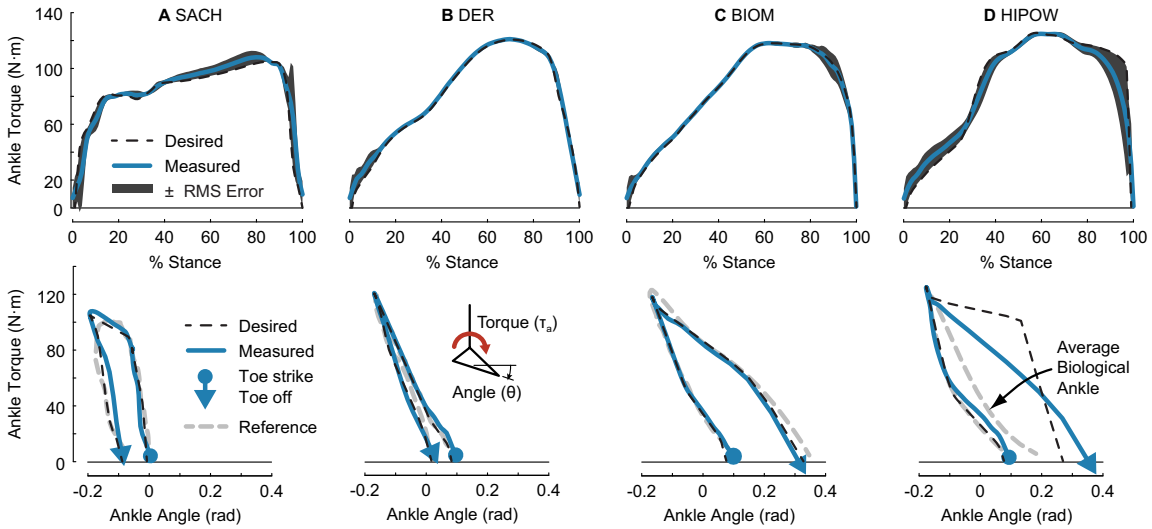

Figure 4.3: Emulating ankle torque vs. angle behavior of candidate prostheses. Demonstrated emulations include: **A** solid-ankle cushioned heel (SACH), **B** dynamic-elastic response (DER), **C** an active robotic foot, the BiOM® T2 (BIOM), and **D** a conceptual high-powered robotic foot design (HIPOW) that was designed to maximize torque during plantarflexion, with the expectation that torque would not be tracked precisely. Data in A-D are from a single individual with unilateral transtibial amputation walking at 1.25 m·s^{-1} on level ground over approximately 150 strides. *Top:* Prosthetic ankle torque plotted vs. % stance of the prosthesis-side step. *Bottom:* Prosthetic ankle torque plotted vs. prosthetic ankle angle.

4.3 Results

4.3.1 Torque vs. Angle Control

Mean desired and measured prosthetic ankle torque trajectories during the stance phase of the prosthetic limb for a representative subject during level ground walking are presented in Fig. 4.3. Root mean squared (RMS) error is presented to quantify torque tracking errors. Mean RMS errors across all subjects was 7.8±2.4 N·m, 2.6±0.7 N·m, 3.4±0.9 N·m, and 7.9±1.1 N·m for SACH, DER, BIOM, and HIPOW modes, respectively. Mean measured prosthetic ankle torque vs. angle in each emulation mode is presented for a representative subject in Fig. 4.3, along with the reference data used to design the emulation for comparison.

4.3.2 Walking Performance Outcome Metrics

Measurements of walking performance are listed for each subject in Fig. 4.4. Subject #1, a DER user, used the least metabolic energy and had the lowest heart rate in passive modes (DER and SACH) on level ground, although on inclined ground metabolic energy was minimized in HIPOW. However, this subject always preferred and walked fastest with the robotic modes (BIOM and HIPOW). Heart rate data were inconsistent with these observations, with passive modes (DER and SACH) always exhibiting the lowest heart rate. Subject #2, a DER user, used the least metabolic energy and had the lowest heart rate in the robotic modes, but always preferred DER. This subject walked fastest in BIOM on level ground but walked fastest in DER when walking uphill. Subject #3, a DER user, used the least metabolic energy and had the lowest heart rate in BIOM, but walked fastest in HIPOW. This subject preferred the passive modes on level walking, but preferred HIPOW on inclined ground. For subject #4, a BiOM® T2 user, DER was optimal by all metrics on level ground. This subject used less metabolic energy in BIOM on inclined ground, but still preferred DER. Subject #5, a DER user, used the least metabolic energy and walked fastest in BIOM on level ground but used the least energy in HIPOW on inclined ground. This subject always preferred to walk in BIOM. Heart rate, inclined SACH, and inclined MSWS data were not available due to equipment failure and scheduling difficulties. Subject #6, a DER user, used the least metabolic energy in HIPOW, although heart rate was minimized and walking speed maximized in BIOM. This subject preferred BIOM on inclined ground but preferred DER on level ground.

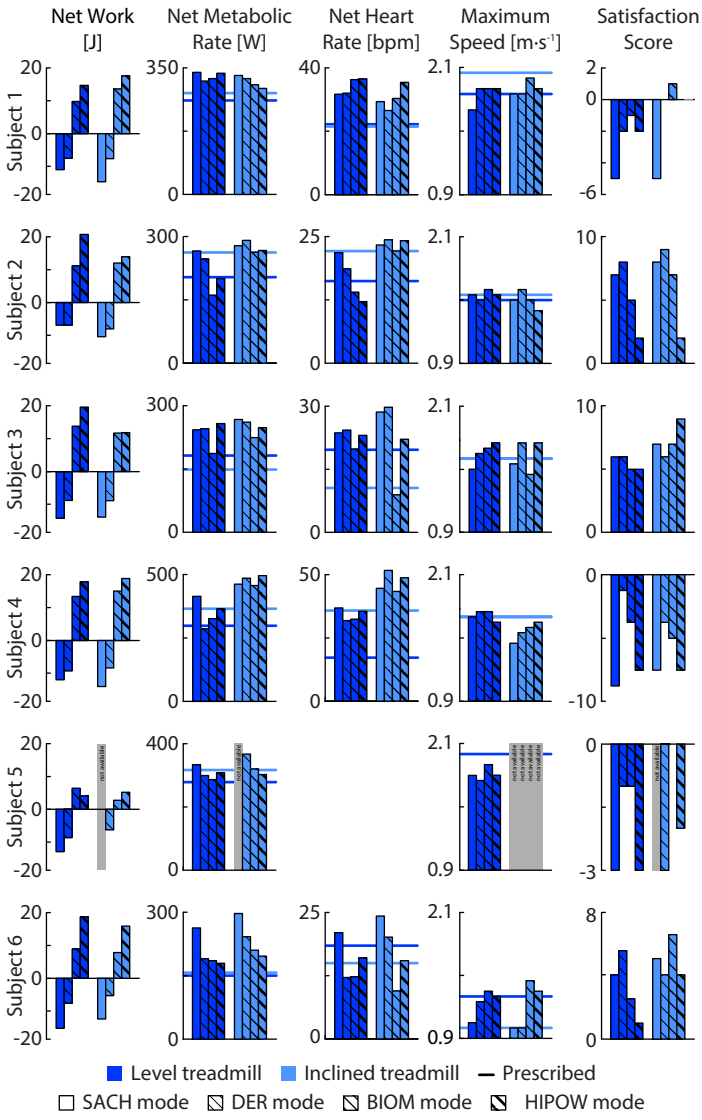

Figure 4.4: Walking performance outcome metrics listed for each subject across different emulator modes and two treadmill incline conditions. Hatching indicates different modes, colors indicate different inclines, and horizontal lines indicate reference measurements taken during a condition where the user walked with their prescribed prosthesis.

4.4 Discussion

4.4.1 Quality of Prosthesis Emulation

We demonstrated a haptic emulator that exhibited high-quality tracking of the ankle torque vs. angle relationships of an array of commercially-available prostheses. The emulator tracked the desired torque vs. angle relationships with average RMS error between 2 and 4% of the maximum ankle torque, depending on the mode (Fig. 4.3). The largest tracking errors were exhibited early in stance when torque was below 30 N·m and just after the transition from dorsiflexion to plantarflexion. Because of torque sensor noise and nonlinearities, motor position was held constant below a 30 N·m torque threshold, leading to reduced emulation quality in this region. In future versions we will improve sensor linearity and signal-to-noise ratio by, e.g., implementing a digital ankle encoder and reducing backlash in the series elastic actuator, or through the implementation of strain gauge sensing. The state-based torque vs. angle controller requires some plantarflexion velocity to be certain of the state transition from dorsiflexion to plantarflexion. Variability in the timing of this transition led to reduced emulation quality near the transition. In future versions we will eliminate this state distinction, instead emulating the ankle torque as a function of ankle velocity in addition to ankle angle. Iterative learning control improved torque tracking quality in BIOM but also introduced dynamics that are likely not exhibited by the BiOM® T2. Subjectively, we observed increased step-to-step variability and slow changes in device behavior as it adapted to the user's own slow changes. In future versions of the emulator system we will improve feedback control performance, through improved sensing and actuation as well as by implementing a derivative term in the feedback and improving the hardware to mitigate the deleterious effects of transmission friction and compliance.

We demonstrated successful emulation of different classes of device behavior, but it remains to be seen if the system demonstrated here can successfully differentiate subtle variations within device classes. The current emulator prototype can be programmed to exhibit such subtleties, but a controlled test of quality has yet to be performed. Most unilateral transtibial amputees are prescribed DER feet, so it would be useful if the emulator could differentiate brands, models, and configurations of prostheses, including variations in stiffness, damping, geometry, and weight. For robotic feet with programmable behavior, such as the BiOM® T2, device behavior should be optimized to ensure that prescription decisions are made using the best possible configuration of the emulated device for a given user. To this end, we are currently developing methods for automatic configuration of device behavior to maximize user benefit.

Subjects generally reported that the behavior of the emulator was similar to the devices that were being emulated, with some subtle differences that we will address in future versions. Two subjects had experience walking with a SACH foot. One reported: "[SACH mode was] stiff as a board! Felt just like my old leg and made it hard to walk fast." All subjects had extensive experience walking with DER feet, and all DER users reported that DER mode felt similar to their prescribed device. One subject reported: "This [DER mode emulation] is really good, I'll say my prescribed device is more comfortable, but just barely." The BiOM® T2 user reported that the DER mode felt most similar to his prescribed device, possibly because of the device's ability to be reconfigured to suit an individual's needs. This impression suggests that a fixed reference for BIOM emulation may be too simplistic, but also that this user may find a satisfactory balance of cost and performance with a DER prosthesis.

User feedback on the HIPOW mode demonstrated the emulator's utility as a tool for testing design ideas prior to physical implementation. All users found the HIPOW mode to be much too powerful during steady-state walking on a level treadmill, but

some commented that the additional power was useful during uphill and/or maximum speed walking. For example, one said "The high push-off is hard to control. The region of good places to put my foot is much smaller. If I put my foot in the wrong place I get a lot of push-off in the wrong direction." But, another comment identified benefits during inclined walking: "Push-off with [HIPOW mode] was way too much on the flat treadmill but just now [on the 5° slope] it felt helpful."

4.4.2 Limitations of the Scope of Emulation

Several aspects of prosthesis behavior were not considered in our emulation scheme, which could affect outcomes. We represented different devices by their stance-phase sagittal-plane ankle torque vs. angle relationship as measured in previously published amputee walking experiments. This common model of ankle behavior (Hansen et al., 2004; Shamaei et al., 2013) is limited as it contains only one degree of freedom, ankle plantar/dorsi-flexion, and does not consider the swing phase of gait. This model cannot fully predict the six independent components of force and moments that act on the user's residual limb.

We observed three main limitations of considering just saggital ankle angle in our emulation. First, to emulate the effect of varying foot length independent of joint impedance would require an additional degree of freedom to control the reaction forces independent of the reaction moment. Second, as one user reported, "Because [the emulator] is so stiff, I notice whenever I take a slightly off step. My prescribed foot is compliant in every direction so there's more room for error." In future versions of the emulator system we will characterize the complete force/torque-deflection characteristics of the different commercially available prostheses through amputee-independent benchtop tests (Major et al., 2011; Adamczyk et al., 2013) and through controlled walking trials. It is likely that including passive compliance in the structure of the prosthesis, comparable to what is provided by a DER prosthesis, will improve emu-

lation quality significantly. We are also exploring prosthesis designs with additional controlled degrees of freedom (Collins et al., 2015) to capture differences across device type. Third, robotic feet with programmable behavior, e.g. the BiOM® T2, need not exhibit the same ankle torque vs. angle behavior from one step to the next; their behavior can be a function of inputs other than ankle angle (Eilenberg et al., 2010). To better emulate the behavior of such systems we are developing emulations of device-specific high-level control schemes.

Ankle torque is typically not considered significant during swing, but adding mass to the foot increases metabolic energy consumption by about 9% per added kilogram (Browning et al., 2007), which suggests inertial and gravitational forces during swing are significant. Given that powered ankle-foot prostheses require extra mass for motors, batteries, and electronics, they tend to be about 1 kg heavier than passive prostheses, which would reduce our expectation for the energetic benefits of powered assistance strategies. Future versions of the prosthesis end-effector will be about 30% lighter, matching the mass of the lightest passive prostheses, and modular weights will be added to emulate candidate device mass.

Dorsiflexion torque at the beginning of stance during heel-only ground contact was provided by a passive heel spring, rather than through active control, in order to simplify the design of the emulator. Peak torque and energy absorption/dissipation are relatively small during this relatively short period of stance, so we believe this behavior to be less important than the primary stance phase behavior. However, future versions of the emulator will include active control of dorsiflexion torque to more completely characterize differences across device types.

4.4.3 Utility of Performance Metrics

We demonstrated a protocol for measuring users' walking performance across emulator modes that discerned individuals' needs using simple quantitative measures. All

unilateral transtibial amputees we tested appeared to benefit from robotic assistance strategies to some degree but with individual subject differences. The five DER users we tested appeared to have the potential for improved walking performance and satisfaction with a robotic prosthesis, but were never able to explore this option within the conventional prescription process. The BiOM® T2 user showed benefits from robotic assistance, but only when walking uphill, and always preferred walking in the passive modes. Despite having the good fortune of using the most sophisticated technology available, it is possible that the conventional prescription process falsely identified this individual as one who would benefit most from a robotic device. By exploring candidate device behaviors through haptic emulation, prosthesis prescriptions could be objectively justified and ensure that users reach an appropriate balance of cost and benefit.

Users' comments suggest that a variety of factors contribute to overall level of satisfaction with the various modes. In future protocols we will expand the subjective satisfaction assessment to address contributing factors such as perceived effort, stability, and pain.

While our subjects varied greatly in time since amputation and make and model of prescribed device, they were relatively homogeneous in K-Level, cause of amputation, and weight. We expect that users with lower K-Level, dysvascular amputation, and/or significantly higher or lower body weight could have different needs from the subjects tested here. We are currently recruiting individuals with more diverse medical histories and developing hardware to support a broader group of individuals for future tests of the emulator.

Acknowledgments

This material is based upon work supported by the National Institutes of Health under Award No. 1R43HD076518-01.

The authors thank Dr. Mary Ann Miknevich and Jonathan Akins for subject recruitment; Bambi Brewer for prosthesis emulator fitting; Hartmut Geyer for use of data collection equipment; Gordon Composites for leaf spring material; Julie Renkant, Roberto Jaime, and Anne Alcasid for interpreting reference data from literature; Roberto Quesada, Patrick Sumner, and Alec Assaad for hardware maintenance and assistance with experiments; and three anonymous reviewers for helpful feedback on the manuscript.

4.5 Additional discussion of future work

4.5.1 Customized emulations

Prosthetic devices, of all levels of complexity, are custom-tailored to some degree to suit the individual user. They incorporate adjustable-length pylons with pyramidal adapters that are adjusted to set the alignment of the prosthesis. Devices are selected based on shoe size and body-weight/activity level. Some devices have additional parameters, such as bumpers or wedges. Devices with hydraulic fluid have damping settings. Robotic devices, such the Proprio and BiOM, have software parameters that can be tuned. In future emulation of off-the-shelf feet, all of these aspects of behavior should be optimized prior to conducting the emulation comparison protocol to ensure that the user is experiencing the best possible version of each candidate device. Some of these parameters have nontrivial affects on torque vs. angle behavior, e.g. foot length, so these effects will need to be empirically identified, perhaps through

benchtop testing. This optimization could either be performed manually by a certified prosthetist, as per the conventional approach, or could be performed based on user-feedback as in Chapter 5.

4.5.2 Emulating robotic device control structures

Some robotic devices, such as the BiOM T2, do not exhibit fixed torque vs. ankle behavior because actuator commands are based on measurements of signals other than the kinematic state of the prosthesis. For such robotic devices, emulation would be best performed by copying the emulated device's high-level control architecture. Such control architectures are proprietary and would require collaboration with device manufacturers, who may be hesitant to share such information due to intellectual property concerns. Perhaps by providing manufacturers with a mechanism for implement their control code as a secured black-box module, such emulations could be feasible.

4.5.3 Measuring device behavior in-house

Emulating device behavior based on measurements reported in the literature is ultimately limiting since it is typically averaged across users and device types and literature data is not available for all devices. Therefore, in future work we will obtain an array of candidate prosthetic feet and characterize their torque vs. angle relationships through in-house benchtop characterization (Major et al., 2011; Adamczyk et al., 2013). This will involve fixturing the prosthesis, loading it with bodyweight, rotating the prosthesis about the ground plane, and measuring the reaction torque. This ideal torque vs. angle behavior is likely affected by, for example, off-axis behavior (e.g. stepping on a stone) and subject loading and range of motion (e.g. different bodyweights or walking speeds). Therefore it will be important for benchtop tests to resemble actual walking conditions as closely as possible. Also, with roughly 450

candidate devices to chose from, it will be important to first meaningfully categorize the different devices (perhaps by CMS L-Code) and pick representative examples for characterization. Ultimately, I hope to build a database of all available devices.

4.5.4 Improvements to end-effector comfort

To improve comfort and the accuracy of emulation, we will include greater off-axis passive compliance and damping in the structure of the end-effector. For example, during initial ground contact, the heel component of the prosthesis is more rigid than a typical shod foot, so we will modify the design of the end-effector to fit inside a conventional walking shoe. In Chapters 2 and 3, prosthesis emulator conditions were less preferable compared to normal walking conditions with users' prescribed feet by most measures. Learning is probably a significant cause, as users have much more experience with their prescribed feet than with the emulator, but perhaps this can also be partly explained by the lack of compliance and damping in the end-effector. Such improvements would improve all experiments that used the prosthesis emulator, as improving overall comfort could affect relationships between certain parameters and outcomes of interest.

4.5.5 Expanding the scope of emulation

The current emulator is limited to emulating the plantarflexion torque vs. angle relationship of candidate devices–other forces and kinematics are likely to govern the interactions between the user, their prosthesis, and the ground. An emulation approach that controls the full 3D forces and moments exerted by the device on the user as a function of the full state of the device would be more accurate than one which controls just ankle moment as a function of joint angle.

Unfortunately the independent measurement and control of each of these forces and moments would be quite complex, requiring a prosthesis with six actuated de-

grees of freedom. However, some relatively straightforward modifications might yield most of the potential benefits. The weight of the candidate devices could be emulated by lightening the prosthesis end-effector to the mass of the lightest conventional prosthetic feet and adding dead-weight to the end-effector. Adding inversion/eversion actuation (Collins et al., 2015) could capture the behavior of multiaxial feet, which are typically preferred by active users for their performance over uneven terrain. Actuating the heel segment of the prosthesis end-effector would capture the differences in how different prosthetic feet bear load upon leading leg ground impact. Finally, an adjustable-length toe component could better match the geometry of the emulator end-effector to the user's intact limb (as done in conventional prescription).

Chapter 5

User-optimal prosthesis design

The process of selecting from an array of off-the-shelf ankle-foot prosthesis could be superseded by custom prosthesis design. Because patients' and practitioners' time is limited, a custom design process would need to be rapid while also exploring a large-enough design space to ensure that all possibilities are considered. The experimental methods used in Chapters 2 and 3 are far too time-consuming, so we developed a new approach. We evaluated candidate device behaviors using only user-reported satisfaction–this outcome can be an order of magnitude quicker to asses than most alternatives, and includes a subjective measurement and weighing of many outcomes of interest. We demonstrate a procedure for the simultaneous optimization of three behavior parameters, which is sufficient to optimize the behavior of a typical passive-elastic ankle-foot prosthesis. In clinical practice, the resultant behaviors from such a process could then be sent to device manufacturers for the manufacture of user-optimal custom prostheses.

The contents of this chapter have not been previously published, but will appear in:

Caputo, J. M., Adamczyk, P. G., Collins, S. H. (2015) Optimization of ankle-foot prosthesis behavior to maximize patient-specific performance outcome metrics, **in preparation**.

This work will be presented at:

Caputo, J. M., Adamczyk, P. G., Collins, S. H. (2015) Optimizing prosthesis design to maximize user satisfaction using a tethered robotic ankle-foot prosthesis. *Dynamic Walking*.

Abstract

Imperfect matching of prosthesis design to users' needs likely contributes to the reduced walking ability and quality of life endured by lower-limb amputees. Conventional design methods rely on observational data from general populations to inform design. We demonstrate a method that instead optimizes prosthesis design to the needs of individual users. Using a tethered robotic prosthesis, users systematically explore a parameterized design space that encompasses the scope of behaviors which can be provided using conventional passive-elastic materials. Exploration of the design space is guided by users' verbal cues, provided during steady-speed walking on a treadmill. We demonstrate that this approach results in designs which are on-average preferred to common alternative design guidelines. Optimal personalized design parameters determined through such a process could be recommended to prosthetists and manufacturers for physical implementation in a mobile device for daily use. This approach could eliminate uncertainty in device prescription, thereby reducing waste and conflicts with payers, as well as improving patient-specific locomotion outcomes.

5.1 Introduction

5.1.1 State-of-the-art design and prescription

About 630,000 people in the United States have a major lower-limb amputation, and prevalence is rising (Ziegler-Graham et al., 2008). The use of prosthetic limbs following amputation, as prescribed using current practices, tends to result in reduced walking ability, satisfaction, and quality of life compared to non-amputees (Miller et al., 2001; Hagberg and Brånemark, 2001; Zidarov et al., 2009). Some of the functional limitations experienced by amputees are likely caused by imperfect device behavior.

Prosthetic devices are typically designed according to low-level objectives, such

as mimicking the kinematic time-trajectory (Herr and Wilkenfeld, 2003; Au et al., 2005; Hitt et al., 2007), kinetic time-trajectory (Eilenberg et al., 2010; Versluys et al., 2009b), joint impedance (Au et al., 2006; Cherelle et al., 2012; Sup et al., 2008), or rollover shape (Hansen et al., 2000), of the biological ankle-foot. Devices are optimized to achieve these objectives either through hand tuning (Hitt et al., 2007; Cherelle et al., 2012; Huang et al., 2014) or, particularly in the case of robotic devices, through off-line numerical optimization (Herr and Grabowski, 2012; Herr and Wilkenfeld, 2003; Au et al., 2005; Versluys et al., 2009b; Au et al., 2006; Sup et al., 2008). In either case, it is unclear if these low-level design objectives translate into desirable high-level outcomes such as reduced walking effort or improved balance. A design optimization system in which high-level outcomes were instead the objective, with low-level behaviors a means to those outcomes, might more effectively achieve favorable high-level outcomes.

Clinicians adjust the behavior of off-the-shelf prostheses based on subjective observation of an individual's gait in an attempt to optimize these high-level outcomes. In the case of conventional passive-elastic devices used by most amputees, several physical features, such as the length and stiffness of keel components, can be chosen to match the foot's behavior to an individual's needs. Modest variations in these properties can give rise to large changes in functional outcomes for an individual, such as energy cost or user satisfaction (Adamczyk et al., 2015; Klodd et al., 2010; Lehmann et al., 1993). Such parameters are typically selected on the basis of body weight, height, and self-reported activity level, without iterative testing (Michael and Bowker, 2004). When testing is performed during prescription, it is typically limited to subjective comparison of a few different models or iterations of a given model–a process that is inefficient, poorly controlled, and narrow in scope. Recently developed robotic devices offer additional features for improved performance over passive feet and are gaining popularity (Schwartz, 2013), but their complexity also makes identify-

ing optimal parameters even more challenging. These prostheses have a large number of software control parameters that affect device behavior (Eilenberg et al., 2010), creating a high-dimensional design space. Very little of this space can be explored through hand tuning. As with passive devices, the responses of individual users vary widely (Herr and Grabowski, 2012; Esposito et al., 2015), and small changes in parameters have large and disparate effects across individuals (Quesada et al., 2015). Given individual differences in physiology, motor control, and gait coordination patterns, this current prescription approach is unlikely to achieve any patient's optimal gait. A means of systematically identifying the optimal device behavior for each individual person could dramatically improve this process and improve mobility outcomes.

5.1.2 Alternative approaches

Computational models might eventually be used to optimize prosthesis designs, but are as yet inadequate for the task. Simple dynamic walking models and joint-level models based on robotics concepts make incorrect predictions about basic mechanical and energetic outcomes of prosthesis function (Quesada et al., 2015; Caputo and Collins, 2014b; Malcolm et al., 2015). Forward-dynamic neuromuscular models with subject-specific parameters might eventually allow rapid computational optimization of device function (Thelen and Anderson, 2006; Fey et al., 2013; Song et al., 2013; Laprè et al., 2014), but as yet are not able to accurately estimate muscle activity even when resulting biomechanical performance data are already available (Fregly et al., 2012). Even simple empirically-derived walking models may not predict responses across populations (Zelik et al., 2011) or for individual users (Quesada et al., 2015; Caputo and Collins, 2014b; Malcolm et al., 2015). Though these modeling approaches will undoubtedly advance, determining subject-specific values of crucial parameters, such as muscle cross-sections or moment arms, will remain challenging in a clinical environment due to inter-subject variability, especially for damaged limbs. Models

inspire qualitative device designs, but optimization of device features through experimentation seems a more plausible means of improving clinical prosthesis prescription.

Some individualized prosthesis design optimization techniques have been demonstrated in the past, but these address only low-level mechanical parameters rather than functional outcomes. For example, Herr et al. (Herr and Wilkenfeld, 2003) used iterative tuning of impedance to maintain desired peak knee flexion during walking. This is useful, but requires knowledge of the values mechanical parameters, e.g. peak flexion, which maximize benefit for a given individual. Directly optimizing functional outcomes would have greater impact.

5.1.3 Functional outcomes

There are many possible optimization criterion, and it is likely that the choice of criterion will have an effect on the efficiency of the optimization. The subject's energy consumption, walking speed, stability, and pain are each examples of relevant criteria. Some criteria are time-consuming to measure, which puts practical limits the scope of search within a single session, while others are difficult or even impossible to objectively measure. And, it is unclear how to appropriately combine these different criteria for use in design optimization–it is likely that the weightings in this combination depend on the subject. "User satisfaction" includes a subjective combination of different relevant criterion, such as perceived effort and stability, comfort, and symmetry.

Satisfaction is rapid to assess, which makes it an attractive optimization criterion for design optimization, but it is not without limitations. Due to learning effects, users' perception of optimal behavior is likely to drift, so design optimization should be repeated over time to demonstrate that such learning has stabilized. Because of this drift and imprecision in users' feedback, we found absolute measurements of user satisfaction to be less reliable than relative scores.

5.1.4 Our approach

We propose a rapid, empirically-driven process to identify ankle-foot prosthesis behavior that maximizes user satisfaction. In this approach, candidate behaviors are rapidly implemented using a universal ankle-foot prosthesis emulator (Caputo and Collins, 2014a). Behavior is systematically adjusted according to users' verbal cues during steady-speed treadmill walking. We hypothesize that A) such a system can rapidly identify user-optimal prosthesis design parameters and that B) this optimized behavior will be user-preferred compared to common design alternatives. We conduct an experimental test of the concept, considering a 3-dimensional design space which includes behaviors exhibited by most conventional dynamic elastic response (DER) ankle-foot prostheses.

5.2 Methods

5.2.1 Prosthesis design optimizer overview

Passive-elastic ankle-foot prosthesis behavior was optimized through a series of treadmill walking tests and validated against common alternative designs. Subjects walked while wearing a universal ankle-foot prosthesis emulator (Caputo and Collins, 2014a) which was programmed to provide the experience of candidate behaviors. The emulator system is comprised of a lightweight ankle-foot prosthesis which is actuated and controlled through a flexible tether by a powerful servomotor and real time controller (Fig. 5.1). During optimization, device behavior was systematically varied according to users' verbal cues while they walked. To test the efficacy of the proposed method, we validate the resultant optimized behavior against common alternative design targets.

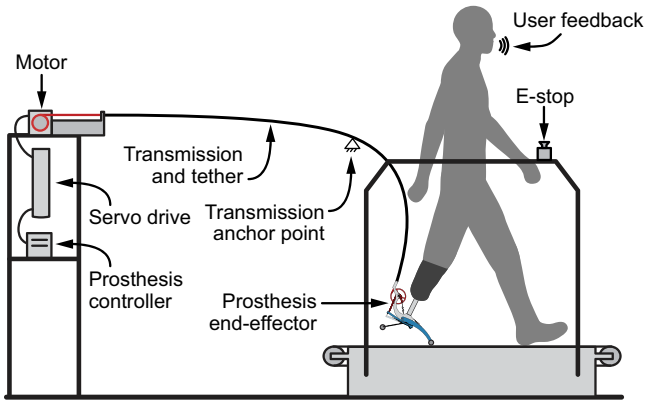

Figure 5.1: Schematic of ankle-foot prosthesis emulator system. The user walks on a treadmill while wearing a lightweight ankle-foot prosthesis which is powered through a flexible tether to a high performance actuation and control system. In the optimization phase, user feedback provides verbal cues to guide design optimization. In the validation phase, user feedback is used to compare the optimized behavior against standard design alternatives.

5.2.2 Control of prosthesis behavior

The prosthesis provides torque-controlled ankle plantarflexion while a passive-elastic heel section provides dorsiflexion torques early in stance (Caputo and Collins, 2014a). Ankle plantarflexion is controlled as a function of ankle angle, emulating the behavior of a nonlinear spring. Desired ankle torque (τ_{des}) is controlled as a function of ankle angle (θ) according to:

$$\tau_{des} = K \cdot \tau_{recip}(\theta - \theta_0) \text{ where } \tau_{recip} = \frac{c_1}{(\theta - \theta_0) - c_2} + c_3 \tag{5.1}$$

The nature of this spring-like behavior is adjusted in three ways (Fig. 5.2): the alignment of the nonlinear spring (θ_0), the overall stiffness of the spring-like behavior (K), and the nonlinear shape of the spring ($c2$) ($c1$ and $c3$ are determined from $c2$ by constraint). The effect of adjustments to stiffness, alignment, and shape are independent of each other, as visualized in Fig. 5.2. Nominal operating parameter values (stiffness of 1, alignment of 0, and shape of 1.8) are chosen to match a typical non-amputee's ankle torque-angle curve at the same walking speed.

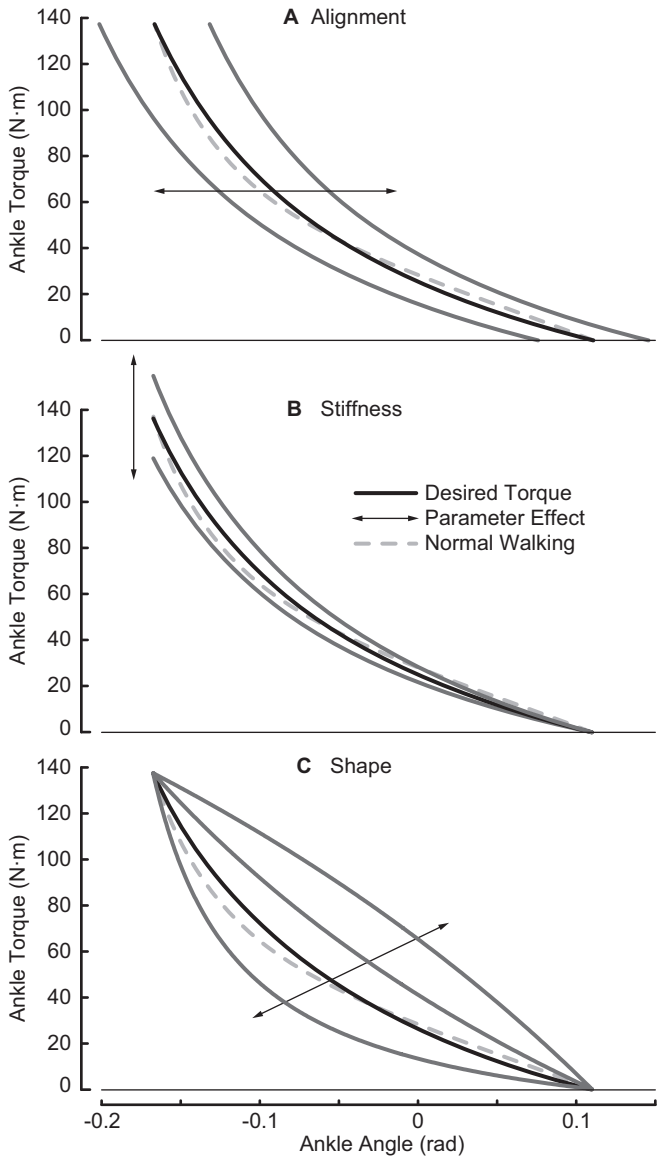

Figure 5.2: Three aspects of ankle-foot prosthesis behavior are adjusted in the design optimization system. These parameters control aspects of the ankle torque vs. angle relationship exhibited by the prosthesis emulator. **A** Alignment, an angular shift in the resting point of the joint's virtual spring. **B** Stiffness, a scaling of the stiffness of the joint's virtual spring. **C** Shape, a parameter that controls the non-linearity of the virtual spring without changing the endpoints.

5.2.3 Optimization

Prosthesis behavior parameters were optimized through three successive parameter optimizations wherein each parameter was adjusted in isolation. The order of parameter optimizations was randomized for each subject. Optimization was performed according to the following procedure:

1. The experimenter adjusted Parameter 1 incrementally, once per stride.

2. The user was instructed to inform the experimenter when they noticed a decrease in their level of satisfaction with the device behavior.

3. Upon receiving 'worsening' feedback, the experimenter reversed the direction of adjustment, began again with Step 1, and repeated the process three times.

4. Upon reaching the final reversal, the optimal parameter value was taken to be the midpoint between the nearest reversals in search direction.

5. The experimenter then moved on to Parameter 2, and then Parameter 3, beginning each time with Step 1.

The magnitude of incremental adjustment depended on the parameter and subject such that once per stride adjustments were barely perceptible but the worsening threshold was reached after roughly 10 strides.

Some parameters were observed to have coupled effects on satisfaction during pilot tests with some users, so the above procedure was repeated five times to ensure convergence to the globally optimal parameter values. The order of parameter optimizations remained consistent across repetitions. The initial search direction was switched with each repetition. Initial parameter values were randomly selected for the first repetition, and then updated with the most recently measured optimal value for subsequent trials (as in hill climbing (Russell and Norvig, 2003)). The final optimal

value of each parameter was taken to be the mean of optimal parameter values from each trial, with values lying outside of one standard deviation of the mean considered outliers and ignored.

In pilot testing, it was observed that linearly varying $c2$ had a highly non-linear effect on user satisfaction. Therefore, the integral of τ_{recip} was computed as a function of $c2$ (referred to as $\int$ Shape) and was used as a surrogate for $c2$. Thus, $\int$ Shape was linearly varied, leading to non-constant steps $c2$.

5.2.4 Validation

The resultant optimized behavior (OPT) was then validated against alternative device behaviors during through an additional set of walking trials. Alternative behaviors mimicked four typical reference conditions: an average healthy ankle (NORM), the user's prescribed prosthesis (PRE, a dynamic elastic response prosthesis), the user's intact ankle (INT), and an average solid ankle cushioned heel prosthesis (SACH). Reference data for the NORM and SACH conditions came from previously reported walking data ((Caputo and Collins, 2014b) and (Torburn et al., 1990) respectively). Reference data for PRE and INT conditions was measured by inverse dynamics analysis.

These different behaviors were compared based marks made by the user on a paper Likert Scale (Likert, 1932) ranging from "walking is impossible" to "walking is effortless", where the center of the scale was indicated to be "similar to my prescribed prosthesis". These marks were quantified by measuring the distance of each mark from the center of the scale. This process was repeated across three trials and the order of conditions was randomized in each trial. Data are reported as mean $\pm$ standard deviation across the three trials.

5.2.5 Experimental methods

Three unilateral transtibial amputees (N = 3, male, traumatic, 186 lb, aged 41.7 yr, 12.5 yr since amputation) participated in the experimental test of the design optimization procedure. Subjects walked on a level treadmill at 1.25 $m \cdot s^{-1}$ during both the optimization and validation components of the experiment. The protocol was repeated across three days with data reported on the final day.

5.3 Results

Optimal parameter values varied across subjects. For Subject 1, optimal parameter values were 1.15±0.05, 0.105±0.002, and 3.58±0.15 (for stiffness, alignment, and shape, respectively). For Subject 2, optimal parameters were 1.47±0.03, 0.0385±0.0111, and 2.28±0.02. And for Subject 2, optimal parameters were 1.20±0.09, -0.0212±0.0111, and 3.25±0.40. Representative raw optimization data is provided for Subject 1 in Figure 5.3. Standard deviation is indicative of random error, not drift in users preference–optimized values typically stabilized over the course of the five trials.

Each subject's optimized ankle torque vs. angle relationship appears in Figure 5.4.

Subjects 1 and 2 preferred the optimized behavior, while Subject 3 rated the behavior second best to the behavior which emulated their prescribed prosthesis (Fig. 5.5). Paired t-test p-values for these comparisons were 0.133, 0.000, and 0.018, for Subjects 1 through 3, respectively. Subject 2 completed completed only 2 of the 3 validation trials, however, due to scheduling constraints.

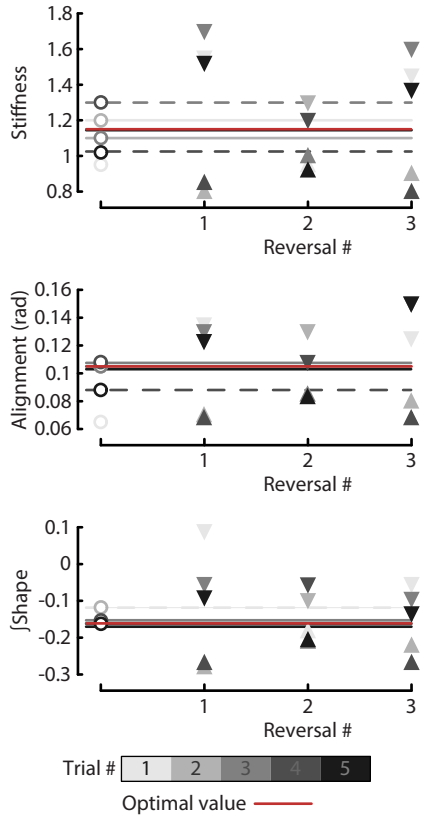

Figure 5.3: Optimization of the stiffness, alignment, and shape parameters for a representative subject over the course of five trials, each with three reversals of the parameter search direction. Open circles indicate initial conditions for each parameter at the start of the trial. Triangles indicate value at which subjects indicated behavior was worsening and direction of parameter change after reversal. Optimal parameter values were taken to be the mean optimal value measured across the five trials (horizontal lines), with outliers ignored (dashed lines).

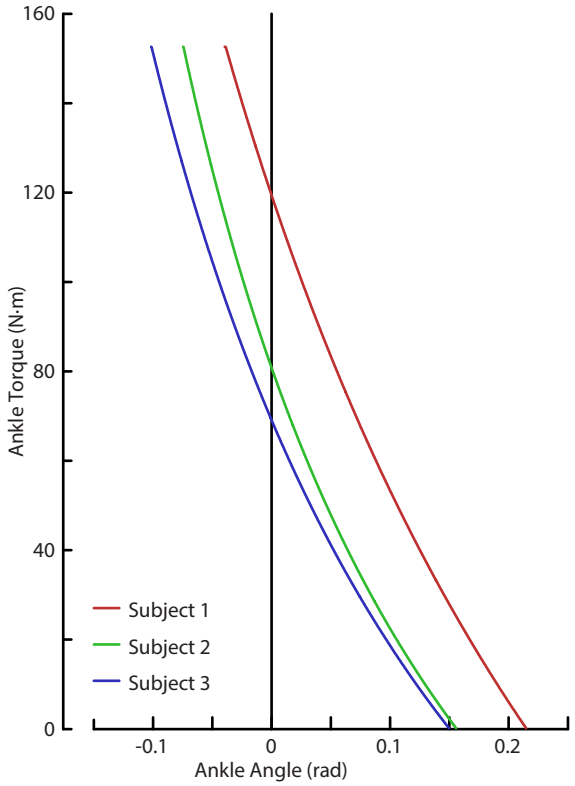

Figure 5.4: The optimized ankle torque vs. angle relationship for each subject. Colors indicate different subjects and correspond to Figure 5.3.

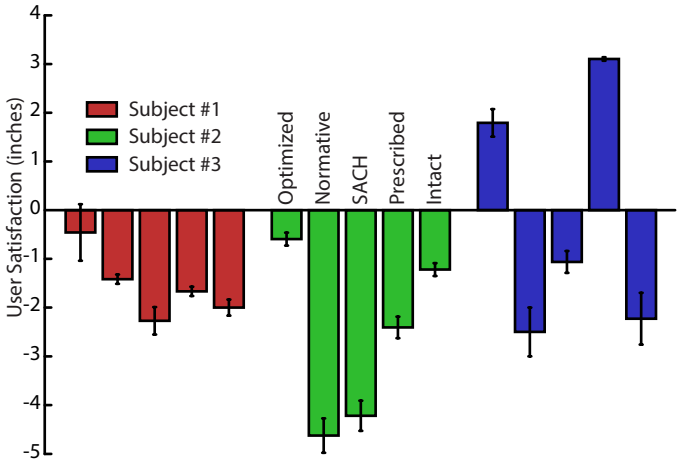

Figure 5.5: Comparison of the effect of candidate prosthesis behaviors on subject's subjective satisfaction. Data are plotted on a scale where 0 indicates that the behavior is as comfortable as walking with the subject's prescribed prosthesis, positive numbers indicate the behavior is more comfortable that the prescribed prosthesis, and negative numbers indicate that it is less comfortable. Data are averaged across three trials. Colors indicate different subjects and correspond to Figure 5.4.

5.4 Discussion

5.4.1 A new approach to design and prescription

The demonstrated design optimization approach differentiates users based on their subjective needs and results in designs that are on-average user-preferred over typical design alternatives. The reported optimal designs could be implemented physically using conventional means in clinical practice–prosthetists could send user-optimized specifications to device manufacturers for fabrication into user-customized prostheses. Such an approach could address longstanding uncertainty in both the design and the prescription of prosthetic limbs.

5.4.2 Interpretation of optimal parameter values

Ankle-foot prostheses are typically prescribed and customized based on simple observations, clinicians' intuition, and user feedback. We proposed that these processes are unlikely to result in user-optimal designs and that a empirically-driven design optimization process could result in designs that are user-preferred compared to conventionally-designed behaviors. We optimized three aspects of device behavior based on user feedback, and some aspects of the optimized behaviors were not as one might expect. Given the small sample size and lack of quantitative outcome measures, such as subjects' metabolic energy consumption, we cannot mechanistically explain these results, so we suggest further exploration of stiffness, alignment, and shape through 1- or 2-D parameter sweep studies using a full suite of biomechanical analyses. It is apparent, however, that the proposed method is a practical means of differentiating users based on their subjective needs.

Individuals with higher body mass and/or activity level are typically prescribed stiffer prosthetic feet. Perhaps this practice is a result of the observation that the

stiffness of the biological ankle joint scales roughly with body mass. The biological ankle joint torque vs. angle relationship is often reported normalized to body mass, which makes the implicit assumption that the joint stiffness scales linearly with body mass (Hansen et al., 2004). Our results suggest that, while user-preferred stiffness appeared to roughly scale with body mass, this practice may result in suboptimal device behavior for some individuals, as the lightest subject tested did not have the lowest preferred stiffness.

Prosthetists typically set alignment by observing subjects' symmetry during standing and a brief bout of walking. In this study, mechanical alignment was set by a certified prosthetist before optimization. However, subjects preferred alignments that differed by as much as 6^{deg} from the default setting. This result could suggest a limit for the resolution with which a prosthetist is able to optimize alignment.

The shape of the torque vs. angle relationship of the ankle joint is not typically advertised by manufacturers or adjustable by prosthetists. All subjects distinctly preferred a shape that was more linear than the shape observed in the normal walking reference data. This result might suggest yet another example of inconsistency between biological mimicry and user optimality.

5.4.3 Choice of optimization scheme

The demonstrated design optimization procedure appears to be well-suited for optimizing a 3-dimensional parameterization of prosthesis behavior on the basis of user satisfaction, but other methods may be more efficient, enabling searching in larger design spaces, or more appropriate for other optimization criteria.

In our first attempt to optimize design for user satisfaction we performed a grid search optimization, where users provided absolute measures of their level of satisfaction on a scale of -10 to 10 for each behavior. We fit a quadratic model, with and without interaction terms, to these responses and took the optimized behavior to be

that which corresponded to the minimum of this fit model over the range of the grid search. We observed that the approach was unreliable, given considerable measurement noise and drift in subjects' absolute scale reference point over time. For other optimization criterion where outcome measure are more reliable, e.g. metabolic rate, the grid search method could be effective and would provide the added bonus of generating a mathematical model of the design landscape. In such an approach, Design of Experiments techniques could improve efficiency by strategically omitting points in the grid based on known characteristics of the model being fitted (Taguchi et al., 2004). If such absolute measurements were possible, it would also be possible to utilize gradient-based optimization methods, such as Gradient Descent, which could be more efficient since they avoid sampling the entire design space by locally estimating the gradient and searching for the optimum in the direction of the gradient.

An alternative to absolute measures of satisfaction is to make pairwise comparisons across sets of parameter values. In such an approach, the experimenter would ask users if the current behavior was "better or worse" than the previous behavior. As in the grid search approach, a quadratic model of satisfaction could be built based on such data, for example, as in an Ordinal Support Vector Machine (Herbrich et al., 1999). This approach is attractive since pairwise comparisons are likely to be more reliable (less subject to drift) than absolute satisfaction scores, but it is unclear if they will be reliable enough to build a model of the design space. Again, a local search method could avoid sampling the entire design space. Though the gradient cannot be measured absolutely with pairwise comparisons, the pairwise comparison provides the sign of the gradient. This is the strategy employed in the routine subjective refraction procedure used in the clinical practice of determining optimal eyeglass parameters with a phoropter (Kurtz and Carlson, 2003). The method we employed to optimize prosthesis behavior works in this way but instead of asking "better or worse" and computing the sign of the gradient accordingly, we ask users to estimate the sign of

the gradient directly. Regardless of the technique, a methodology for systematically searching the space is required. Perhaps the simplest is univariate search, where parameters are independently adjusted sequentially. This process can be repeated indefinitely in an attempt to converge to the optimal design (as in the method we employed), though in some cases, for example optimizing eyeglass parameters (Kurtz and Carlson, 2003), one pass through the different parameters is deemed sufficient. Alternatively, a method such as Powell's Conjugate Direction Method could be used to update the direction of search according to the direction that the optimized behavior moves across trials (Powell, 1964). Such a method could reduce the number of trials required to reach the global optimum.

5.4.4 Effects of adaptation

Humans exhibit adaptation dynamics in response to novel lower-limb assistive devices on timescales ranging from minutes to days, weeks, and even years (Gordon and Ferris, 2007; Kent et al., 2015). The demonstrated method for optimizing device behavior presents users with a continuum of different behaviors and provides just seconds of experience with any single behavior. Thus, the behaviors that result from the demonstrated design optimization method could be suboptimal over longer timescales, despite appearing optimal over short timescales.

Design optimization could conceivably be performed across longer timescales but would be limited in scope by the practical considerations such as the time that practitioners' and patients' are willing to spend on design optimization. Anecdotally, users struggle to compare levels of satisfaction across different behaviors on longer time scales and become confident of their perception of satisfaction after just several strides with a particular behavior. The balance of these trade-offs will likely differ for different optimization criteria. Optimized behavior does not appear to systematically drift across trials in tests conducted so far. For the three subjects tested here, design

optimization was repeated across three days; optimized behavior changed considerably from Day 1 to 2 but appeared roughly consistent from days 2 to 3, which is consistent with previous work (Chapters 3 and 4, (Gordon and Ferris, 2007)). In our follow-up to the push-off work magnitude experiment with amputee subjects, we repeated the experimental protocol across 10 days for one subject and observed consistency across days 2 to 10 (Quesada et al., 2015). We do expect that as users adapt to a novel customized prosthesis over the scale of weeks, months, and years since their neural coordination and physiology will change. Thus, repeating the design optimization process weekly, monthly, or yearly (standard practice in optimization of eyeglass parameters) would likely be beneficial.

5.4.5 Choice of outcome measures

User satisfaction is but one of many possible design optimization objectives, and it is unclear which objectives are most appropriate. Effort related measures, such as metabolic rate or heart rate, could be measured in real time to discover behaviors that minimize walking effort (Felt et al., 2014). Other outcomes such as maximum walking speed, stability, comfort, or muscle activity might also be measured rapidly and used as inputs to a design optimization scheme. It is likely that some combination of these outcomes are relevant to the quality of life of amputees, but it is unclear what weighting of these outcomes is most appropriate. We expect that users' own subjective weighting of these factors is relevant to their overall quality of life, but alternative weightings, such as that of the user's prosthetist, might also be worth consideration.

5.4.6 Platforms for design optimization

The tethered robotic ankle-foot prosthesis used here is a versatile platform for design optimization, but the approach could also be applied using different types of devices. Behavior of mobile prostheses with easily swappable components (Adamczyk et al.,

2013) or programmable behavior (Eilenberg et al., 2010) could be similarly optimized. These devices have more limited capabilities, but would allow design optimization to occur during activities and over time scales that are not feasible with a tethered device (e.g. walking throughout a user's home over the course of a normal day). Design optimization through computer simulation is another promising approach (van Dijk and van der Kooij, 2013), but it is not yet clear if mathematical models can accurately predict an individual's response to changes in device behavior.

5.4.7 Other parameters to optimize

The demonstrated approach could be extended in many ways, e.g. a parameter that encodes net work provided by the prosthesis could be added to explore the potential benefits of providing a particular user with a powered prosthesis. In a clinical setting, including such a parameter could help reduce uncertainty in determining users who will benefit from expensive robotic devices, helping to realize the promise of next-generation prosthetic technology, and help manufacturers to appropriately size motor and battery components in these robotic devices. Adding parameters to the demonstrated optimization approach increases the duration of the optimization process. In the experiment described here, one session of optimization spanned approximately 1 hr. Refinements to the process could likely reduce this time to 0.75 hr. Some parameters are likely decoupled, especially for certain subjects, which would allow optimization to be split across multiple sessions.

Chapter 6

Summary of conclusions

Robotic prostheses are a promising solution to the reductions in walking performance experienced by lower-limb amputees (Herr and Grabowski, 2012; Esposito et al., 2015; Zelik et al., 2011), but it is unclear which aspects of their behavior are most important to improving outcomes and which users will derive enough benefit to justify the increased costs associated with robotic technology. Motivated by the limitations of physically prototyping mobile prostheses, I developed a new experimental approach to the design and prescription of prosthetic legs, which utilizes a novel high-performance tethered robotic ankle-foot prosthesis emulator.

First, I demonstrated that this tethered prosthesis is the lightest, most powerful, and most responsive robotic lower-limb assistive device to date (Caputo and Collins, 2014a). The key to these achievements is the use of a powerful off-board electric motor and real-time control system which actuates a simple, lightweight prosthesis end-effector through a flexible Bowden cable transmission. This device introduces a new paradigm of systematic human experimentation. In this approach, prosthesis behaviors can be quickly implemented in software, rather than through time-consuming physical prototyping. This thesis focuses on the design and prescription of ankle-foot prostheses, but the system can be re-purposed with relative ease for experimentation with knee prostheses, or ankle, knee, and hip exoskeletons. All of these applications are currently being pursued at the Carnegie Mellon University's Experimental Biomechatronics Laboratory. Though this approached had been conceived of decades

ago (Flowers and Mann, 1977), the work described in this thesis seems to have rekindled interest in the approach and several other laboratories across the United States have begun to explore this new experimental paradigm.

I then conducted an experimental test of the simple dynamic walking model prediction that providing net-positive prosthetic ankle push-off work would lead to reduced leading limb collision losses, improved gait efficiency, and reduced metabolic rate (Kuo and Donelan, 2010). I found that increasing ankle push-off reduced metabolic energy consumption during walking, but that simple dynamic walking models do not accurately predict the cause (Caputo and Collins, 2014b; Malcolm et al., 2015; Esposito et al., 2015). Metabolic reductions seemed primarily associated with reductions in prosthesis-side hip power during push-off and early swing, which has been associated with initiation of leg swing (Fox and Delp, 2010; Lipfert et al., 2014). Furthermore, other recent research has shown that not all amputees benefit from increased ankle push-off work (Quesada et al., 2015; Caputo et al., 2015), and even that not all amputees experience greater metabolic energy consumption during walking (Esposito et al., 2014). While there must be a mechanistic explanation for these mixed results, it appears that current mathematical models of human walking cannot predict these differences across individuals.

In lieu of models that can make such predictions, individualized empirical approaches to designing prosthesis behavior may provide practical solutions to the uncertainty faced in the design and prescription of current commercially-available prosthetic limbs. Based on the hardware and methodologies I had developed thus far, I developed two novel empirical processes for individualized prosthesis design and selection. First, I demonstrated an approach wherein the behavior of off-the-shelf prostheses was emulated in order to give patients the opportunity to test-drive candidate devices prior to purchase. I show that the optimal device selection is highly depended on the individual, the choice of outcome measures, and walking conditions

(Caputo et al., 2015). This suggests that it would be beneficial to include a greater degree of experimentation in the prescription process. I also demonstrate an approach that supersedes the need for selection, by designing user-customized prostheses from scratch. In this approach, device behavior is systematically varied while the user walks to discover behaviors which maximize user-reported satisfaction. I demonstrate that a simple univariate search can rapidly optimize a clinically-relevant three-parameter design space, and that users prefer optimized designs compared to designs based on other common design targets. This process generates a blueprint that could be used for the manufacture of a customized mobile prosthesis, which is likely to be more satisfying than an off-the-shelf device. These individualized procedures are promising approaches to improving the quality of prescription and the likelihood that payers will be convinced to reimburse prosthetists for the purchase of more sophisticated robotic prostheses. I demonstrated the efficacy of these methods in pilot studies, and am currently working towards larger-scale double-blind validation and clinical deployment.

Bibliography

Abul-Haj, C. J. and Hogan, N. (1987). An emulator system for developing improved elbow prosthesis designs. *IEEE Transactions on Biomedical Engineering*, 34(9):724–37.

Adamczyk, P. G., Collins, S. H., and Kuo, A. D. (2006). The advantages of a rolling foot in human walking. *The Journal of Experimental Biology*, 209(20):3953–63.

Adamczyk, P. G., Roland, M., and Hahn, M. E. (2013). Novel method to evaluate angular stiffness of prosthetic feet from linear compression tests. *Journal of Biomechanical Engineering*, 135(10):104502.

Adamczyk, P. G., Roland, M., and Hahn, M. E. (2015). Sensitivity of biomechanical outcomes to independent variations of hindfoot and forefoot stiffness in foot prostheses. *Human Movement Science*, **in review**.

Agarwal, G. C. and Gottlieb, G. L. (1977). Oscillation of the human ankle joint in response to applied sinusoidal torque on the foot. *The Journal of Physiology*, 268(1):151–76.

Andersen, J. B. and Sinkjaer, T. (1995). An actuator system for investigating electrophysiological and biomechanical features around the human ankle joint during gait. *IEEE Transactions on Rehabilitation Engineering*, 3(4):299–306.

Anderson, F. C. and Pandy, M. G. (2001). Dynamic optimization of human walking. *Journal of Biomechanical Engineering*, 123(5):381–90.

Aoyagi, D., Ichinose, W. E., Harkema, S. J., Reinkensmeyer, D. J., and Bobrow, J. E. (2007). A robot and control algorithm that can synchronously assist in naturalistic motion during body-weight-supported gait training following neurologic injury. *IEEE Transactions on Neural Systems and Rehabilitation Engineering*, 15(3):387–400.

Au, S. K., Bonato, P., and Herr, H. M. (2005). An EMG-position controlled system for an active ankle-foot prosthesis: an initial experimental study. *Proceedings of IEEE International Conference on Rehabilitation Robotics*, pages 375–9.

Au, S. K., Dilworth, P., and Herr, H. M. (2006). An ankle-foot emulation system for the study of human walking biomechanics. *Proceedings of IEEE International Conference on Robotics and Automation*, pages 2939–45.

Au, S. K. and Herr, H. M. (2008). Powered ankle-foot prosthesis. *IEEE Robotics & Automation Magazine*, 15(3):52–9.

Au, S. K., Weber, J., and Herr, H. M. (2007). Biomechanical design of a powered ankle-foot prosthesis. *Proceedings of IEEE International Conference on Rehabilitation Robotics*, pages 298–303.

Barr, A. E., Siegel, K. L., Danoff, J. V., McGarvey, C. L., Tomasko, A., Sable, I., and Stanhope, S. J. (1992). Biomechanical comparison of the energy-storing capabilities of SACH and Carbon Copy II prosthetic feet during the stance phase of gait in a person with below-knee amputation. *Physical Therapy*, 72(5):344–54.

Barth, D. G., Schumacher, L., and Thomas, S. S. (1992). Gait analysis and energy cost of below-knee amputees wearing six different prosthetic feet. *Journal of Prosthetics and Orthotics*, 4(2):63–75.

Bawa, P. and Stein, R. B. (1976). Frequency response of human soleus muscle. *Journal of Neurophysiology*, 39(4):788–93.

Bertram, J. E. A. and Gutmann, A. (2009). Motions of the running horse and cheetah revisited: fundamental mechanics of the transverse and rotary gallop. *Journal of the Royal Society of London: Interface*, 6(35):549–59.

Bhounsule, P. A. (2012). A controller design framework for bipedal robots: trajectory optimization and event-based stabilization. *Dissertation*, pages 1–172.

Brockway, J. M. (1987). Derivation of formulae used to calculate energy expenditure in man. *Human Nutrition, Clinical Nutrition*, 41(6):463–71.

Browning, R. C., Modica, J. R., Kram, R., and Goswami, A. (2007). The effects of adding mass to the legs on the energetics and biomechanics of walking. *Medicine and Science in Sports and Exercise*, 39(3):515–25.

Bruijn, S. M., Meijer, O. G., Beek, P. J., and van Dieën, J. H. (2010). The effects of arm swing on human gait stability. *The Journal of Experimental Biology*, 213(23):3945–52.

Budynas, R. G. and Nisbett, J. K. (2011). *Shigley's Mechanical Engineering Design*. McGraw-Hill, New York, 9th edition.

Burse, R. L., Pandolf, K. B., and Goldman, R. F. (1979). Physical conditioning of sedentary young men with ankle weights during working hours. *Ergonomics*, 22(1):69–78.

Byl, K. and Tedrake, R. (2008). Approximate optimal control of the compass gait on rough terrain. *Proceedings of IEEE International Conference on Robotics and Automation*, pages 1258–63.

Caputo, J. M., Adamczyk, P. G., and Collins, S. H. (2015). Informing ankle-foot prosthesis prescription through haptic emulation of candidate devices. *Proceedings of IEEE International Conference on Robotics and Automation*, pages 1–6.

Caputo, J. M. and Collins, S. H. (2013). An experimental robotic testbed for accelerated development of ankle prostheses. *IEEE International Conference on Robotics and Automation*, pages 2645–50.

Caputo, J. M. and Collins, S. H. (2014a). A universal ankle-foot prosthesis emulator for human locomotion experiments. *Journal of Biomechanical Engineering*, 136(3):035002.

Caputo, J. M. and Collins, S. H. (2014b). Prosthetic ankle push-off work reduces metabolic rate but not collision work in non-amputee walking. *Nature Scientific Reports*, 4:7213.

Casillas, J. M., Dulieu, V., Cohen, M., Marcer, I., and Didier, J. P. (1995). Bioenergetic comparison of a new energy-storing foot and SACH foot in traumatic below-knee vascular amputations. *Archives of Physical Medicine and Rehabilitation*, 76(1):39–44.

Cherelle, P., Grosu, V., Matthys, A., Vanderborght, B., and Lefeber, D. (2013). Design and validation of the ankle mimicking prosthetic (AMP-) foot 2.0. *IEEE Transactions on Neural Systems and Rehabilitation Engineering*, 22(1):138–48.

Cherelle, P., Matthys, A., Grosu, V., Vanderborght, B., and Lefeber, D. (2012). The AMP-foot 2.0: mimicking intact ankle behavior with a powered transtibial prosthesis. *International Conference on Biomedical Robotics and Biomechatronics*, pages 544–9.

Collins, S. H. and Jackson, R. W. (2013). Inducing self-selected human engagement in robotic locomotion training. *Proceedings of IEEE International Conference on Rehabilitation Robotics*, pages 1–6.

Collins, S. H., Kim, M., Chen, T., and Chen, T. (2015). An ankle-foot prosthesis emulator with control of plantarflexion and inversion-eversion torque. *Proceedings of IEEE International Conference on Robotics and Automation*, pages 1–6.

Collins, S. H. and Kuo, A. D. (2010). Recycling energy to restore impaired ankle function during human walking. *PloS One*, 5(2):e9307.

Collins, S. H., Ruina, A. L., Tedrake, R., and Wisse, M. (2005). Efficient bipedal robots based on passive-dynamic walkers. *Science*, 307(5712):1082–5.

Composites, G. (2012). GC-67-UB: Unidirectional Fiberglass Bar Stock. http://www.gordoncomposites.com/product-gc67ub.htm.

de Leva, P. (1996). Adjustments to Zatsiorsky-Seluyanov's segment inertia parameters. *Journal of Biomechanics*, 29(9):1223–30.

Doets, H. C., Vergouw, D., Veeger, H. E. J. D., and Houdijk, H. (2009). Metabolic cost and mechanical work for the step-to-step transition in walking after successful total ankle arthroplasty. *Human Movement Science*, 28(6):786–97.

Donelan, J. M., Kram, R., and Kuo, A. D. (2002). Mechanical work for step-to-step transitions is a major determinant of the metabolic cost of human walking. *The Journal of Experimental Biology*, 205(23):3717–27.

Drillis, R., Contini, R., and Bluestein, M. (1964). Body segment parameters: a survey of measurement techniques. *Artificial Limbs*, 8(1):44–66.

Eilenberg, M. F., Geyer, H., and Herr, H. M. (2010). Control of a powered ankle-foot prosthesis based on a neuromuscular model. *IEEE Transactions on Neural Systems and Rehabilitation Engineering*, 18(2):164–73.

Ellis, R. E., Ismaeil, O. M., and Lipsett, M. G. (1996). Design and evaluation of a high-performance haptic interface. *Robotica*, 14(3):321–7.

Esposito, E. R., Rodriguez, K. M., Ràbago, C. A., and Wilken, J. M. (2014). Does unilateral transtibial amputation lead to greater metabolic demand during walking? *Journal of Rehabilitation Research and Development*, 51(8):1287–1296.

Esposito, E. R., Whitehead, J. M. A., and Wilken, J. M. (2015). Step-to-step transition work during level and inclined walking using passive and powered ankle-foot prostheses. *Prosthetics and Orthotics International*, pages 1–9.

Felt, W., Selinger, J., Donelan, J. M., and Remy, C. D. (2014). Body-in-the-loop optimizing actual human walking. *Proceedings of Dynamic Walking*, pages 1–2.

Ferris, A. E., Aldridge, J. M., Rábago, C. A., and Wilken, J. M. (2012). Evaluation of a powered ankle-foot prosthetic system during walking. *Archives of Physical Medicine and Rehabilitation*, 93(11):1911–8.

Fey, N. P., Klute, G. K., and Neptune, R. R. (2013). Altering prosthetic foot stiffness influences foot and muscle function during below-knee amputee walking: a modeling and simulation analysis. *Journal of biomechanics*, 46(4):637–44.

Fey, N. P., Silverman, A. K., and Neptune, R. R. (2010). The influence of increasing steady-state walking speed on muscle activity in below-knee amputees. *Journal of electromyography and Kinesiology*, 20(1):155–61.

Flowers, W. C. and Mann, R. W. (1977). An electrohydraulic knee-torque controller for a prosthesis simulator. *Journal of biomechanical engineering*, 99(1):3–8.

Fox, M. D. and Delp, S. L. (2010). Contributions of muscles and passive dynamics to swing initiation over a range of walking speeds. *Journal of Biomechanics*, 43(8):1450–5.

Fregly, B. J., Besier, T. F., Lloyd, D. G., Delp, S. L., Banks, S. A., Pandy, M. G., and D'Lima, D. D. (2012). Grand challenge competition to predict in vivo knee loads. *Journal of Orthopaedic Research*, 30(4):503–13.

Gailey, R. S., Allen, K., Castles, J., Kucharik, J., and Roeder, M. (2008). Review of secondary physical conditions associated with lower-limb amputation and long-term prosthesis use. *Journal of Rehabilitation Research and Development*, 45(1):15–29.

Gailey, R. S., Roach, K. E., Applegate, E., Cho, B., Cunniffe, B., Licht, S., Maguire, M., and Nash, M. S. (2002). The Amputee Mobility Predictor: An instrument to assess determinants of the lower-limb amputee's ability to ambulate. *Archives of Physical Medicine and Rehabilitation*, 83(5):613–27.

Gates, D. H., Su, J. L.-S., and Dingwell, J. B. (2007). Possible biomechanical origins of the long-range correlations in stride intervals of walking. *Physica A: Statistical Mechanics and its Applications*, 380:259–70.

Geil, M. D. (2001). Energy loss and stiffness properties of dynamic elastic response prosthetic feet. *Journal of Prosthetics and Orthotics*, 13(3):70–3.

Genin, J. J., Bastien, G. J., Franck, B., Detrembleur, C., and Willems, P. A. (2008). Effect of speed on the energy cost of walking in unilateral traumatic lower limb amputees. *European Journal of Applied Physiology*, 103(6):655–63.

Glantz, S. A. (2011). The special case of two groups: the t-test. In *Primer of Biostatistics*. McGraw-Hill Medical, New York.

Goldfarb, M., Lawson, B. E., and Shultz, A. H. (2013). Realizing the promise of robotic leg prostheses. *Science Translational Medicine*, 5(210):210ps15.

Gordon, K. E. and Ferris, D. P. (2007). Learning to walk with a robotic ankle exoskeleton. *Journal of Biomechanics*, 40(12):2636–44.

Gordon, K. E., Ferris, D. P., and Kuo, A. D. (2009). Metabolic and mechanical energy costs of reducing vertical center of mass movement during gait. *Archives of Physical Medicine and Rehabilitation*, 90(1):136–44.

Gordon, K. E., Sawicki, G. S., and Ferris, D. P. (2006). Mechanical performance of artificial pneumatic muscles to power an ankle-foot orthosis. *Journal of Biomechanics*, 39(10):1832–41.

Grabowski, A. M., Rifkin, J., and Kram, R. (2010). K3 Promoter prosthetic foot reduces the metabolic cost of walking for unilateral transtibial amputees. *Journal of Prosthetics and Orthotics*, 22(2):113–20.

Griffiths, P. G., Gillespie, R. B., and Freudenberg, J. S. (2011). A fundamental linear systems conflict between performance and passivity in haptic rendering. *IEEE Transactions on Robotics*, 27(1):75–88.

Hafner, B. J., Sanders, J. E., Czerniecki, J. M., and Fergason, J. (2002). Energy storage and return prostheses: does patient perception correlate with biomechanical analysis? *Clinical Biomechanics*, 17(5):325–44.

Hagberg, K. and Brånemark, R. (2001). Consequences of non-vascular trans-femoral amputation: a survey of quality of life, prosthetic use and problems. *Prosthetics and Orthotics International*, 25(3):186–94.

Hansen, A. H., Childress, D. S., and Knox, E. H. (2000). Prosthetic foot roll-over shapes with implications for alignment of trans-tibial prostheses. *Prosthetics and Orthotics International*, 24(3):205–15.

Hansen, A. H., Childress, D. S., Miff, S. C., Gard, S. A., and Mesplay, K. P. (2004). The human ankle during walking: implications for design of biomimetic ankle prostheses. *Journal of Biomechanics*, 37(10):1467–74.

Hawes, M. R. and Sovak, D. (1994). Quantitative morphology of the human foot in a North American population. *Ergonomics*, 37(7):1213–26.

Herbrich, R., Graepel, T., and Obermayer, K. (1999). Support vector learning for ordinal regression. *Science*, 1:97–102.

Herr, H. M. and Grabowski, A. M. (2012). Bionic ankle-foot prosthesis normalizes walking gait for persons with leg amputation. *Proceedings of the Royal Society of London B*, 279(1728):457–64.

Herr, H. M. and Wilkenfeld, A. (2003). User-adaptive control of a magnetorheological prosthetic knee. *Industrial Robot: An International Journal*, 30(1):42–55.

Hidler, J., Nichols, D., Pelliccio, M., Brady, K., Campbell, D. D., Kahn, J. H., and Hornby, T. G. (2009). Multicenter randomized clinical trial evaluating the effectiveness of the Lokomat in subacute stroke. *Neurorehabilitation and Neural Repair*, 23(1):5–13.

Hirtz, J., Stone, R., and McAdams, D. (2002). A functional basis for engineering design: reconciling and evolving previous efforts. *Research in Engineering Design*, 13(2):65–82.

Hitt, J. K., Bellman, R., Holgate, M., Sugar, T. G., and Hollander, K. W. (2007). The SPARKy (spring ankle with regenerative kinetics) project: design and analysis of a robotic transtibial prosthesis with regenerative kinetics. *Proceedings of ASME International Conference on Multibody Systems, Nonlinear Dynamics, and Control*, pages 1587–96.

Hitt, J. K., Sugar, T. G., Holgate, M. A., Bellman, R., and Hollander, K. W. (2009). Robotic transtibial prosthesis with biomechanical energy regeneration. *Industrial Robot: An International Journal*, 36(5):441–7.

Hobbelen, D. G. E. and Wisse, M. (2008). Ankle actuation for limit cycle walkers. *The International Journal of Robotics Research*, 27(6):709–35.

Hoffman, M. D., Sheldahl, L. M., Buley, K. J., and Sandford, P. R. (1997). Physiological comparison of walking among bilateral above-knee amputee and able-bodied subjects, and a model to account for the differences in metabolic cost. *Archives of Physical Medicine and Rehabilitation*, 78(4):385–92.

Hofstad, C., Linde, H., Limbeek, J., and Postema, K. (2004). Prescription of prosthetic ankle-foot mechanisms after lower limb amputation. *The Cochrane Database of Systematic Reviews*, 1:CD003978.

Houdijk, H., Pollmann, E., Groenewold, M., Wiggerts, H., and Polomski, W. (2009). The energy cost for the step-to-step transition in amputee walking. *Gait & Posture*, 30(1):35–40.

Hsu, M.-J., Nielsen, D. H., Lin-Chan, S.-J., and Shurr, D. (2006). The effects of prosthetic foot design on physiologic measurements, self-selected walking velocity, and physical activity in people with transtibial amputation. *Archives of Physical Medicine and Rehabilitation*, 87(1):123–9.

Huang, S., Wensman, J. P., and Ferris, D. P. (2014). An experimental powered lower limb prosthesis using proportional myoelectric control. *Journal of Medical Devices*, 8(2):024501.

Jackson, R. W. and Collins, S. H. (2015). An experimental comparison of the relative benefits of work and torque assistance in ankle exoskeletons. *Journal of Applied Physiology*, **in review**.

Kent, J. A., Stergiou, N., and Wurdeman, S. R. (2015). Does dynamic balance of transtibial amputees change after a three week adaptation period on a new prosthetic foot? *Proceedings of the 39th Annual Meeting of the American Society of Biomechanics*.

Kim, M. and Collins, S. H. (2015). Once-per-step control of ankle push-off work improves balance in a three-dimensional simulation of bipedal walking. *Transactions on Robotics*, **in review**.

Klodd, E., Hansen, A. H., Fatone, S., and Edwards, M. (2010). Effects of prosthetic foot forefoot flexibility on oxygen cost and subjective preference rankings of unilateral transtibial prosthesis users. *Journal of Rehabilitation Research and Development*, 47(6):543–552.

Kuo, A. D. (2001). Energetics of actively powered locomotion using the simplest walking model. *Journal of Biomechanical Engineering*, 124(1):113–120.

Kuo, A. D. and Donelan, J. M. (2010). Dynamic principles of gait and their clinical implications. *Physical Therapy*, 90(2):157–74.

Kuo, A. D., Donelan, J. M., and Ruina, A. L. (2005). Energetic consequences of walking like an inverted pendulum: step-to-step transitions. *Exercise and Sport Sciences Reviews*, 33(2):88–97.

Kurtz, D. and Carlson, N. B. (2003). In *Clinical Procedures for Ocular Examination*. McGraw-Hill Medical, 3rd edition.

Laprè, A. K., Umberger, B. R., and Sup, F. (2014). Simulation of a powered ankle prosthesis with dynamic joint alignment. *Proceedings of IEEE Engineering in Medicine and Biology Society*, pages 1618–21.

Legro, M. W., Reiber, G., del Aguila, M., Ajax, M. J., Boone, D. a., Larsen, J. a., Smith, D. G., and Sangeorzan, B. (1999). Issues of importance reported by persons with lower limb amputations and prostheses. *Journal of Rehabilitation Research and Development*, 36(3):155–63.

Lehmann, J. F., Price, R., Boswell-Bessette, S., Dralle, A., Questad, K., and DeLateur, B. J. (1993). Comprehensive analysis of energy storing prosthetic feet: Flex Foot and Seattle Foot Versus Standard SACH foot. *Archives of Physical Medicine and Rehabilitation*, 74(11):1225–31.

Lenzi, T., Hargrove, L. J., and Sensinger, J. W. (2014). Preliminary evaluation of a new control approach to achieve speed adaptation in robotic transfemoral prostheses. *Proceedings of IEEE/RSJ International Conference on Intelligent Robots and Systems*, pages 2049–54.

Lewis, C. L. and Ferris, D. P. (2008). Walking with increased ankle pushoff decreases hip muscle moments. *Journal of biomechanics*, 41(10):2082–9.

Likert, R. (1932). A technique for the measurement of attitudes. *Archives of Psychology*, 22(140):1–55.

Lipfert, S. W., Günther, M., Renjewski, D., and Seyfarth, A. (2014). Impulsive ankle push-off powers leg swing in human walking. *The Journal of Experimental Biology*, 217(8):1218–28.

Madden, J. D. (2007). Mobile robots: motor challenges and materials solutions. *Science*, 318(5853):1094–7.

Major, M. J., Twiste, M., Kenney, L. P. J., and Howard, D. (2011). Amputee independent prosthesis properties: a new model for description and measurement. *Journal of Biomechanics*, 44(14):2572–5.

Major, M. J., Twiste, M., Kenney, L. P. J., and Howard, D. (2014). The effects of prosthetic ankle stiffness on ankle and knee kinematics, prosthetic limb loading, and net metabolic cost of trans-tibial amputee gait. *Clinical biomechanics*, 29(1):98–104.

Malcolm, P., Derave, W., Galle, S., and De Clercq, D. (2013). A simple exoskeleton that assists plantarflexion can reduce the metabolic cost of human walking. *PloS One*, 8(2):e56137.

Malcolm, P., Quesada, R. E., Caputo, J. M., and Collins, S. H. (2015). The influence of push-off timing in a robotic ankle-foot prosthesis on the energetics and mechanics of walking. *Journal of Neuroengineering and Rehabilitation*, 12(21):1–14.

Malone, L. A., Bastian, A. J., and Torres-Oviedo, G. (2012). How does the motor system correct for errors in time and space during locomotor adaptation? *Journal of Neurophysiology*, 108(2):672–83.

Margaria, R. (1976). Biomechanics and energetics of muscular exercise. In *Biomechanics of human locomotion*, pages 126–39. Clarendon Press, Oxford.

Michael, J. W. and Bowker, J. H. (2004). *Atlas of amputations and limb deficiencies: surgical, prosthetic, and rehabilitation principles*. American Academy of Orthopaedic Surgeons, Rosemont, IL.

Miller, W. C., Speechley, M., and Deathe, A. B. (2002). Balance confidence among people with lower-limb amputations. *Physical Therapy*, 82(9):856–65.

Miller, W. C., Speechley, M., and Deathe, B. (2001). The prevalence and risk factors of falling and fear of falling among lower extremity amputees. *Archives of Physical Medicine and Rehabilitation*, 82(8):1031–7.

Morgenroth, D. C., Segal, A. D., Zelik, K. E., Czerniecki, J. M., Klute, G. K., Adamczyk, P. G., Orendurff, M. S., Hahn, M. E., Collins, S. H., and Kuo, A. D. (2011). The effect of prosthetic foot push-off on mechanical loading associated with knee osteoarthritis in lower extremity amputees. *Gait & Posture*, 34(4):502–7.

Noël, M., Cantin, B., Lambert, S., Gosselin, C. M., and Bouyer, L. J. (2008). An electrohydraulic actuated ankle foot orthosis to generate force fields and to test proprioceptive reflexes during human walking. *IEEE Transactions on Neural Systems and Rehabilitation Engineering*, 16(4):390–9.

Powell, M. J. D. (1964). An efficient method for finding the minimum of a function of several variables without calculating derivatives. *The Computer Journal*, 7(2):155–62.

Pratt, G. A. and Williamson, M. M. (1995). Series elastic actuators. *Proceedings of IEEE/RSJ International Conference on Intelligent Robots and Systems*, 1:399–406.

Pratt, J. E., Krupp, B., and Morse, C. (2002). Series elastic actuators for high fidelity force control. *Industrial Robot: An International Journal*, 29(3):234–41.

Pratt, J. E., Krupp, B. T., Morse, C. J., and Collins, S. H. (2004). The RoboKnee: an exoskeleton for enhancing strength and endurance during walking. *Proceedings of IEEE International Conference on Robotics and Automation*, 3:2430–5.

Quesada, R. E., Caputo, J. M., and Collins, S. H. (2015). Increased robotic ankle-foot prosthesis push-off work does not necessarily reduce metabolic rate for unilateral trans-tibial amputees. **in review**.

Ralston, H. J. (1958). Energy-speed relation and optimal speed during level walking. *Internationale Zeitschrift für Angewandte Physiologie Einschliesslich Arbeitsphysiologie*, 17(4):277–83.

Ren, L. and Hutchinson, J. R. (2008). The three-dimensional locomotor dynamics of African (Loxodonta africana) and Asian (Elephas maximus) elephants reveal a smooth gait transition at moderate speed. *Journal of the Royal Society of London: Interface*, 5(19):195–211.

Requião, L. F., Nadeau, S., Milot, M. H., Gravel, D., Bourbonnais, D., and Gagnon, D. (2005). Quantification of level of effort at the plantarflexors and hip extensors and flexor muscles in healthy subjects walking at different cadences. *Journal of Electromyography and Kinesiology*, 15(4):393–405.

Roy, A., Krebs, H. I., Williams, D. J., Bever, C. T., Forrester, L. W., Macko, R. M., and Hogan, N. (2009). Robot-aided neurorehabilitation: a novel robot for ankle rehabilitation. *IEEE Transactions on Robotics*, 25(3):569–82.

Ruina, A. L., Bertram, J. E. A., and Srinivasan, M. (2005). A collisional model of the energetic cost of support work qualitatively explains leg sequencing in walking and galloping, pseudo-elastic leg behavior in running and the walk-to-run transition. *Journal of Theoretical Biology*, 237(2):170–92.

Russell, S. J. and Norvig, P. (2003). Beyond classical search. In *Artificial Intelligence: A Modern Approach*, pages 122–5. Prentice Hall, Upper Saddle River, NJ.

Sawicki, G. S. and Ferris, D. P. (2008). Mechanics and energetics of level walking with powered ankle exoskeletons. *The Journal of Experimental Biology*, 211(9):1402–13.

Sawicki, G. S. and Ferris, D. P. (2009). Powered ankle exoskeletons reveal the metabolic cost of plantar flexor mechanical work during walking with longer steps at constant step frequency. *The Journal of Experimental Biology*, 212(1):21–31.

Sawicki, G. S., Lewis, C. L., and Ferris, D. P. (2009). It pays to have a spring in your step. *Exercise and Sport Sciences Reviews*, 37(3):130–8.

Schiele, A. (2008). Performance difference of Bowden Cable relocated and non-relocated master actuators in virtual environment applications. *Proceedings of IEEE/RSJ International Conference on Intelligent Robots and Systems*, pages 3507–12.

Schiele, A., Letier, P., Der Linde, R., and Der Helm, F. (2006). Bowden cable actuator for force-feedback exoskeletons. *Proceedings of IEEE/RSJ International Conference on Intelligent Robots and Systems*, pages 3599–604.

Schwartz, J. (2013). A brand-new kick: How an mit spinoff is revolutionizing prosthetics one motor-driven ankle at a time. http://www.bostonmagazine.com/health/article/2013/11/26/prosthetics-research-boston-biom-ankle-prosthetic/.

Segal, A. D., Zelik, K. E., Klute, G. K., Morgenroth, D. C., Hahn, M. E., Orendurff, M. S., Adamczyk, P. G., Collins, S. H., Kuo, A. D., and Czerniecki, J. M. (2012). The effects of a controlled energy storage and return prototype prosthetic foot on transtibial amputee ambulation. *Human Movement Science*, 31(4):918–31.

Shamaei, K., Sawicki, G. S., and Dollar, A. M. (2013). Estimation of quasi-stiffness and propulsive work of the human ankle in the stance phase of walking. *PloS One*, 8(3):e59935.

Silverman, A. K., Fey, N. P., Portillo, A., Walden, J. G., Bosker, G., and Neptune, R. R. (2008). Compensatory mechanisms in below-knee amputee gait in response to increasing steady-state walking speeds. *Gait & Posture*, 28(4):602–9.

Skinner, H. B. and Effeney, D. J. (1985). Gait analysis in amputees. *American Journal of Physical Medicine & Rehabilitation*, 64(2).

Snaterse, M., Ton, R., Kuo, A. D., and Donelan, J. M. (2011). Distinct fast and slow processes contribute to the selection of preferred step frequency during human walking. *Journal of Applied Physiology*, 110(6):1682–90.

Song, S. and Geyer, H. (2012). Regulating speed and generating large speed transitions in a neuromuscular human walking model. *Proceedings of IEEE International Conference on Robotics and Automation*, pages 511–6.

Song, S., LaMontagna, C., Collins, S. H., and Geyer, H. (2013). The effect of foot compliance encoded in the windlass mechanism on the energetics of human walking. *Proceedings of International Conference of the IEEE Engineering in Medicine and Biology Society*, pages 3179–82.

Soo, C. H. and Donelan, J. M. (2012). Coordination of push-off and collision determine the mechanical work of step-to-step transitions when isolated from human walking. *Gait & Posture*, 35(2):292–7.

Spurr, G. B., Prentice, A. M., Murgatroyd, P. R., Goldberg, G. R., Reina, J. C., and Christman, N. T. (1988). Energy expenditure from minute-by-minute heart-rate recording: comparison with indirect calorimetry. *The American Journal of Clinical Nutrition*, 48(3):552–9.

Sreenath, K., Park, H. W., Poulakakis, I., and Grizzle, J. W. (2010). A compliant hybrid zero dynamics controller for stable, efficient and fast bipedal walking on MABEL. *The International Journal of Robotics Research*, 30(9):1170–93.

Srinivasan, M. and Ruina, A. L. (2006). Computer optimization of a minimal biped model discovers walking and running. *Nature*, 439:72–5.

Stephens, B. J. and Atkeson, C. G. (2010). Dynamic balance force control for compliant humanoid robots. *Proceedings of IEEE/RSJ International Conference on Intelligent Robots and Systems*, pages 1248–55.

Stienen, A. H. A., Hekman, E. E. G., ter Braak, H., Aalsma, A. M. M., van der Helm, F. C. T., and van der Kooij, H. (2010). Design of a rotational hydroelastic actuator for a powered exoskeleton for upper limb rehabilitation. *IEEE Transactions on Biomedical Engineering*, 57(3):728–35.

Su, J. L.-S. and Dingwell, J. B. (2007). Dynamic stability of passive dynamic walking on an irregular surface. *Journal of Biomechanical Engineering*, 129(6):802–10.

Sulzer, J. S., Roiz, R. a., Peshkin, M. a., and Patton, J. L. (2009). A highly backdrivable, lightweight knee actuator for investigating gait in stroke. *IEEE Transactions on Robotics*, 25(3):539–48.

Sup, F., Bohara, A., and Goldfarb, M. (2008). Design and control of a powered transfemoral prosthesis. *The International Journal of Robotics Research*, 27(2):263–73.

Sup, F., Varol, H. A., Mitchell, J., Withrow, T. J., and Goldfarb, M. (2009). Self-contained powered knee and ankle prosthesis: initial evaluation on a transfemoral amputee. *Proceedings of IEEE International Conference on Rehabilitation Robotics*, pages 638–44.

Taguchi, G., Chowdhury, S., and Wu, Y. (2004). In *Taguchi's quality engineering handbook*. John Wiley & Sons, Hoboken, New Jersey.

Thelen, D. G. and Anderson, F. C. (2006). Using computed muscle control to generate forward dynamic simulations of human walking from experimental data. *Journal of Biomechanics*, 39(6):1107–15.

Torburn, L., Perry, J., Ayyappa, E., and Shanfield, S. L. (1990). Below-knee amputee gait with dynamic elastic response prosthetic feet: a pilot study. *The Journal of Rehabilitation Research and Development*, 27(4):369–84.

Torburn, L., Powers, C. M., Guiterrez, R., and Perry, J. (1995). Energy expenditure during ambulation in dysvascular and traumatic below-knee amputees: a comparison of five prosthetic feet. *Journal of Rehabilitation Research and Development*, 32(2):111–9.

Usherwood, J. R., Williams, S. B., and Wilson, A. M. (2007). Mechanics of dog walking compared with a passive, stiff-limbed, 4-bar linkage model, and their collisional implications. *The Journal of Experimental Biology*, 210(3):533–40.

van Dijk, W. and van der Kooij, H. (2013). Optimization of human walking for exoskeletal support. *Proceedings of IEEE International Conference on Rehabilitation Robotics*, pages 1–6.

Vanderpool, M. T., Collins, S. H., and Kuo, A. D. (2008). Ankle fixation need not increase the energetic cost of human walking. *Gait & Posture*, 28(3):427–33.

Veneman, J. F., Kruidhof, R., Hekman, E. E. G., Ekkelenkamp, R., Van Asseldonk, E. H. F., and van der Kooij, H. (2007). Design and evaluation of the LOPES exoskeleton robot for interactive gait rehabilitation. *IEEE Transactions on Neural Systems and Rehabilitation Engineering*, 15(3):379–86.

Versluys, R., Deckers, K., Van Damme, M., Van Ham, R., Steenackers, G., Guillaume, P., and Lefeber, D. (2009a). A study on the bandwidth characteristics of pleated pneumatic artificial muscles. *Applied Bionics and Biomechanics*, 6(1):3–9.

Versluys, R., Desomer, A., Lenaerts, G., Pareit, O., Vanderborght, B., der Perre, G. V., Peeraer, L., and Lefeber, D. (2008). A biomechatronical transtibial prosthesis powered by pleated pneumatic artificial muscles. *International Journal of Modelling, Identification and Control*, 4(4):394–405.

Versluys, R., Lenaerts, G., van Damme, M., Jonkers, I., Desomer, A., Vanderborght, B., Peeraer, L., Van der Perre, G., and Lefeber, D. (2009b). Successful preliminary walking experiments on a transtibial amputee fitted with a powered prosthesis. *Prosthetics and Orthotics International*, 33(4):368–77.

Waters, R. L. and Mulroy, S. (1999). The energy expenditure of normal and pathologic gait. *Gait & Posture*, 9(3):207–31.

Whittle, M. W. (1996). Normal gait. In *Gait Analysis: An Introduction*, pages 48–90. Butterworth-Heinemann, Oxford.

Winter, D. A. (1990). In *Biomechanics and Motor Control of Human Movement*. John Wiley & Sons, Hoboken, New Jersey, 4th edition.

Winter, D. A. (1991). In *The Biomechanics and Motor Control of Human Gait: Normal, Elderly and Pathological*. Waterloo Biomechanics, Waterloo, Canada, 2nd edition.

Winter, D. A. and Sienko, S. E. (1988). Biomechanics of below-knee amputee gait. *Journal of Biomechanics*, 21(5):361–7.

Witte, K. A., Zhang, J., Jackson, R. W., and Collins, S. H. (2015). Design of two lightweight, high-bandwidth torque-controlled ankle exoskeletons. *Proceedings of IEEE International Conference on Robotics and Automation*, pages 1–6.

Wutzke, C. J., Sawicki, G. S., and Lewek, M. D. (2012). The influence of a unilateral fixed ankle on metabolic and mechanical demands during walking in unimpaired young adults. *Journal of Biomechanics*, 45(14):2405–10.

Wyeth, G. (2006). Control issues for velocity sourced series elastic actuators. *Proceedings of Australasian Conference on Robotics and Automation*, pages 6–8.

Yeom, J. and Park, S. (2011). A gravitational impulse model predicts collision impulse and mechanical work during a step-to-step transition. *Journal of Biomechanics*, 44(1):59–67.

Zelik, K. E., Collins, S. H., Adamczyk, P. G., Segal, A. D., Klute, G. K., Morgenroth, D. C., Hahn, M. E., Orendurff, M. S., Czerniecki, J. M., and Kuo, A. D. (2011). Systematic variation of prosthetic foot spring affects center-of-mass mechanics and metabolic cost during walking. *IEEE Transactions on Neural Systems and Rehabilitation Engineering*, 19(4):411–9.

Zhang, J., Cheah, C. C., and Collins, S. H. (2015). Experimental comparison of torque control methods on an ankle exoskeleton during human walking. *Proceedings of IEEE International Conference on Robotics and Automation*, pages 1–6.

Zidarov, D., Swaine, B., and Gauthier-Gagnon, C. (2009). Quality of life of persons with lower-limb amputation during rehabilitation and at 3-month follow-up. *Archives of Physical Medicine and Rehabilitation*, 90(4):634–45.

Ziegler-Graham, K., MacKenzie, E. J., Ephraim, P. L., Travison, T. G., and Brookmeyer, R. (2008). Estimating the prevalence of limb loss in the United States: 2005 to 2050. *Archives of Physical Medicine and Rehabilitation*, 89(3):422–9.

Zmitrewicz, R. J., Neptune, R. R., Walden, J. G., Rogers, W. E., and Bosker, G. W. (2006). The effect of foot and ankle prosthetic components on braking and propulsive impulses during transtibial amputee gait. *Archives of Physical Medicine and Rehabilitation*, 87(10):1334–9.

Zoss, A. B., Kazerooni, H., and Chu, A. (2005). On the mechanical design of the Berkeley lower extremity exoskeleton (BLEEX). *Proceedings of IEEE/RSJ International Conference on Intelligent Robots and Systems*, pages 3465–72.